MICROCOPY RESOLUTION TEST CHART

NATIONAL BUREAU OF STANDARDS-1963-A

019795-1-T

⑫

AD-A135 335

OPTIMUM DESIGN OF MILLIMETER-WAVE IMPATT DIODE OSCILLATORS

TECHNICAL REPORT NO. 165

October 1983

By

Y. S. HWANG

ELECTRON
PHYSICS
LABORATORY

DTIC
S ELECTE D
DEC 0 2 1983
E

DEPARTMENT OF ELECTRICAL AND COMPUTER ENGINEERING
THE UNIVERSITY OF MICHIGAN, ANN ARBOR

83 12 02 009

This report has also been submitted as a dissertation in
partial fulfillment of the requirements for the degree of
Doctor of Philosophy in The University of Michigan, 1983.

OPTIMUM DESIGN OF MILLIMETER-WAVE IMPATT DIODE OSCILLATORS

by

Y. S. Hwang

Technical Report No. 165
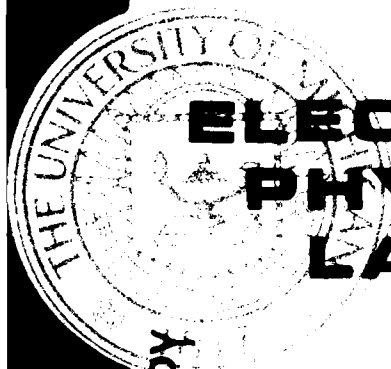
Electron Physics Laboratory
Department of Electrical and Computer Engineering
The University of Michigan
Ann Arbor, MI 48109-1109

Approved for public release; distribution unlimited.

Grant No. DAAG29-82-K-0083

U. S. Army Research Office
Research Triangle Park, NC 27709

October 1983

ABSTRACT

The limitations and control of pulsed IMPATT diode millimeter-wavelength oscillators are described. A quasi-static oscillator model is established for characterizing amplitude and frequency behavior during pulsed operation in response to external influences such as bias current, temperature, optical injection, locking signal injection and RF circuit. The effect of these external parameters in oscillator turn-on, turn-off, frequency chirp during the pulse, and start-up jitter are given for a millimeter-wavelength oscillator using a Si double-drift diode. Methods of controlling the pulsed behavior including bias current compensation, optical compensation and injection locking are analyzed and applied to a pulsed millimeter-wave oscillator example. The optimum bias current and optical current waveforms which eliminate post turn-on frequency drift are presented.

Accession For	
NTIS GRA&I	☒
DTIC TAB	☐
Unannounced	☐
Justification	
By	
Distribution/	
Availability Codes	
Dist	Avail and/or Special
A-1	

TABLE OF CONTENTS

LIST OF ILLUSTRATIONS

LIST OF SYMBOLS

A	Device area, cm^2.
B_c	Circuit susceptance, mho.
B_d	Device susceptance, mho.
C	Capacitance, F.
C_d	Device capacitance, F.
C_p	Parasitic capacitance, F.
c	Heat capacity of the material, $J/^{\circ}C$.
c'	Specific Heat, $J/g^{\circ}C$.
d	Duty cycle.
d	Device width, cm.
d_i	Material thickness of the ith layer, cm.
f, f_o	Frequency, Hz.
f_i	Frequency of the locking signal, Hz.
G, G_c	Circuit conductance, mho.
G_d	Device conductance, mho.
I_{dc}	Dc bias current, A.
I_i	Injection current, A.
I_{op}	Photon injection current, A.
J_{dc}	Dc bias current density, A/cm^2.
J_{op}	Photon injection current density, A/cm^2.
k	Thermal conductivity, $W/cm^{\circ}C$.
k_i	Thermal conductivity of the ith layer, $W/cm^{\circ}C$.
L	Inductance, H.
L_p	Parasitic inductance, H.

P_{av}	Average power, W.
P_d	Dissipated power, W.
P_{dc}	Dc power, W.
P_{in}	Injection power of the locking signal, W.
P_{mean}	Mean power, W.
PRF	Pulse repetition frequency, Hz.
P_{RF}	Oscillator power, W.
P_r	Rayleigh probability distribution.
Q	Quality factor.
Q_L	Loaded oscillator quality factor.
$Q_{L,C}$	Loaded circuit quality factor.
R	Radius of the diode, cm.
R	Resistance, Ω.
R_{HS}	Thermal resistance due to the heat sink, °C/W.
R_{ind}	Negative resistance induced by the back-bias effect, Ω.
R_s	Thermal resistance due to the Si and thin layers of contact metallization, °C/W.
R_{sc}	Space-charge resistance, Ω.
R_{th}	Thermal resistance, °C/W.
r	Thermal resistance, °C/W.
r_{max}	Maximum range.
s	Complex frequency.
T, T_J	Junction temperature of the device, °K.
T	Period, s.
T_a	Ambient temperature, °K.
t	Time, s.
t_1	Pulsewidth, s.

t_{on}	Turn-on time, s.
V, V_{RF}	Amplitude of RF voltage, V.
V_B	Breakdown voltage, V.
V_{dc}	Dc voltage, V.
V_R	Rectification voltage, V.
V_s	Amplitude of constant voltage source, V.
V_{ss}, V_o	RF voltage at steady state, V.
v	Instantaneous voltage, V.
Y_c	Circuit admittance, mho.
Y_d	Device admittance, mho.
α	Thermal diffusivity, cm^2/s.
Δf	Frequency drift, Hz.
ΔI_{dc}	Change of dc bias current, A.
ΔI_{op}	Change of photon injection current, A.
ΔT	Temperature rise of the diode, ^oK.
ε	Dielectric constant, F/cm.
η	Operating efficiency.
θ	Phase angle, rad.
ρ	Density, g/cm^3.
σ	Growth rate, s^{-1}.
σ_{jitter}	Standard deviation of turn-on time.
τ_{th}	Thermal-time constant, s.
ω	Angular frequency, rad/s.
ω_i	Angular frequency of the locking signal, rad/s.

CHAPTER I.   INTRODUCTION

1.1 Millimeter-Wave Applications of IMPATT Diodes

Impact ionization avalanche transit time (IMPATT) devices
provide an extremely important source of solid-state power generation,
particularly in the millimeter-wave frequency range from 30 to 300 GHz
(10- to 1-mm wavelength). While atmospheric absorption caused by a
combination of water vapor and oxygen molecular resonances[1] are sig-
nificant in this region of the spectrum, relatively transparent win-
dows exist at 35, 94, 140 and 225 GHz where the advantages of
millimeter-wave systems are possible. These advantages are large data
bandwidth, small antenna size, low detection probability, and high
anti-jam capability.[2]

Millimeter waves have applications in radar, communication and
medicine. Millimeter-wave radar systems make use of a variety of
coherent, noncoherent pulse, pulse doppler FM-CW and pulse compression
techniques. The size, reliability, and power generating capability of
IMPATT devices are particularly well suited to many of these applications.

1.2 Pulsed Oscillators and their Applications

A fundamental problem with all solid-state devices including
IMPATT diodes is the reduction in their power generating capability
as frequency increases[3] (Pf^2 = constant). RF power generated from
the active device becomes limited at millimeter-wave frequencies.
For CW operation the maximum current density, and hence power output,
is limited thermally, while pulsed operation can increase this peak
power depending on the pulsewidth and duty cycle. For very

short pulsewidth and low duty cycle as required in many millimeter-wave pulsed applications, the generated power is no longer thermally limited. The current density can be increased to obtain more power until space-charge effects cause power and efficiency to decline. Since the diode output power increases with current density, pulsed operation is often required to generate the power levels necessary in this frequency range. Other problems of the pulsed oscillator include turn-on jitter in the leading edge envelope of the output power and power variation or amplitude modulation (AM) and frequency chirp or frequency modulation (FM) during the pulse.

One important application of pulsed oscillators is as transmitters in pulsed radar systems. Resolution and maximum range are two of the important parameters of radar systems, and the range resolution of a radar set is determined by pulsewidth. High resolution requires short pulsewidth with stable, clean operation of the transmitter oscillator. The maximum range (r_{max}) attainable depends on the reflecting properties of the object as well as the characteristics of the radar. The effectiveness of the transmitter in making r_{max} large is measured by the product of peak power and pulsewidth (the energy of each pulse transmitted). Hence, it is important in these systems that the transmitter provide high-power, stable and clean operation.

1.3 Goals of the Present Study

Significant research has been done on the device properties and design criteria for optimizing the output power. However, additional work is required for improved understanding of

device-circuit interaction, noise reduction techniques, and methods to control the oscillator frequency, particularly in pulsed operation.

The purpose of this study is to develop an oscillator model which can be used to investigate the behavior of pulsed and CW oscillators. Analytical equations, adequate device characterization, RF circuit models, bias circuit considerations, and computer simulations are used to study the starting transients and behavior of the pulsed IMPATT oscillators.

With this model, a more comprehensive understanding of oscillator properties primarily in the millimeter-wave frequency range can be achieved. These properties are transient and dynamic effects in pulsed and injection locked oscillators, the relation of circuit to oscillator behavior and design criteria for stable ("clean") operation, the effect of external influences (such as bias current, bias circuit, RF circuit, temperature and light) on device behavior and performance as oscillators. Techniques and device design to control the post turn-on transients are important and require further study.

In Chapter II an oscillator model is developed, and the equations governing the behavior of oscillators and device junction temperature are given. Device parameters (device admittance, thermal resistance and thermal-time constant) and circuit admittance presented to the device which are required for the oscillator analysis are discussed briefly. The usefulness of this model to predict the behavior of pulsed oscillators and their limitations is described. Turn-on, post turn-on and turn-off transients of a pulsed IMPATT oscillator are demonstrated through an example.

In Chapter III the dependence of oscillator turn-on transients on the device and circuit parameters is investigated. Effects of bias current, RF circuit, bias circuit, injection locking, photon injection and ambient temperature on the frequency response, RF power buildup and generated output power of a millimeter-wave IMPATT oscillator are described.

In Chapter IV techniques to control the oscillation frequency of pulsed and CW oscillators are described. Techniques and examples including bias current compensation, optical injection compensation and injection locking to control the post turn-on transients of pulsed oscillators are presented.

Chapter V presents a summary and conclusions of this study. Suggestions for further study are also described.

CHAPTER II. MODEL FOR CHARACTERIZING THE

OSCILLATOR STATICS AND DYNAMICS

2.1 Analysis of the Oscillator Model

The purpose of this chapter is to develop a simple oscillator

model such that the static and dynamic behavior of a free-running or

injection locked pulsed oscillator can be investigated. Although

only the IMPATT diode oscillators are discussed, this analysis can

be applied to any two-terminal active device or three-terminal device

(such as a field-effect transistor) in an appropriate circuit.

The IMPATT device exhibits negative resistance when its bias

current exceeds the threshold level, and the circuit can be designed

to utilize this negative-resistance property. For CW operation, the

diode is usually biased with constant current instead of constant

voltage, while a constant current or constant voltage source with

finite impedance may be used under pulsed operation. The bias

circuit constrains the bias current passing through the diode and the

dc voltage across it, thereby affecting the dynamic behavior of a

pulsed oscillator.

Part of the dc power delivered to the diode is converted to

ac power, and the remainder generates heat. The generated heat in

turn contributes to the increase of device temperature. Since the

device characteristics are dependent upon junction temperature, the

oscillator frequency and output power will vary accordingly as a

result of the device-circuit interaction. Thus the turn-on, post

turn-on and turn-off transients of pulsed oscillators can be

obtained by solving the oscillator equation, the thermal equation, and the bias circuit equation simultaneously.

2.1.1 Quasi-Statics. An analytical treatment of pulsed and injection locked oscillator dynamics is possible if the oscillator amplitude and frequency are assumed to vary sufficiently slowly over an average cycle of the RF or microwave signal. That is, the oscillator signal is assumed to be a quasi-sinusoid of the form

$$v(t) = Ve^{j\omega t} , \qquad (2.1)$$

where $V = V(t)$ and $\omega = \omega(t)$ are real slowly varying functions of time. Slowly varying can be stated as

$$\frac{\Delta V}{V}\bigg|_{\text{one cycle}} \ll 1 \quad \text{or} \quad \frac{1}{V}\frac{dV}{dt} \ll \omega \qquad (2.2a)$$

and

$$\frac{\Delta \omega}{\omega}\bigg|_{\text{one cycle}} \ll 1 \quad \text{or} \quad \frac{1}{\omega}\frac{d\omega}{dt} \ll \omega . \qquad (2.2b)$$

In a small neighborhood of a time t_o, $V(t)$ can be approximated by $V^*(t)$ as

$$V^*(t) = V_o e^{\sigma_o t} ,$$

where

$$V^*(t_o) = V(t_o) = V_o e^{\sigma_o t}$$

or

$$\sigma_o \triangleq \frac{\dot{V}(t_o)}{V(t_o)} \qquad (2.3a)$$

with

$$\omega_o = \omega(t_o) . \qquad (2.3b)$$

Then,

$$v^*(t) = V_o e^{s_o t} , \qquad (2.4)$$

where $s_o = \sigma_o + j\omega_o$ is a quasi-sinusoidal approximation to $v(t)$ in the neighborhood of t_o.

The dynamics of the oscillator are thus embedded in the evolution of $s(t) \triangleq \sigma(t) + j\omega(t)$. This frequency can be found by examining the interaction between a nonlinear active device and a microwave circuit.

2.1.2 Device Describing Function. The describing function concept[4] is appropriate and useful in characterizing nonlinear quasi-static, quasi-sinusoidal oscillators. It can be used to describe the RF properties of the nonlinear device when device parameters are slowly varying in time. When used with IMPATT devices, the describing function is usually defined as the ratio of fundamental RF current to the amplitude of the sinusoidal RF voltage across the diode. Hence, it is an admittance Y_d which can depend on several slowly varying parameters, i.e.,

$$Y_d = Y_d(V_{RF}, I_{dc}, I_{op}, T, j\omega) , \qquad (2.5)$$

where Y_d = the IMPATT admittance describing function (mho),

V_{RF} = the fundamental RF voltage across the diode (V),

I_{dc} = the low-frequency bias current (A),

I_{op} = the photon injection current (A),

T = the junction or device temperature (°K), and

ω = the frequency.

Other parameters may also affect Y_d, but the ones given above are of most interest in the present study.

2.1.3 Oscillator Equation. In order to produce oscillation at microwave frequency, the active device must exhibit negative resistance. For the IMPATT diode, the negative-resistance conditions can be achieved by applying adequate dc bias current to the diode. The oscillator can then be properly designed to make use of the negative-resistance property and obtain oscillation at the desired frequency. The equivalent circuit of an oscillator[5] generally consists of the large-signal model of the diode admittance Y_d, the equivalent circuit of the microwave circuit admittance Y_c, and injection current I_i, as shown in Fig. 2.1.

2.1.4 Free-Running Oscillator. In the free-running case, I_i is set to zero which yields

$$[Y_d(V_{RF}, I_{dc}, I_{op}, T, j\omega) + Y_c(j\omega)]V_{RF}e^{j\omega t} = 0$$

or, since $V_{RF} \neq 0$ for all t,

$$Y_d(V_{RF}, I_{dc}, I_{op}, T, s) + Y_c(s) = 0 \qquad (2.6)$$

for all time, where s has replaced $j\omega$ to indicate a generally complex frequency as the solution to Eq. 2.6. The solution to Eq. 2.6 will be of the form

$$s = s(V_{RF}, I_{dc}, I_{op}, T) = \sigma + j\omega , \qquad (2.7)$$

so that the dynamic equation for $V_{RF}(t)$ is given by

$$\frac{1}{V_{RF}} \frac{dV_{RF}}{dt} = \sigma(V_{RF}, I_{dc}, I_{op}, T) \qquad (2.8a)$$
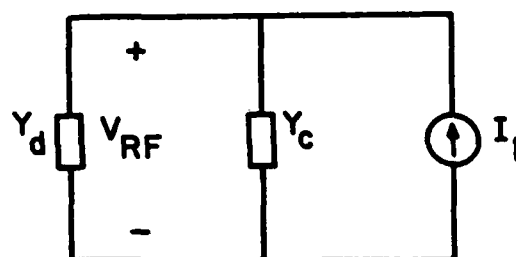
FIG. 2.1 OSCILLATOR EQUIVALENT CIRCUIT USED TO STUDY THE

BEHAVIOR OF A FREE-RUNNING OR INJECTION LOCKED

OSCILLATOR.

with the frequency of oscillation determined as

$$\omega(t) = \omega(V_{RF}, I_{dc}, I_{op}, T) \quad . \qquad (2.8b)$$

If $\sigma > 0$, V_{RF} grows with time. If $\sigma < 0$, V_{RF} decays and steady state occurs for $\sigma = 0$. Oscillator stability requires that $d\sigma/dV_{RF}|_{\sigma=0} < 0$. Hence, to describe the oscillator trajectory in time, the nonlinear differential equation (Eq. 2.8a) must be solved along with other equations governing the other time-dependent variables I_{dc}, I_{op} and T.

2.1.5 Injection Locked Oscillator. In the case of a locked oscillator, a locking signal of amplitude I_i at frequency ω_i is applied to the circuit as shown in Fig. 2.1. The locking equation can then be written as

$$[Y_d(V_{RF}, I_{dc}, I_{op}, T, s) + Y_c(s)]V_{RF}e^{j(\omega_i t + \theta)} = I_i e^{j\omega_i t} \quad ,$$

where θ is the angle between the RF voltage and injection current and is a slowly varying parameter (the locking angle). The equation for a locked oscillator can be rewritten as

$$Y_d(V_{RF}, I_{dc}, I_{op}, T, s) + Y_c(s) = \frac{I_i e^{-j\theta}}{V_{RF}} \quad . \qquad (2.9)$$

The solution to Eq. 2.9 for s at time t, given all the other variables at time t, will give

$$s = s(V_{RF}, I_{dc}, I_{op}, T, I_i, \theta) = \sigma + j\omega \qquad (2.10)$$

and, as before,

$$\frac{1}{V_{RF}} \frac{dV_{RF}}{dt} = \sigma(V_{RF}, I_{dc}, I_{op}, T, I_i, \theta) \qquad (2.11a)$$

with

$$\omega \triangleq \omega_i + \frac{d\theta}{dt} = \omega(V_{RF}, I_{dc}, I_{op}, T, I_i, \theta)$$

or

$$\frac{d\theta}{dt} = \omega - \omega_i \quad . \tag{2.11b}$$

Now both V_{RF} and θ evolve in time as determined by the solution to the nonlinear differential equations and the other slowly varying parameters. The solutions to Eq. 2.11 are straightforward using numerical integration techniques.

When it is assumed that $I_{dc} = 0$ during the "off" period and the injection signal is present all the time, an initial RF voltage exists before the bias pulse is turned on. The diode is passive when $I_{dc} = 0$ and can be represented by a capacitor ($C_d = \epsilon A/d$). Initial RF voltage and phase angle can be determined from the equation:

$$Y_d(T=T_a, j\omega_i, I_{dc}=0) + Y_c(j\omega_i) = \frac{I_i}{V_{RF}(0)} e^{-j\theta(0)} \quad , \tag{2.12}$$

where ω_i = the frequency of the injection signal,

T_a = the ambient temperature,

$Y_d = j\omega_i C_d$,

$V_{RF}(0)$ = the initial RF voltage at $t = 0$, and

$\theta(0)$ = the initial phase angle at $t = 0$.

2.1.6 Thermal Equation. The dc power required to generate RF oscillations also produces heat in the diode and raises its temperature. Since heat generation is proportional to the electric field,[1] most of the heat in IMPATT devices is generated in the

space-charge region and removed through the semiconductor, metal contact and heat sink. The temperature response of the device is then approximated by the following equation:

$$\frac{dT}{dt} + \frac{T - T_a}{\tau_{th}} = \frac{R_{th} \cdot P_d}{\tau_{th}} \, , \qquad (2.13)$$

where   T = the junction temperature of the device,

T_a = the ambient temperature,

τ_{th} = the device thermal-time constant, and

P_d = the dissipated power which is related to the dc power delivered to the diode P_{dc}, and the oscillator power P_{RF} generated by the active device, i.e.,

$$P_d = P_{dc} - P_{RF} = V_{dc} I_{dc} - P_{RF} \, . \qquad (2.14)$$

Constant thermal-time constant and constant thermal resistance are used in the analysis although both are dependent on the temperature and several thermal-time constants may be involved. In Sections 2.2 and 2.3, τ_{th} and R_{th} are described further.

An estimate of the junction temperature at steady state (dT/dt = 0) can be obtained from the device thermal resistance and dissipated power at the junction as

$$T_f = T_a + R_{th} \cdot P_d \, . \qquad (2.15)$$

The maximum bias current that can be used for a safe operating condition of the device is limited by the maximum allowed junction temperature. Normal operating bias current is constrained by the maximum bias current and the required reliability which decreases with the increasing operating device temperature.

2.1.7 Low-Frequency Bias Circuit Equation. In the absence
of RF oscillations, the dc voltage across the IMPATT diode is given
by

$$V_{dc} = V_B(T) + I_{dc}(t)R_{sc} \quad , \qquad (2.16)$$

where $V_B(T)$ is the temperature-dependent breakdown voltage, $I_{dc}(t)$
is the low-frequency bias current, and R_{sc} is the space-charge
resistance.

The ionization rates of electrons and holes decrease with
increasing temperature.[3] Thus, for an IMPATT diode with a given
doping profile, the breakdown voltage will increase with increasing
temperature. The space-charge effect is the variation of electric
field in the depletion region due to the generated carrier space
charge. This effect gives rise to a positive space-charge resis-
tance for the IMPATT diode.

Since the electron and hole ionization rates are highly non-
linear functions of the electric field, the dc voltage is reduced by
an amount V_R which depends upon the amplitude of the RF oscillation
and bias-current level when microwave oscillations are present. The
magnitude of this rectification voltage generally increases with
increased RF voltage level and decreases with increased current
level.[6] Figure 2.2 shows the bias circuit approximation, where the
dc voltage is given by

$$V_{dc} = V_B(T) + I_{dc}(t)R_{sc} + V_R(V_{RF},T,I_{dc}) \quad . \quad (2.17)$$

Equation 2.17 is the bias circuit equation which describes the
relationship between dc voltage and bias current at a different RF
voltage level and junction temperature. The bias source applied to
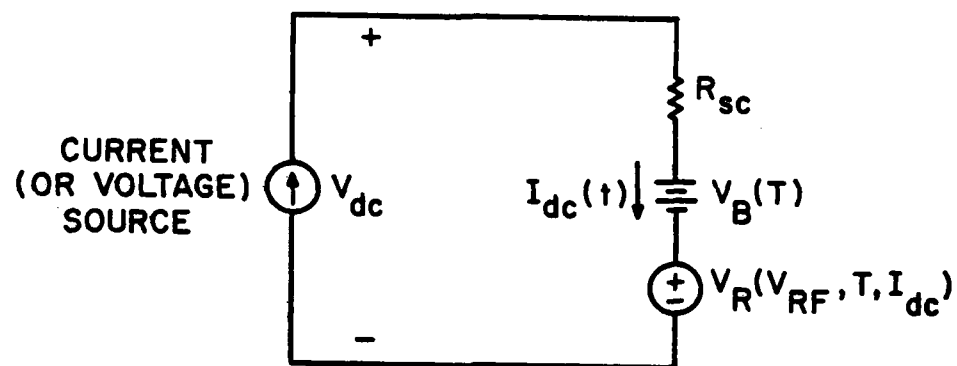
FIG. 2.2 LOW-FREQUENCY "BIAS CIRCUIT" EQUIVALENT CIRCUIT.

the device can be constant current or constant voltage with finite

impedance. In the case of a constant voltage source V_s with series

resistance R and inductor L as shown in Fig. 2.3, the dc voltage

across the device is

$$V_{dc} = V_s - RI_{dc} - L \frac{dI_{dc}(t)}{dt} . \qquad (2.18)$$

Other, more complicated, bias circuits can be used and will require

several state equations for their dynamic description.

2.2 Device and Circuit Parameters Required for the Analysis

To study the transient behavior of a pulsed oscillator, the

following device and circuit parameters must be obtained by theoret-

ical calculation or measurement:

1. Device admittance Y_d which depends on RF voltage V_{RF}, bias

current I_{dc}, optical current I_{op}, oscillation frequency f, and

junction temperature T.

2. Circuit admittance which is a function of frequency.

3. Thermal resistance R_{th} which depends on device size, device

material, geometry, material of heat sink, bias-current pulsewidth,

and duty cycle.

4. Thermal-time constant which is related to device width.

In this section a more detailed description of these device

and circuit properties and their effects on the oscillator behavior

are described.

2.2.1 Describing Function $Y_d(V_{RF}, I_{dc}, I_{op}, f, T)$. Describing

functions[3] can be used to describe the equivalent circuit of non-

linear devices including IMPATT diodes. Derivation of an appropriate

admittance describing function from large-signal behavior of the
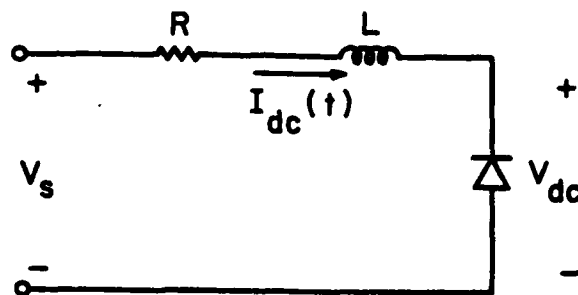
FIG. 2.3   CONSTANT VOLTAGE WITH FINITE IMPEDANCE AS BIAS SOURCE.

active device and its use in the study of pulsed oscillators will
be demonstrated. Initial analysis to illustrate the turn-on, post
turn-on and turn-off transients of a pulsed oscillator has made use
of a uniformly doped double-drift region (DDR) IMPATT diode as an
example. A DDR diode is chosen because the millimeter-wave output
power and efficiency are significantly higher for DDR diodes than for
those obtained with the single-drift region (SDR) diodes. The results
of the large-signal device admittance obtained are being combined
with the RF circuit admittance and bias circuit to study dynamic
effects in the pulsed oscillator under different conditions.

Device admittance data obtained from simulation or measurement
are discrete. For the purpose of analysis, Y_d is expressed as a
continuous function of V_{RF}, I_{dc}, I_{op}, f and T, since then the natural
frequency s can be determined by solving the free-running oscillation
condition given by

$$Y_d(V_{RF}, I_{dc}, I_{op}, s, T) = -Y_c(s) \quad . \qquad (2.19)$$

Analytical expressions for both Y_d and Y_c as functions of
frequency are desired. The device conductance G_d is an even function
of frequency, while device susceptance is an odd function.[7] These
even and odd properties are useful for constructing an approximate
expression for Y_d. For certain bias currents, optical currents, and
junction temperatures, Y_d is a function of RF voltage and frequency.
Therefore, G_d and B_d can be expressed as shown in Eqs. 2.20:

$$G_d = \sum_{k=0}^{R} \sum_{n=0}^{S} A_{kn} V_{RF}^k (f^2)^n \qquad (2.20a)$$

and

$$B_d = \sum_{k=0}^{R} \sum_{n=0}^{S} B_{kn} V_{RF}^k (f^{2n+1}) \quad . \qquad (2.20b)$$

Values of A_{kn} and B_{kn} can be found in the least mean-squared error sense.

If f is replaced by $s/j2\pi$, Y_d can be represented as a continuous function of V_{RF} and s, i.e.,

$$Y_d = G_d + jB_d$$

$$= \sum \sum A_{kn} V_{RF}^k (-1)^n \left(\frac{s}{2\pi}\right)^{2n} + \sum \sum B_{kn} V_{RF}^k (-1)^n \left(\frac{s}{2\pi}\right)^{2n+1} \quad .$$

$$(2.21)$$

Large-signal properties including optical effects of millimeter-wave IMPATT diodes have been studied extensively and are given by Burmawi.[8] Figure 2.4 shows the large-signal device admittance with 60 kA/cm^2 bias-current density and 300°K junction temperature. This figure is the plot of Eq. 2.21 after the discrete data are treated as described.

2.2.2 The Circuit Model. To study the dynamic behavior of a pulsed oscillator, it is essential to have a model for the microwave circuit. The most straightforward method of modeling is by means of a lumped equivalent network representing the RF circuit. Although an equivalent circuit of a practical oscillator may be more complex in general, it can often be reduced to a simple form over a limited frequency range of interest. The RF circuit can be represented by a lumped RLC series or parallel network as shown in Fig. 2.5. These
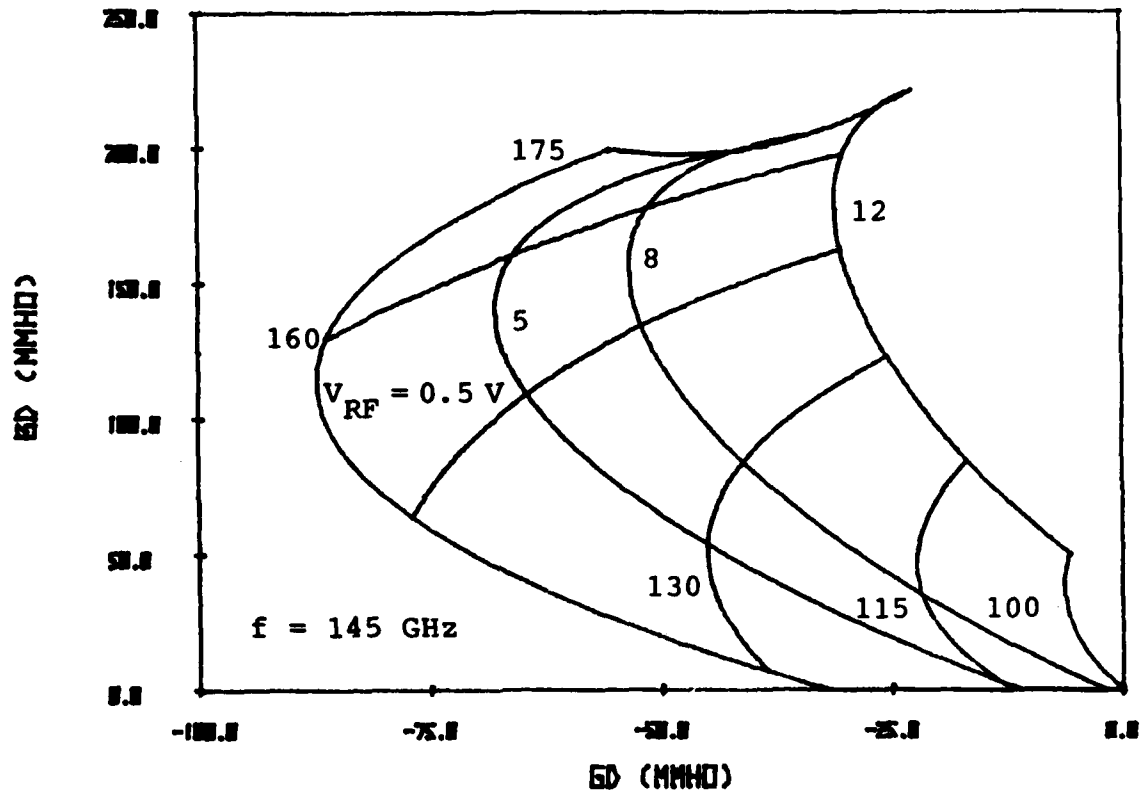
$J_{dc} = 60$ kA/cm^2, Device Diameter = 50 μm and T$_j$ = 300°K

FIG. 2.4   G-B LOCUS FOR DIFFERENT VALUES OF V$_{RF}$.
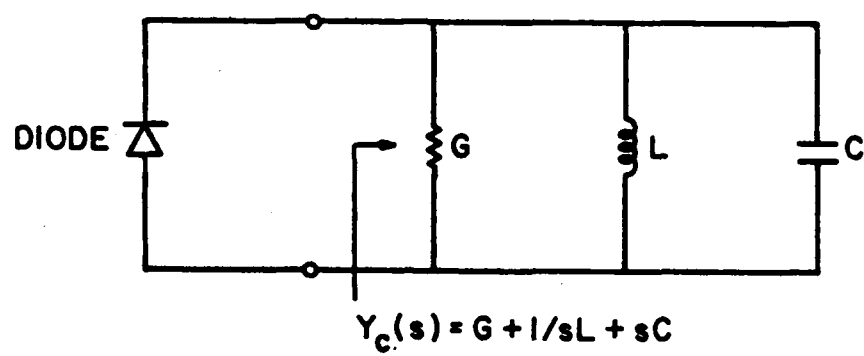
FIG. 2.5 A SIMPLIFIED RF EQUIVALENT CIRCUIT.

RLC elements are frequency independent, and the circuit admittance presented to the diode is a simple function of frequency.

A millimeter-wave diode can be mounted in a waveguide or microstrip circuit to generate RF power. In many cases the diode is mounted in a reduced-height waveguide with a tuning short. This waveguide oscillator circuit consists of an IMPATT diode mounted on a copper heat sink, a rectangular waveguide of reduced height, a movable short, a dc bias post, and a waveguide taper. The reduced-height portion of the waveguide provides a low impedance necessary for proper matching of the load to the diode. The waveguide taper is for impedance matching between reduced- and full-height waveguides.

A theoretical analysis of this post-in-waveguide circuit has been studied, and the calculated results can be applied to the circuit design in optimizing the oscillator performance. This more complex equivalent circuit is based on the analysis of Lewin[9] and modified by Chang and Ebert.[10] The results obtained for the RF circuit can then be combined with the device to predict the oscillator behavior.

2.2.3 Thermal Resistance. The maximum dissipated power is determined by the safe operating temperature of the junction (approximately 300°C for Si) and the total thermal resistance which is a measure of the efficiency of heat removal. Thermal resistance is related to diode area, diode geometry, and the thermal properties of the semiconductor, diode metallization, and the heat sink. When a Si diode is mounted on a heat sink and an ideal thermal contact between all the metallic layers is assumed, total thermal resistance R_{th} is given by

$$R_{th} = R_s + R_{HS} ,$$

where R_s is the thermal resistance caused by the Si and the thin layers of contact metallization, and R_{HS} is the thermal resistance caused by the heat sink.

For the pulsewidth larger than several thermal-time constants, R_s is approximately equal to its CW value, i.e.,

$$R_s = \frac{1}{A} \sum \frac{d_i}{k_i} \; ,$$

where A is the diode area, k_i is the thermal conductivity of the ith layer, and d_i is the material thickness of the ith layer.

For a pulsed oscillator, heat is supplied to the surface of the heat sink in periodic pulses. The thermal-resistance caused by the heat sink R_{HS} can be calculated for an avalanche diode under periodic pulses. The diode is under a periodic heating and cooling cycle caused by the bias pulses. In an actual diode, the heat generation is confined primarily to the active layer close to the diode junction. This generated heat flows through the semiconductor before reaching the heat sink. R_{HS} depends on the pulsewidth t_1 and duty cycle $(d = t_1/T)$, where T is the period of successive pulses, and is given by[11]

$$R_{HS} = \frac{d^{1/2}(\alpha t_1)^{1/2}}{(\pi R^2)k} \left[\frac{2}{(\pi d)^{1/2}} \left(1 - e^{-R^2/4\alpha t_1} \right) + I \right.$$

$$\left. + \frac{R}{d^{1/2}(\alpha t_1)^{1/2}} \, \mathrm{erfc} \left(\frac{R}{2(\alpha t_1)^{1/2}} \right) \right] \; ,$$

(2.22)

where R is the radius of the diode, and I is given by

$$I = \frac{2}{\pi d} \int_0^\infty \frac{e^{-dx^2}[e^{-(1-d)x^2} - e^{-x^2}]\left(1 - \cos \frac{Rx}{(\alpha T)^{1/2}}\right)}{x^2(1 - e^{-x^2})} dx \quad .$$

For a copper heat sink, the thermal conductivity k is 3.96 W/cm°C, and thermal diffusivity α is 1.14 cm²/s. Figure 2.6 shows R_{HS} as a function of a pulsewidth at a 40-kHz pulse repetition frequency. Within reasonable limits, a short pulsewidth is more effective (i.e., less thermal resistance R_{HS}) than a low duty cycle in preventing diode damage from overheating.

The thermal conductivity of diamond is greater than that of copper. Thus, the thermal resistance of the diode can be reduced with a diamond heat sink and higher power can be handled accordingly. Geometries which distribute the junction area over a much larger heat sink area[12] can also be used to reduce thermal resistance.

2.2.4 Thermal-Time Constant. Calculation of the thermal-time constant can be carried out for a simplified geometrical configuration[13] such as that shown in Fig. 2.7. It consists of a heat source located at the end of a slab of material with the constant cross section A, device width d, thermal conductivity k, specific heat c', and density ρ. The other end is connected to a heat sink of temperature T_a. Heat is stored in the thermal capacitance of the device chip, then passes through the thermal resistance of the semiconductor and the contact metallization to the infinite heat sink. The thermal-time constant due to the device-chip capacitance and thermal resistance of the simplified model is given by
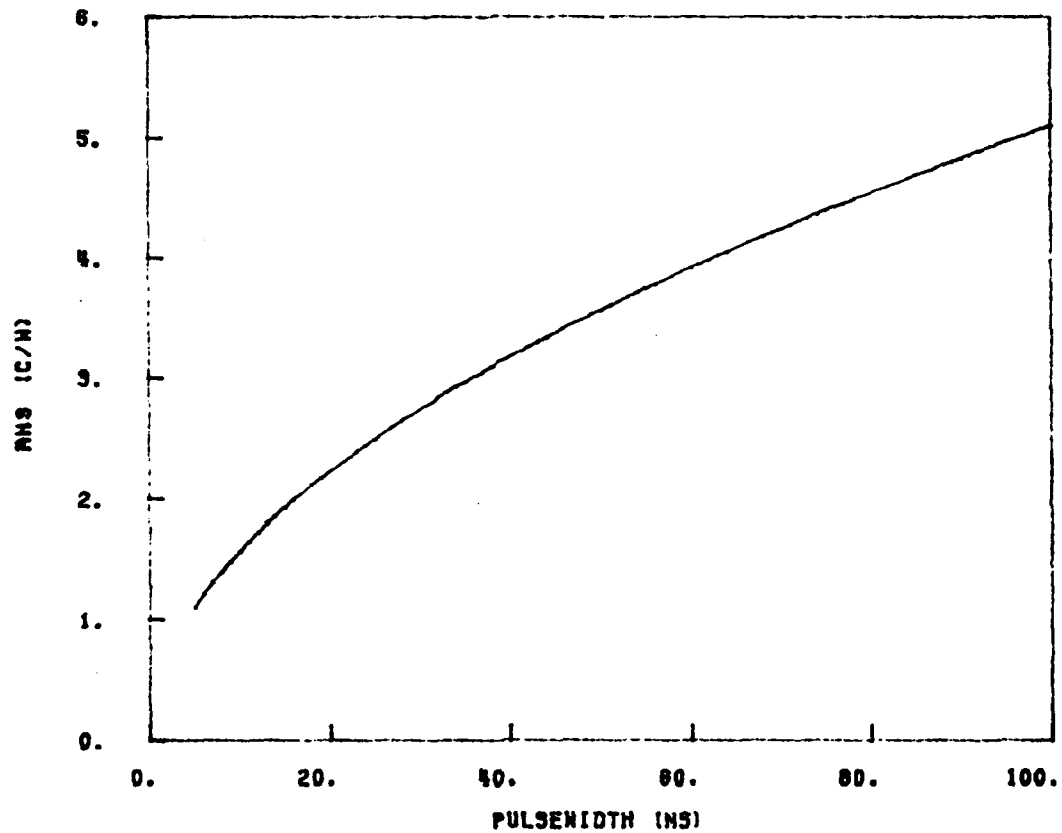
Pulse Repetition Frequency = 40 kHz, Device Diameter = 50 μm

FIG. 2.6 HEAT SINK THERMAL RESISTANCE AS A FUNCTION OF PULSEWIDTH.
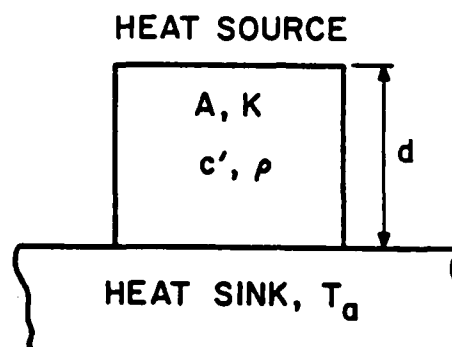
FIG. 2.7 SIMPLIFIED GEOMETRY TO CALCULATE THE THERMAL TIME
CONSTANT.

$$\tau_{th} = rc = \frac{d}{kA} \cdot c'dA\rho = c'\rho d^2/k \quad ,$$

where τ_{th} = the thermal-time constant of the diode (s),

r = the thermal resistance of the slab of material (°C/W),

and

c = the heat capacity of the slab of material (J/°C).

Silicon is often used in millimeter-wave IMPATT diodes, and its properties at 300°K are specific heat $c' = 0.7$ J/g°C, density $\rho = 2.328$ g/cm³, and thermal conductivity $k_{Si} = 1.45$ W/cm°C.

Figure 2.8 shows the thermal-time constant of a Si diode as a function of device width. It can be seen that τ_{th} decreases as the device width decreases. For the double-drift IMPATT diode with an active region width $d = 1$ μm, τ_{th} is 11.2 ns. Since the active region width of the diode decreases as the desired frequency increases, the thermal-time constant is reduced for higher frequency devices. Hence, the temperature rise of pulsed millimeter-wave diodes is faster than that of lower frequency devices.

2.3 Usefulness and Limitations of the Oscillator Model

The oscillator model described in Sections 2.1 and 2.2 is capable of predicting many important effects in CW and pulsed IMPATT oscillators including the following: (1) turn-on transients (oscillation buildup and frequency response) and their dependence on the device (bias current), circuit (bias circuit, RF circuit), and external influences (injection locking, photon injection, ambient temperature), (2) post turn-on transients (frequency chirp, temperature response, and power variation), (3) turn-off transients (device
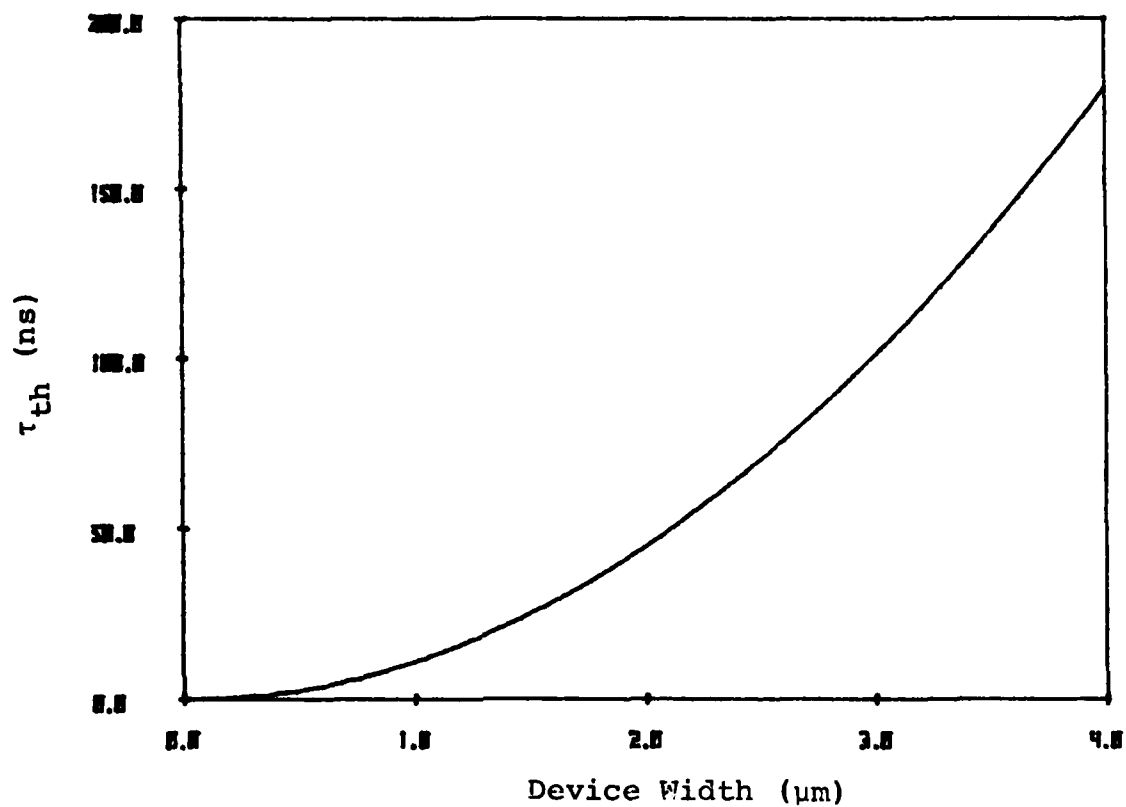
FIG. 2.8   THERMAL-TIME CONSTANT AS A FUNCTION OF DEVICE WIDTH.

cool-off and decay of the output power), (4) control of the post

turn-on transients, and (5) behavior of varactor/photon tuned

oscillators.

The performance of this oscillator model is limited in several

respects. Knowledge of these limitations is necessary for the proper

use of this model. Temperature and photon injection dependence of

the microwave circuit are neglected. In the real oscillator circuit,

the microwave circuit may be dependent on temperature and photon

injection especially when a microstrip is used. The same temperature

is assumed throughout the semiconductor layer while the more realis-

tic thermal distribution is dependent on the location. A single

thermal-time constant is used in the model. The thermal-time constant

may be dependent on the operating temperature, and several time con-

stants may be involved. The value of τ_{th} for the same semiconductor

is approximately 10 ns in the example and that of the heat sink is much

larger (on the order of μs). Variation of the device and circuit

properties due to aging is not considered.

2.4 An Example of a Pulsed Oscillator which Identifies the Various Effects

2.4.1 Introduction. To study the turn-on, post turn-on, and

turn-off transients of pulsed oscillators quantitatively, a quasi-

static device model is used in which it is assumed that the micro-

wave admittance of the diode is an instantaneous function of RF

voltage, dc current, photon injection level, and junction temperature.

This model, which was developed for oscillator analysis, can be used

to determine the dynamic and steady-state behavior of the device

when interacting with a microwave circuit of known admittance.

A constant bias-current pulse is often used in pulsed IMPATT oscillators, such that the oscillator is turned on when adequate current is passing through the device, and the microwave circuit is properly matched. Output power builds up as a result of the device-circuit interaction. A significant portion of the dc power is dissipated which results in the temperature rise and a change of the device properties. Thus, oscillation frequency and output power vary. When the bias pulse is turned off, the RF oscillation cannot sustain, output power decreases, and the junction temperature returns to the ambient temperature.

In this section many important effects of a free-running pulsed IMPATT oscillator are demonstrated through an example. In this example, a flat bias-current (60 kA/cm^2) pulse with a 40-ns pulsewidth and a 40-kHz pulse repetition frequency (period = 25 µs) is applied to a double-drift millimeter-wave diode with a 50-µm diameter. Other important device parameters are the thermal resistance, $R_{th} = 6.7$°C/W, and the thermal-time constant, $\tau_{th} = 11.24$ ns. A simple RLC parallel network represents the passive circuit seen from the device terminals. In this example, the following parameters are used: $G = 24.9$ mmho, $L = 9.39 \times 10^{-13}$ H, and $C = 1.4522$ pF.

2.4.2 _Turn-On Transients of the Pulsed Oscillator_. The device-circuit interaction which results in the buildup of RF oscillation is obtained by using a time-domain computer simulation.

A sudden change in the dc bias current shifts the device admittance from $Y_d(V_{RF}, I_d)$ to $Y_d(V_{RF}, I_d + \Delta I_d)$. Because of the stored-energy requirements of the microwave circuit, the RF voltage cannot change instantaneously. Therefore, immediately after the

change in bias current, the circuit constraint $Y_d(s) + Y_c(s) = 0$
can only be satisfied by the growth of the RF voltage to a new value.
Such growth takes time, and the delay time between the bias pulse and
the output power is related to the amount of current change ΔI_d and
the quality factor Q of the microwave circuit. For the constant
current pulse, the oscillator turn-on is usually characterized by a
rapid decrease in dc voltage across the diode.

The natural frequency s which determines the nature of the
transient response can be solved by numerical methods. The growth
ratio σ is the rate of RF voltage growth given by

$$\frac{1}{V_{RF}} \frac{dV_{RF}}{dt} = \sigma \ .$$

If σ is negative, then any oscillatory response will be damped
out, and the degree of damping depends on the magnitude of σ. An
oscillator will be free running if initially σ is positive. Any dis-
turbance will cause RF voltage to build up. As long as σ remains
positive, the exponential buildup of the free-running oscillator will
continue, and the output will eventually stabilize at some amplitude.
Since the diode conductance G_d and susceptance B_d are generally depen-
dent on the amplitude of the ac voltage, the dc voltage across the
device, and junction temperature, the oscillation frequency and growth
rate of the oscillator are time dependent. This is a result of
device-circuit interaction. There are large transients in the output
frequency during turn-on. This is due to the increase in device
susceptance B_d as the RF voltage swing increases so that the oscilla-
tion frequency decreases continuously during the buildup until the

growth of the oscillation is complete. After steady state is reached, the frequency settling time and the delay time between the bias pulse and full RF power can be determined.

An initial value of RF voltage (V_{RF} = 0.1 V) is used in the calculation. A high growth rate (8.1×10^9) at the start of oscillation and its decrease as the oscillation builds up are illustrated in Fig. 2.9. It can be seen that the growth rate approaches zero when the buildup is complete. Figure 2.10 shows that the RF voltage increases from 0.1 to 12 V within 0.8 ns. Since the initial RF voltage is small, the buildup of the RF voltage is not significant until 0.5 ns, although the growth rate is high at t = 0. Buildup is faster with a higher initial RF voltage.

Figure 2.11 demonstrates the response of device conductance during turn-on. The magnitude of the device conductance $|G_d|$ decreases as RF voltage increases. This fall of $|G_d|$ is a natural phenomenon common to all negative-resistance diode oscillators and is a result of device nonlinearity. When the negative conductance falls to the same value as the circuit conductance ($G_d + G = 0$), where G is the circuit conductance, stable operation is obtained.

RF power ($P_{RF} = - 0.5\ G_d V_{RF}^2$) is determined by the values of device conductance and RF voltage. Figure 2.12 shows the buildup of output power during turn-on. The delay time between the bias pulse and RF power which depends on the initial RF voltage is approximately 0.6 ns. Since the ionization rates of electrons and holes are highly nonlinear functions of the electric field, dc bias voltage across the diode V_{dc} will decrease as the RF voltage builds up as shown in Fig. 2.13. Variation of V_{dc} is negligible when the RF voltage swing is
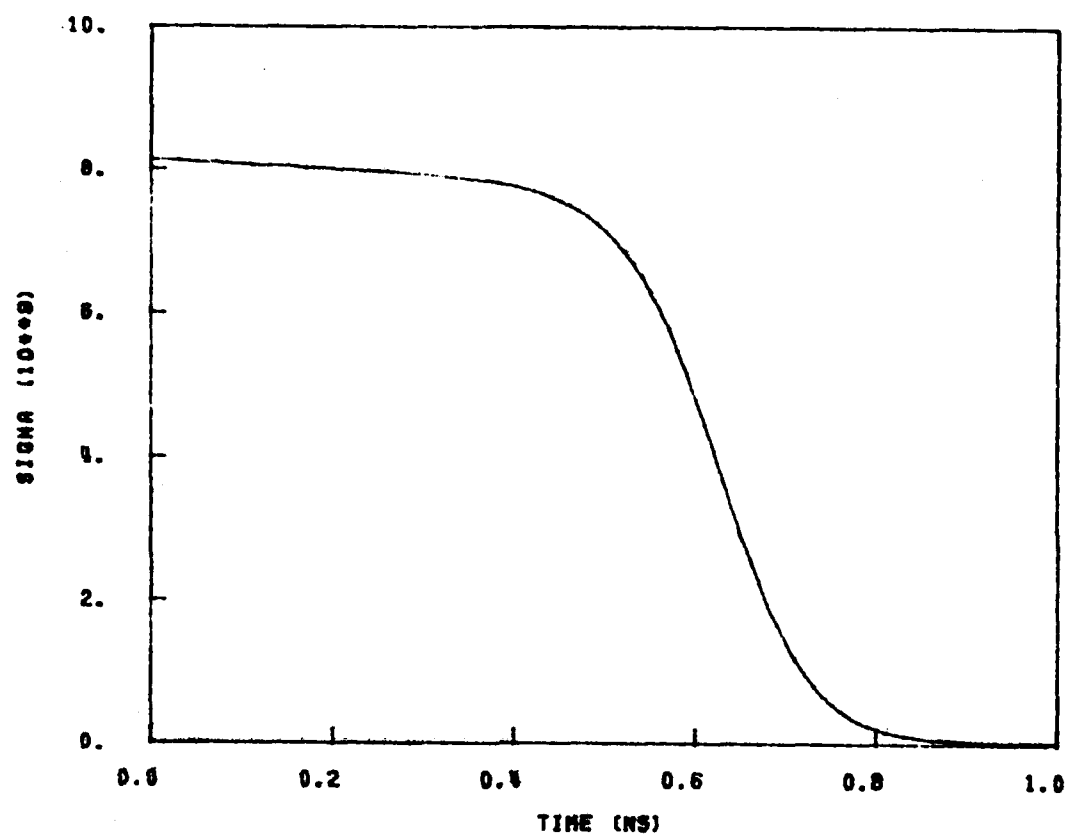
FIG. 2.9   BEHAVIOR OF GROWTH RATE DURING TURN-ON.
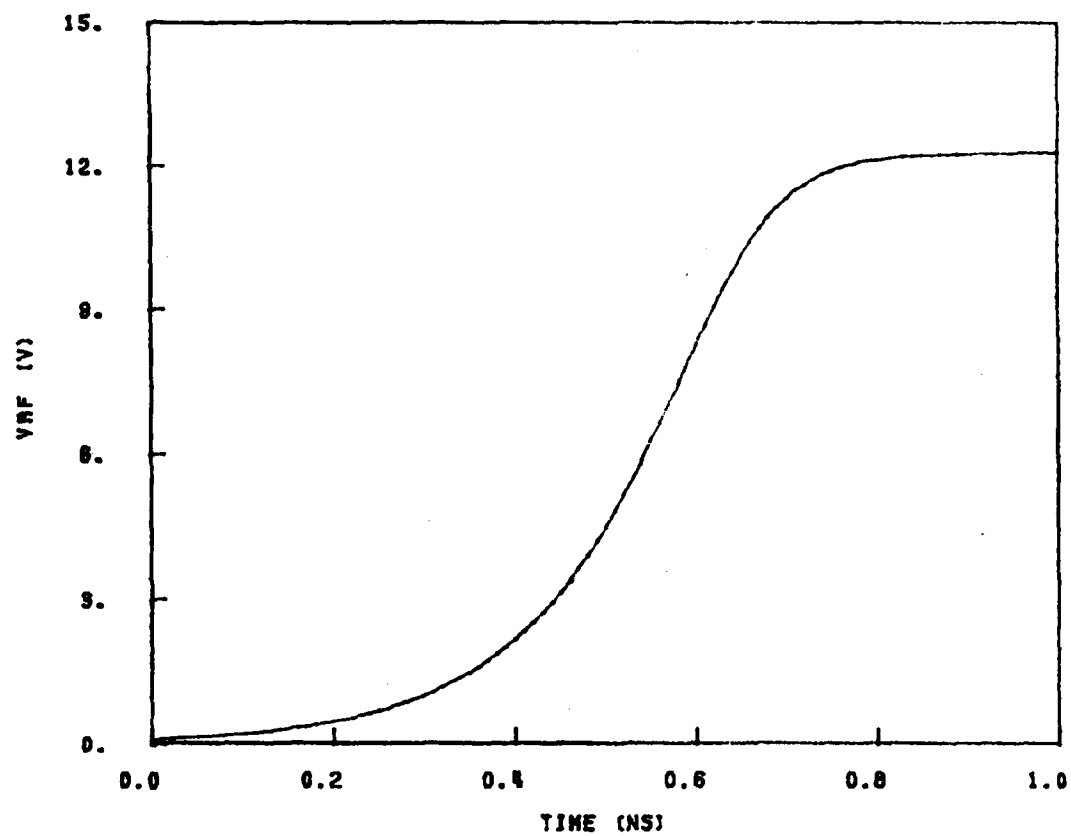
FIG. 2.10 BUILDUP OF RF VOLTAGE DURING TURN-ON.
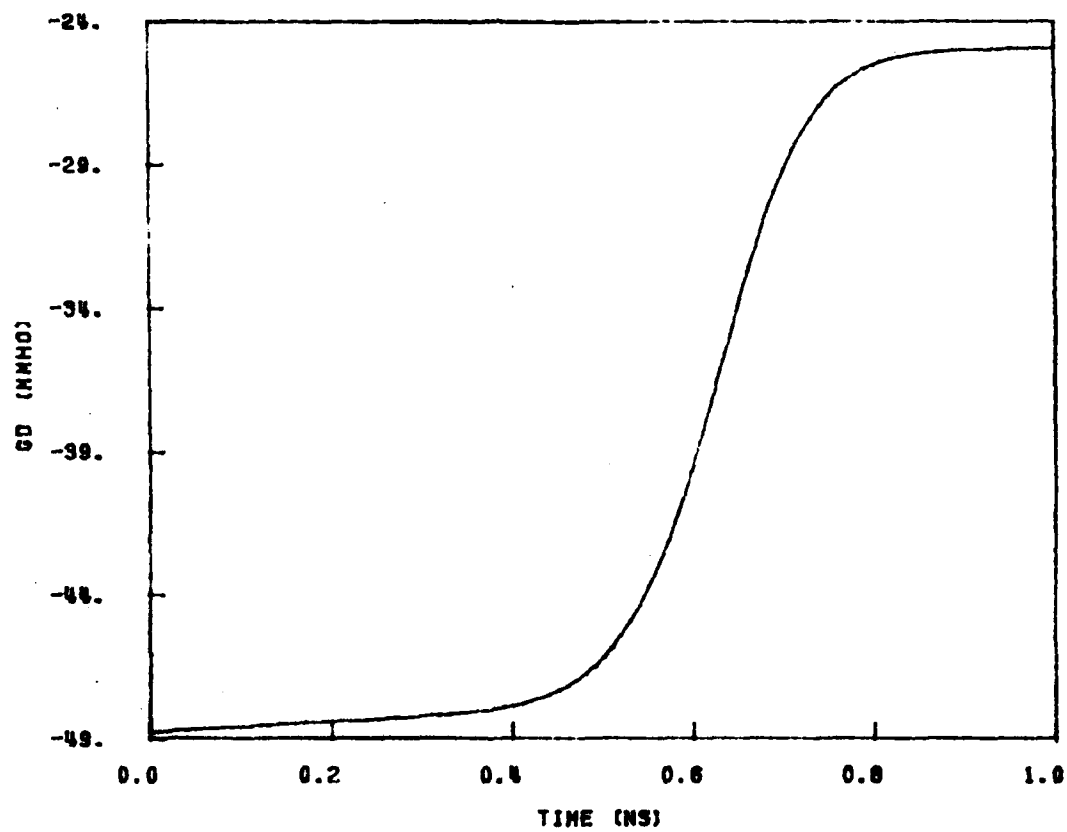
FIG. 2.11 RESPONSE OF DEVICE CONDUCTANCE DURING TURN-ON.
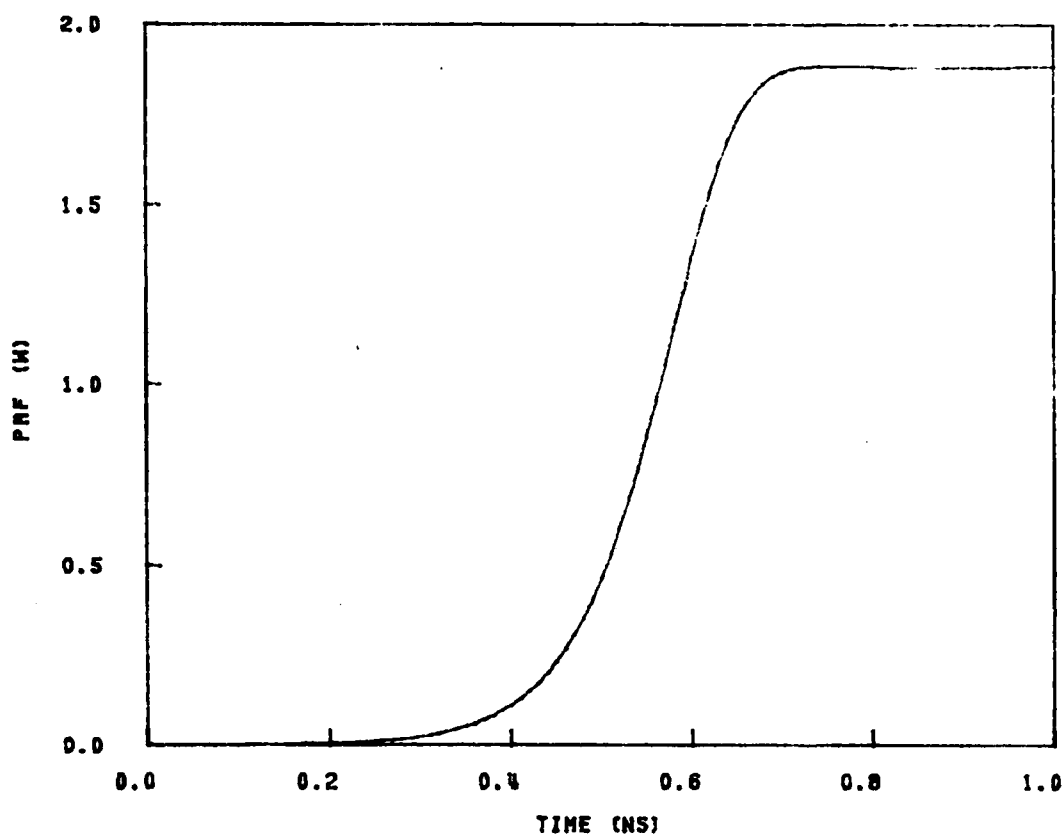
FIG 2.12 BUILDUP OF RF OUTPUT POWER DURING TURN-ON.
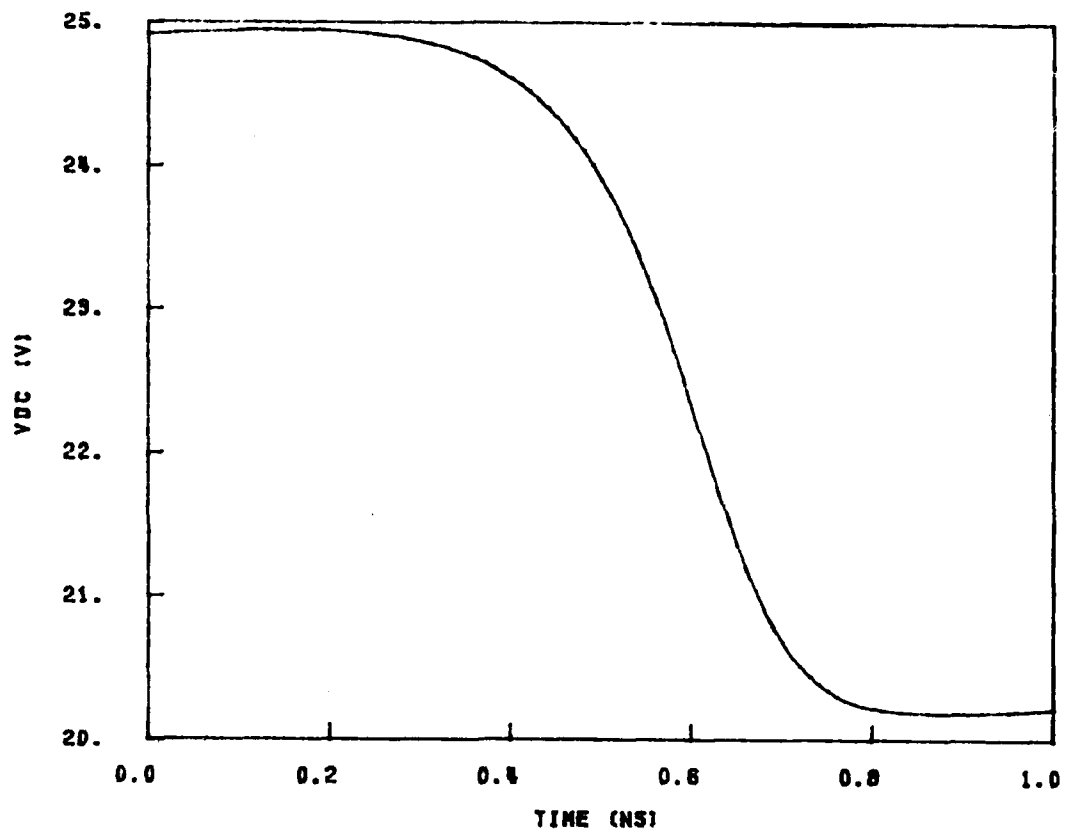
FIG. 2.13 VARIATION OF DC VOLTAGE DURING TURN-ON.

small (< 1 V). V_{dc} decreases from 24.9 to 20.2 V as the RF voltage increases from 0.1 to 12 V and remains relatively constant after the oscillator is turned on. A large decrease of dc voltage can be seen when the RF voltage is building up.

The device susceptance B_d increases with increasing RF voltage, i.e., B_d changes from 24 to 126 mmho during turn-on as shown in Fig. 2.14. This increase of device susceptance causes the oscillation frequency to vary from 135 to 129 GHz when oscillation builds up as shown in Fig. 2.15. Although the device temperature changes from 300 to 315°K during turn-on, it is reasonable to conclude in this example that the turn-on transients are mainly the result of device-circuit interaction. The effect of temperature rise on the oscillator performance begins after the oscillator is turned on. Figure 2.16 and 2.17 show the turn-on transients in the s-plane and the device admittance plane, respectively.

2.4.3 Temperature Response During the Pulse. The device junction temperature, which is determined by ambient temperature, thermal resistance from the junction to the heat sink, and the dissipated power, is an important parameter affecting the performance of IMPATT oscillators. For a given diode under pulsed operation, the temperature behavior during the pulse depends on bias current, pulsewidth, pulse repetition frequency, RF circuit, and ambient temperature.

For low duty cycle operation, the "off" period is much longer than the "on" period and allows the device to cool off to ambient temperature. Therefore, the diode junction is nearly at ambient temperature at the beginning of each heating cycle and gradually heats up because of the dissipated power P_d which varies with the dc power and
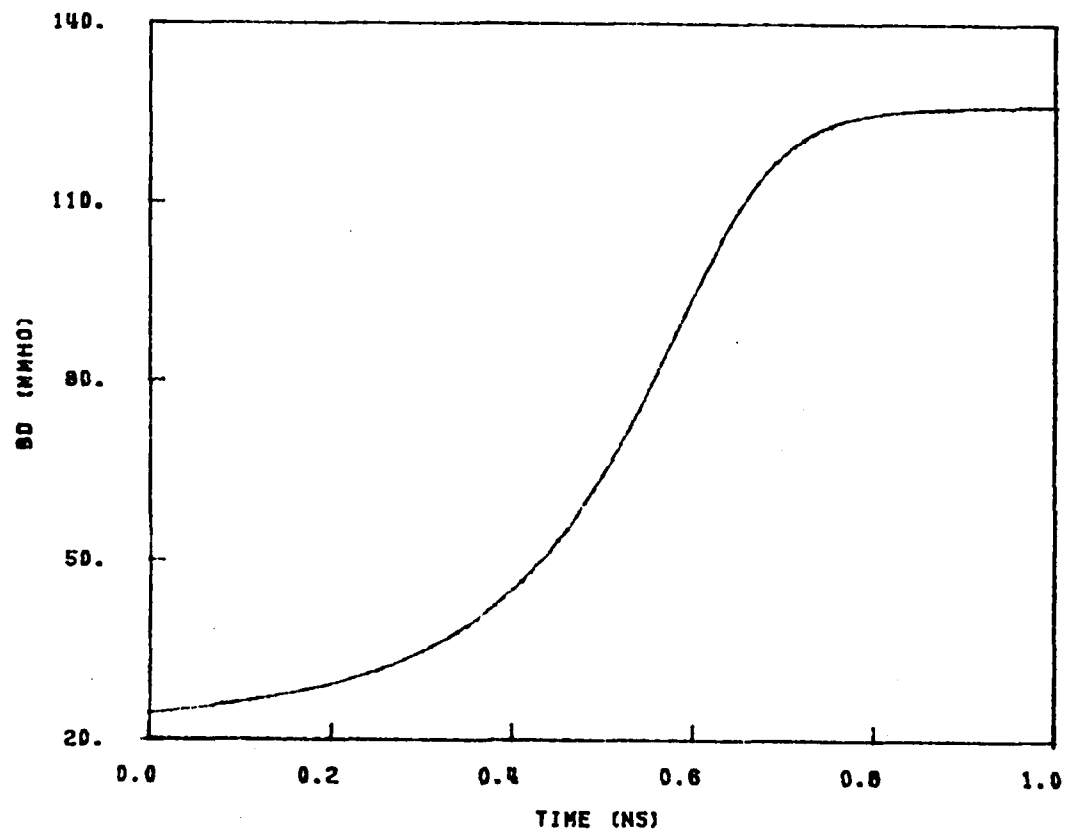
FIG. 2.14 INCREASE OF DEVICE SUSCEPTANCE DURING TURN-ON.
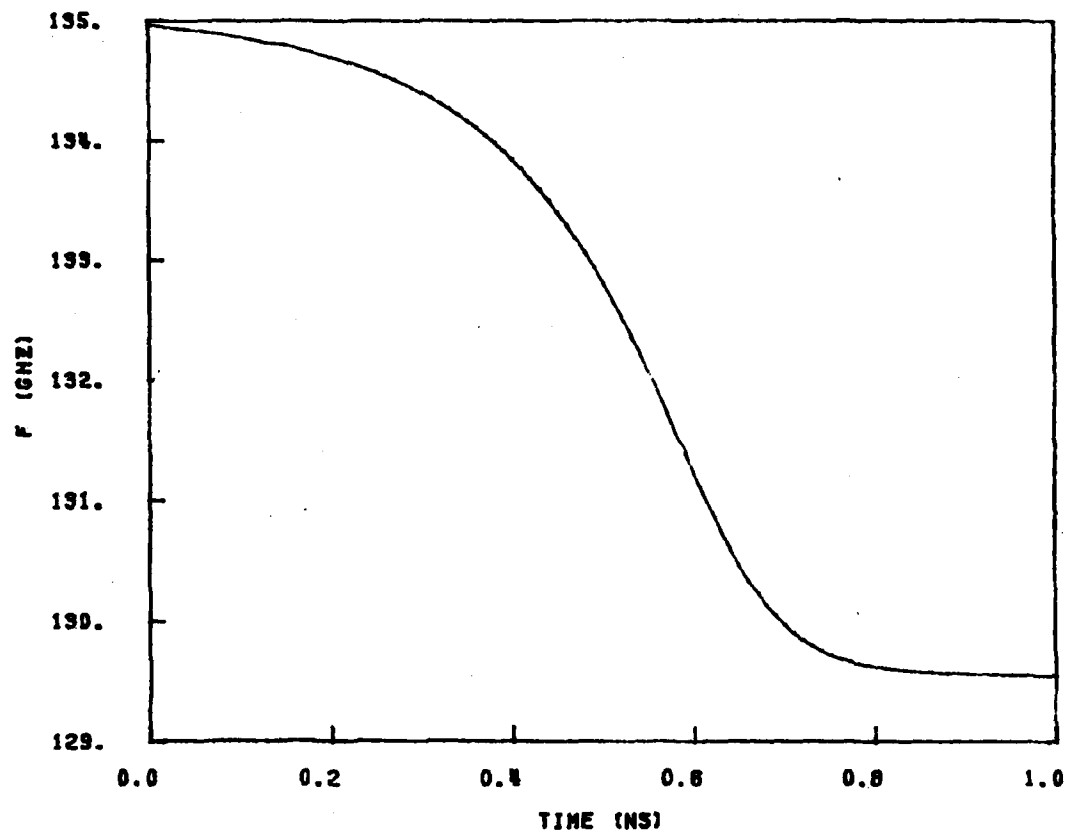
FIG. 2.15   DECREASE OF OSCILLATION FREQUENCY DURING TURN-ON.
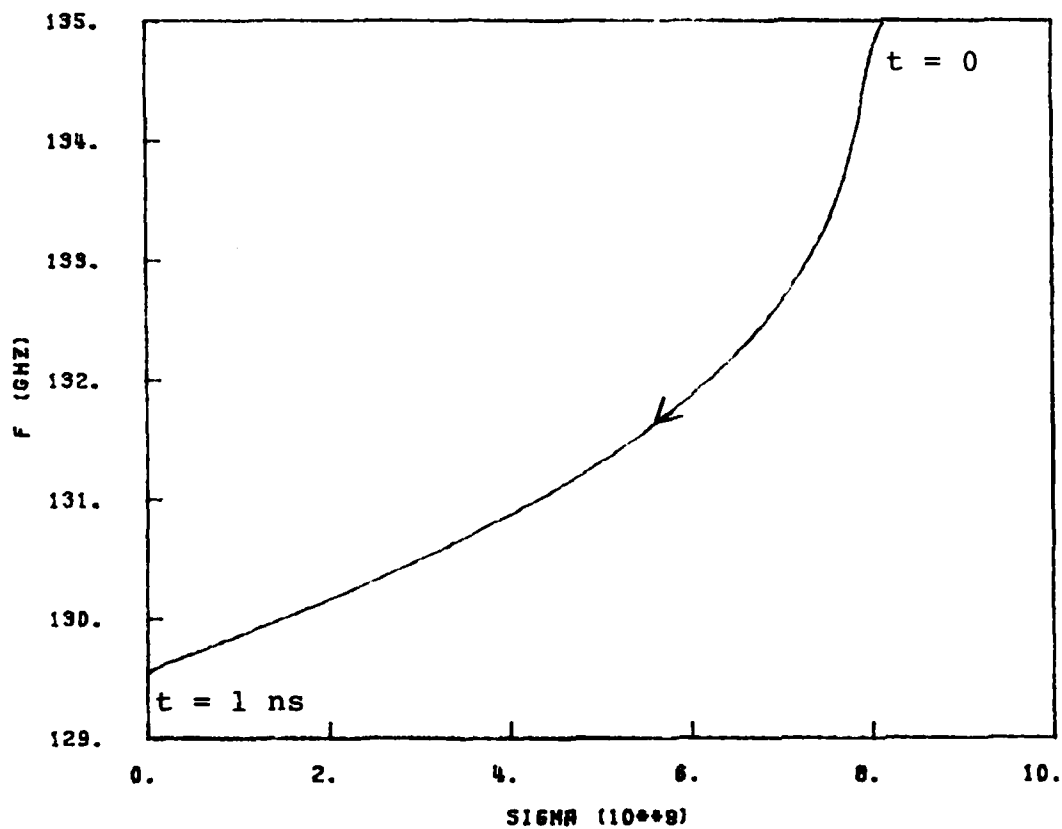
FIG. 2.16   TURN-ON TRANSIENT ON THE s PLANE.   ARROWHEAD REPRESENTS
THE INCREASE OF TIME.
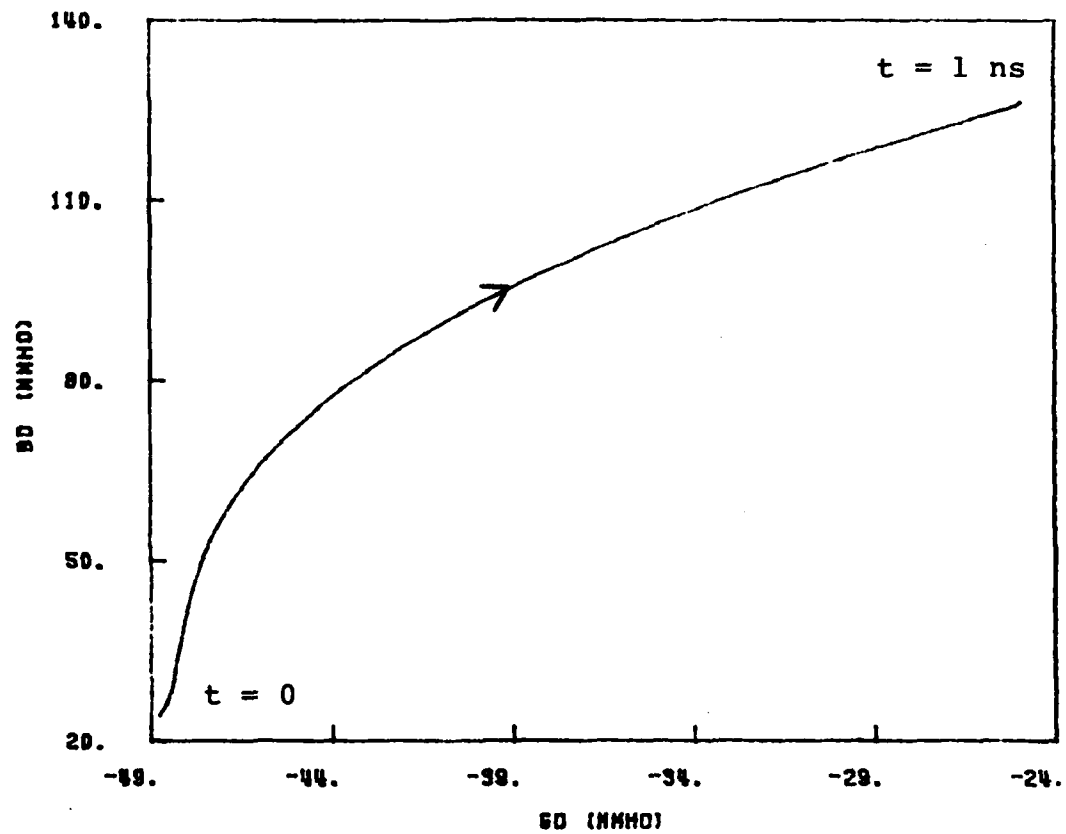
FIG. 2.17 TURN-ON TRANSIENT ON DEVICE ADMITTANCE PLANE. ARROWHEAD

REPRESENTS THE INCREASE OF TIME.

RF oscillation power P_{RF} as

$$P_d = P_{dc} - P_{RF} = V_{dc}I_{dc} - 0.5 \, |G_d|V_{RF}^2 \quad ,$$

where V_{dc} = the dc voltage across the device,

$\quad I_{dc}$ = the dc bias current passing through the device,

$\quad G_d$ = the device admittance, and

$\quad V_{RF}$ = the RF voltage across the device.

The maximum temperature rise of the diode ΔT is related to the dissipated power at the junction P_d and the thermal resistance of the device R_{th} by

$$\Delta T = P_d R_{th} \quad .$$

Given the input bias power, the thermal resistance determines the maximum temperature rise. The actual temperature rise during the pulse is approximately equal to the maximum temperature rise ΔT when pulsewidth is longer than several thermal-time constants τ_{th}.

Semiconductor devices including IMPATT diodes are temperature sensitive. Oscillator performance during the pulse is primarily determined by the temperature dependence of the device properties providing that the temperature dependence of the microwave circuit is negligible. The effect of temperature on the small-signal device admittance has been studied by Schroeder and Haddad.[14] With increasing diode temperature the small-signal negative conductance was found to increase, and the region of negative conductance was shifted toward lower frequencies. This may be caused by several temperature-dependent physical parameters including saturated velocity, dielectric constant, and ionization rates. Intrapulse performance of the

oscillator can be obtained from the temperature dependence of large-signal device properties. For the diode used as an example, the following conclusions which are useful for the intrapulse analysis can be drawn:

1. The absolute value of the device conductance decreases with increasing RF voltage and increases with increasing temperature.

2. The device susceptance has a tendency to increase with RF voltage and operating temperature.

3. Breakdown voltage increases with operating temperature.

On the basis of the same oscillator example, the junction temperature increases from 300 to 470°K during the 40-ns pulsewidth as shown in Fig. 2.18. As the junction temperature rises, the ionization rates and scattering-limited velocities of electrons and holes decrease. Both effects tend to increase breakdown voltage and dc voltage across the device. Figure 2.19 illustrates the increase of dc voltage from 20.2 to 25.1 V during the pulse. The positive temperature-coefficient property of the breakdown voltage can be used to prevent the thermal runaway when the diode is biased under constant-voltage operation.

2.4.4 Frequency Drift During the Pulse. The variation of oscillation frequency due to the change of temperature ΔT can be estimated[15] from the oscillation conditions. The oscillation conditions can be expressed as

$$G_d(V_{RF}, I_{dc}, f, T) + G_c(f, T) = 0$$

and

$$B_d(V_{RF}, I_{dc}, f, T) + B_c(f, T) = 0 \quad ,$$
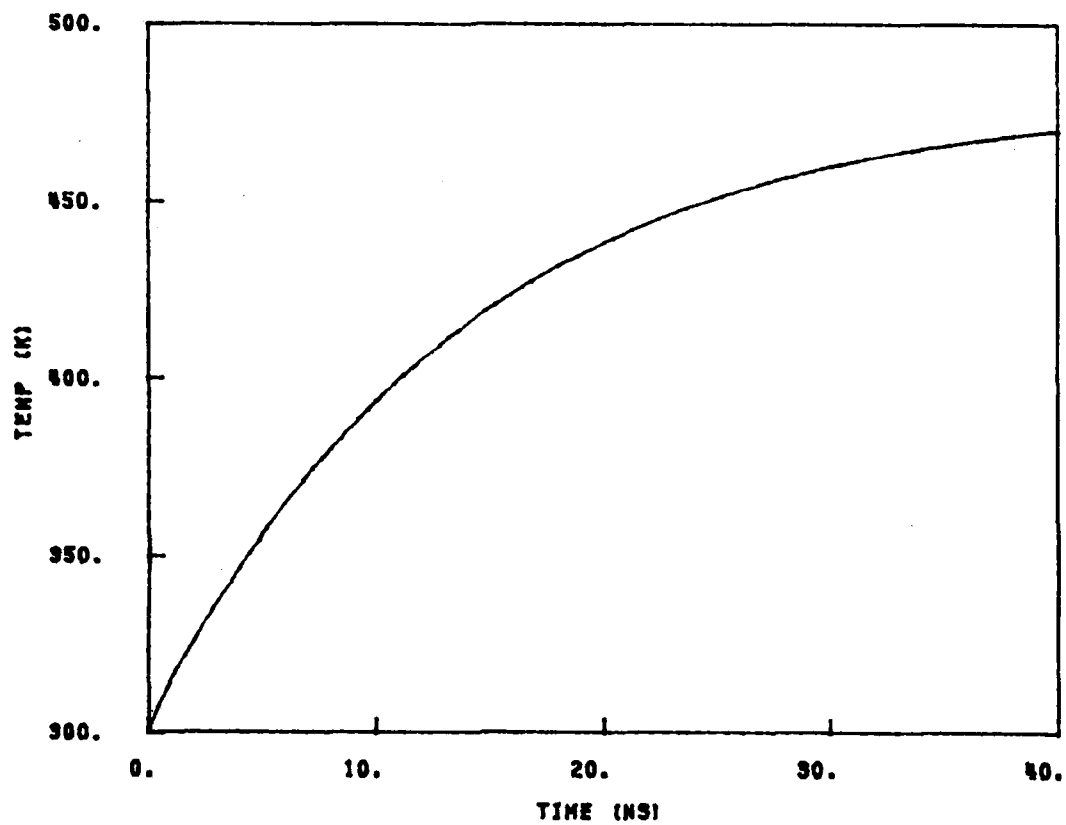
FIG. 2.18 JUNCTION TEMPERATURE RESPONSE DURING THE PULSE.
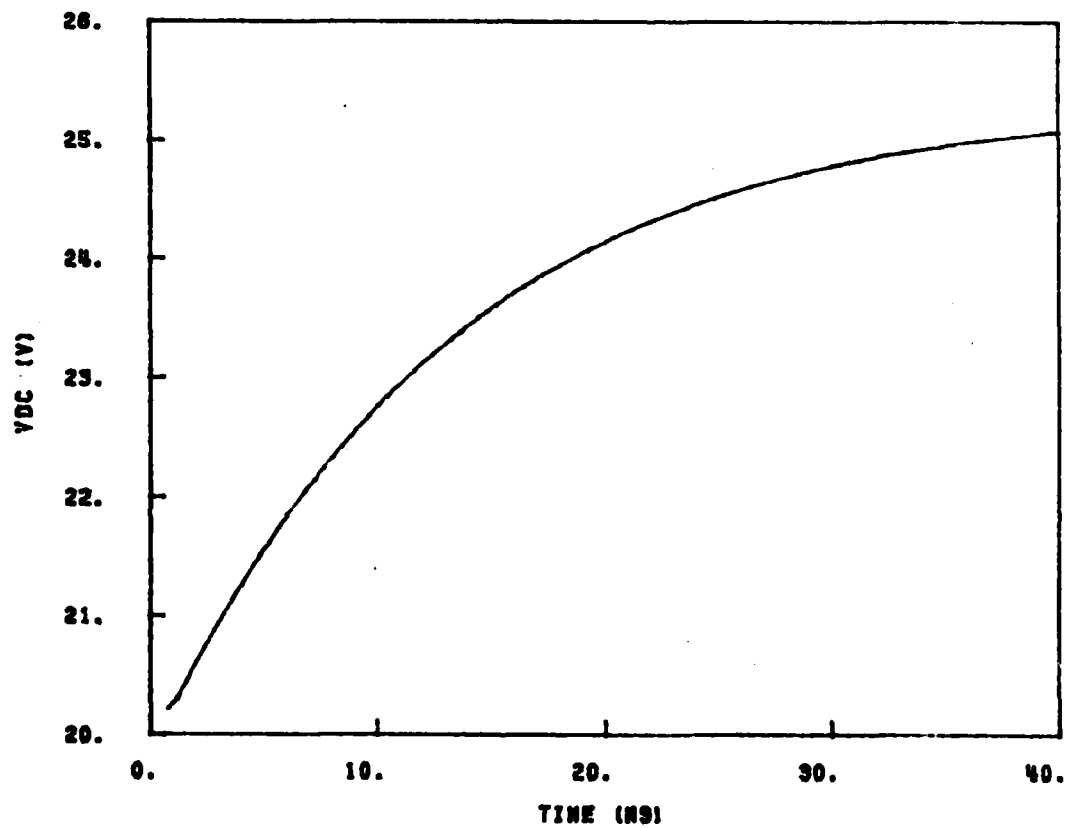
FIG. 2.19   DC VOLTAGE RESPONSE OF POST TURN-ON.

where G_d = the device conductance,

G_c = the circuit conductance,

B_d = the device susceptance, and

B_c = the circuit susceptance.

To obtain analytic results, the following additional assumptions are made: (1) G_c is a constant independent of temperature and frequency, and (2) frequency dependence of G_d is negligible.

The change of G_d due to ΔT must be compensated by that due to the change in RF voltage V_{RF} and dc current I_{dc} to maintain the oscillation conditions, i.e.,

$$\frac{\partial G_d}{\partial V_{RF}} \Delta V_{RF} + \frac{\partial G_d}{\partial I_{dc}} \Delta I_{dc} + \frac{\partial G_d}{\partial T} \Delta T = 0$$

and

$$\frac{\partial B_d}{\partial V_{RF}} \Delta V_{RF} + \left(\frac{\partial B_d}{\partial T} + \frac{\partial B_c}{\partial T}\right)\Delta T + \left(\frac{\partial B_d}{\partial f} + \frac{\partial B_c}{\partial f}\right)\Delta f + \frac{\partial B_d}{\partial I_{dc}} \Delta I_{dc} = 0 .$$

Combining these equations gives

$$\left(\frac{\partial(B_d + B_c)}{\partial f}\right)\Delta f = A_1\Delta T + A_2\Delta I_{dc} , \qquad (2.23)$$

where

$$A_1 = \frac{\partial B_d}{\partial V_{RF}} \frac{1}{\partial G_d/\partial V_{RF}} \frac{\partial G_d}{\partial T} - \frac{\partial(B_d + B_c)}{\partial T}$$

and

$$A_2 = \frac{\partial B_d}{\partial V_{RF}} \frac{1}{\partial G_d/\partial V_{RF}} \frac{\partial G_d}{\partial I_{dc}} - \frac{\partial B_d}{\partial I_{dc}} .$$

Frequency drift due to ΔT is related to the circuit admittance and large-signal device properties of IMPATT diodes. For constant

current operation ($\Delta I_{dc} = 0$), the oscillation frequency decreases with positive temperature change when A_1 is negative. The sign of A_1 is determined by the values of $\partial B_d/\partial V_{RF}$, $\partial G_d/\partial V_{RF}$, $\partial G_d/\partial T$ and $\partial(B_d + B_c)/\partial T$. The temperature dependence of circuit admittance is assumed to be negligible, i.e., $\partial B_c/\partial T = 0$ and $\partial G_c/\partial T = 0$. The large-signal properties including temperature dependence of an IMPATT diode have been studied, and the results are summarized as follows:

1. Device susceptance B_d increases with RF voltage ($\partial B_d/\partial V_{RF} > 0$).

2. Device conductance G_d increases with RF voltage, and this is one of the criteria to achieve stable oscillation ($\partial G_d/\partial V_{RF} > 0$).

3. G_d decreases (more negative G_d) with temperature ($\partial G_d/\partial T < 0$).

4. B_d increases with temperature ($\partial B_d/\partial T > 0$).

5. B_d increases with frequency ($\partial B_d/\partial f > 0$).

6. Circuit susceptance B_c has to increase with frequency to obtain stable oscillation ($\partial B_c/\partial f > 0$).

The sign of A_1 determined from 1 to 4 is negative. Thus, the frequency drifts downward as junction temperature increases. This conclusion is in good agreement with the investigation of Fong and Kuno.[16] Equation 2.23 can be modified when the loaded oscillator quality factor Q_L is introduced. Q_L is defined by

$$Q_L = \frac{f_o}{2G_c} \left.\frac{\partial(B_d + B_c)}{\partial f}\right|_{f=f_o} ,$$

where f_o is the oscillation frequency of the oscillator. Equation 2.23 becomes

$$\Delta f = \frac{f_o}{2G_c Q_L} (A_1 \Delta T + A_2 \Delta I_{dc}) \quad .$$

For a given diode, a higher loaded circuit quality factor $Q_{L,C}$ means higher Q_L. Accordingly, as expected frequency drift Δf decreases with higher $Q_{L,C}$, where

$$Q_{L,C} = \frac{f_o}{2G_c} \left. \frac{\partial(B_c)}{\partial f} \right|_{f=f_o} \quad .$$

During the post turn-on period, device susceptance B_d increases from 126 to 152 mmho, and oscillation frequency decreases from 129.5 to 128.5 GHz as shown in Fig. 2.20. This frequency drift (1.3 GHz) is smaller than the drift during the turn-on period (5.5 GHz), since the increase of B_d caused by temperature rise (26 mmho) is smaller than that caused by the oscillation buildup (102 mmho).

2.4.5 RF Voltage and Power Variations During the Pulse. For the diode used in the example, the drift region is not quite punched through at 300°K and, consequently, a thin layer of high resistivity Si (typically 1 Ω-cm) appears as a parasitic loss element. This undepleted layer degrades the oscillator efficiency. A nonpunched-through diode has been shown[17] to be more temperature sensitive than a punched-through diode. The reduced ionization rates of electrons and holes with increasing temperature have important effects on the electric field profile. Since a higher electric field is required to maintain the same bias current, the space-charge region widens, the parasitic series resistance is appreciably reduced, and efficiency increases at a higher junction temperature.
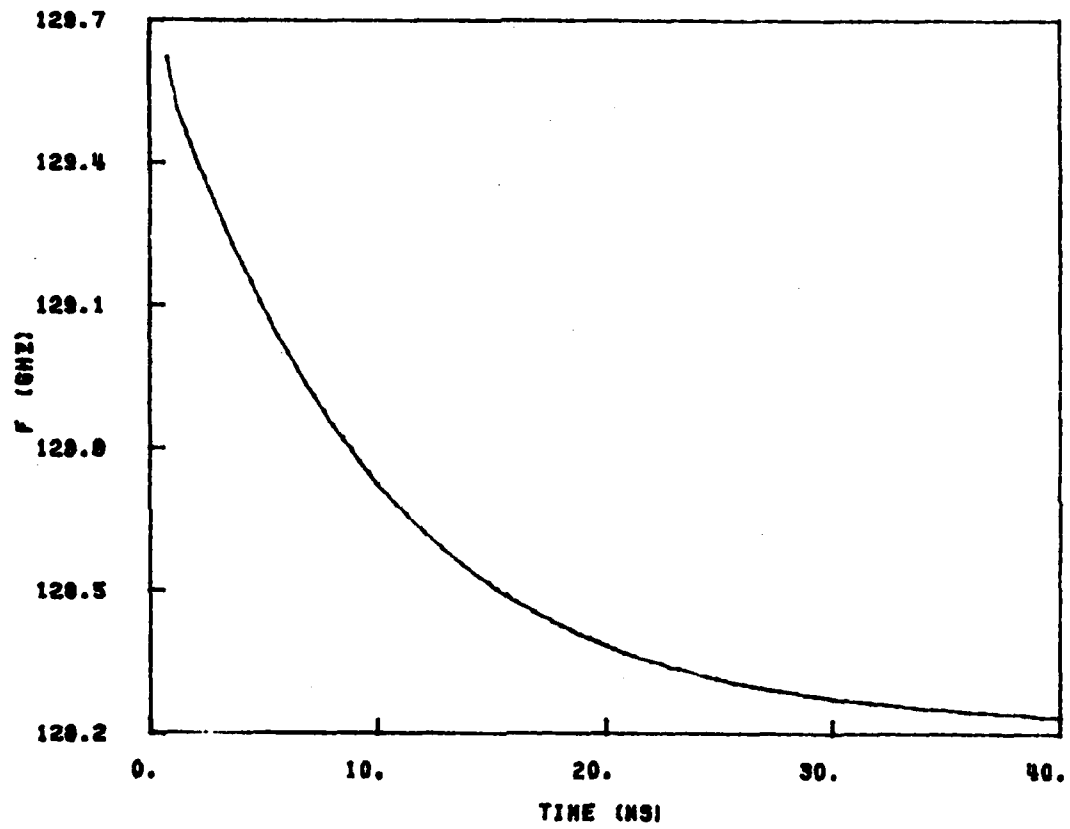
FIG. 2.20   FREQUENCY DRIFT DURING POST TURN-ON.

For a constant current pulse, the RF voltage and output power continue to increase with increasing junction temperature. The output power increases for two reasons. First, as the breakdown voltage increases with temperature, the power input at a constant current source bias increases, and if the efficiency remains constant, the output power must also increase. Second, it has been shown that the efficiency actually increases with temperature, so the output power would increase even if the breakdown voltage remains constant.

Figures 2.21 and 2.22 show the RF voltage and the output power variations of post turn-on transients. The RF voltage increases from 12 to 15.6 V, and the output power increases from 1.8 to 3 W.

2.4.6 Turn-Off Transient of the Pulsed Oscillator. When the bias current pulse is turned off at $t = 40$ ns, the bias current density decreases from 60 kA/cm^2 to 0, and the device admittance changes. The circuit constraint $Y_d(s) + Y_c(s) = 0$ can only be satisfied with $\sigma < 0$. Therefore, the RF oscillation cannot be sustained, and the RF voltage will decrease. Decrease of RF voltage is proportional to the product of RF voltage and the magnitude of the decay rate. RF voltage decreases drastically from 15.6 to 0.1 V within 0.2 ns as shown in Fig. 2.23. The turn-off time (0.2 ns) is smaller than the turn-on time (0.8 ns) as expected since both the RF voltage (15.6 V) and the decay rate ($\sigma = -1.5 \times 10^{10}$) at $t = 40$ ns are large. Since the "off" period (≈ 25 μs) is much larger than the "on" period (40 ns), the junction temperature will cool off from 470 to 300°K during the long "off" period.
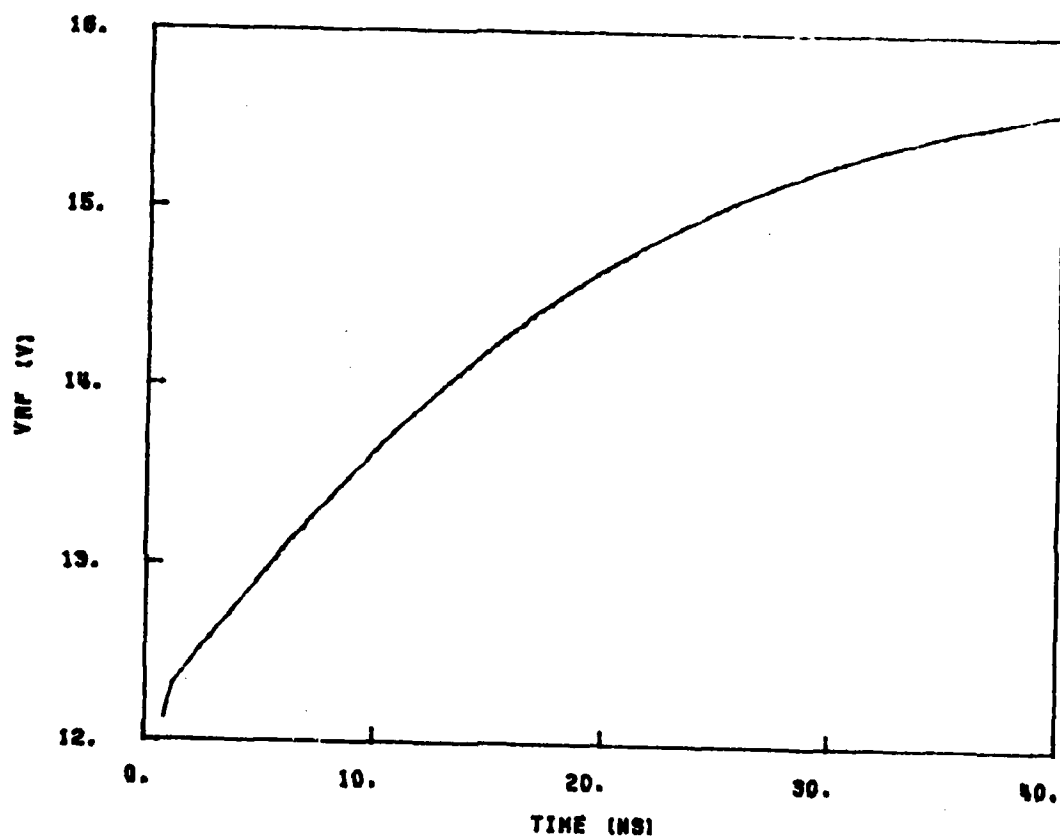
FIG. 2.21 RF VOLTAGE VARIATION DURING POST TURN-ON.
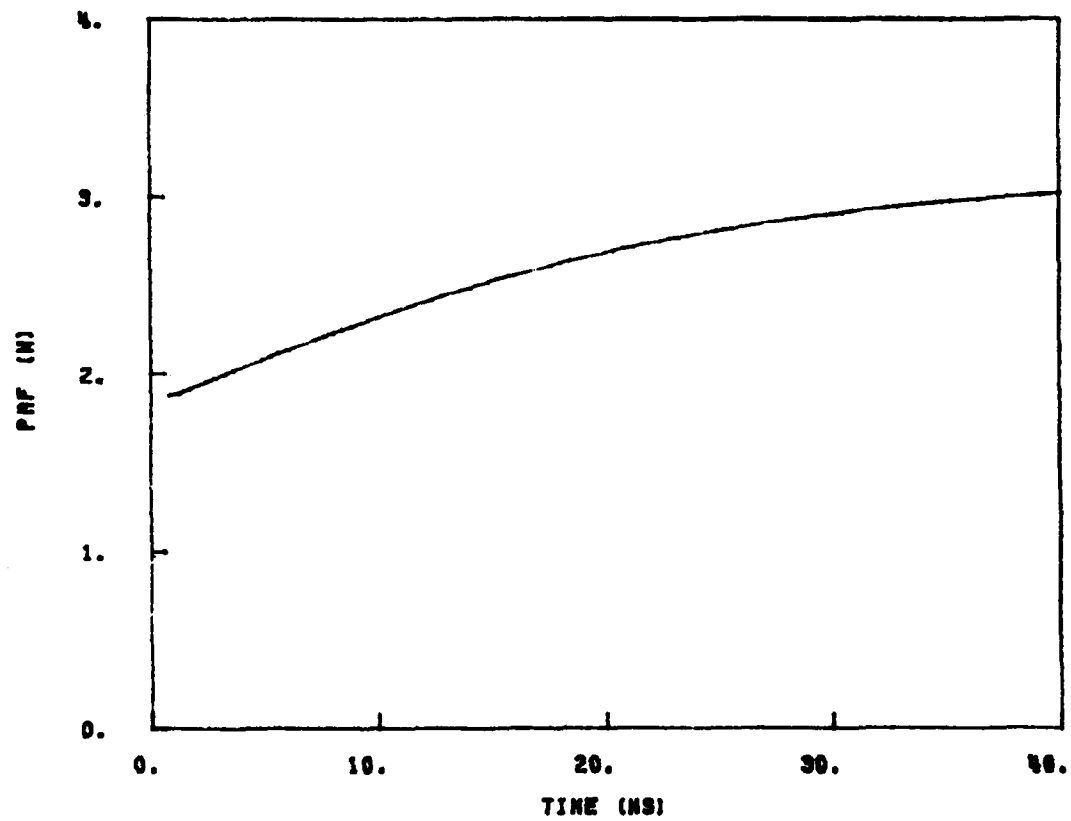
FIG. 2.22 OUTPUT POWER VARIATION DURING POST TURN-ON.
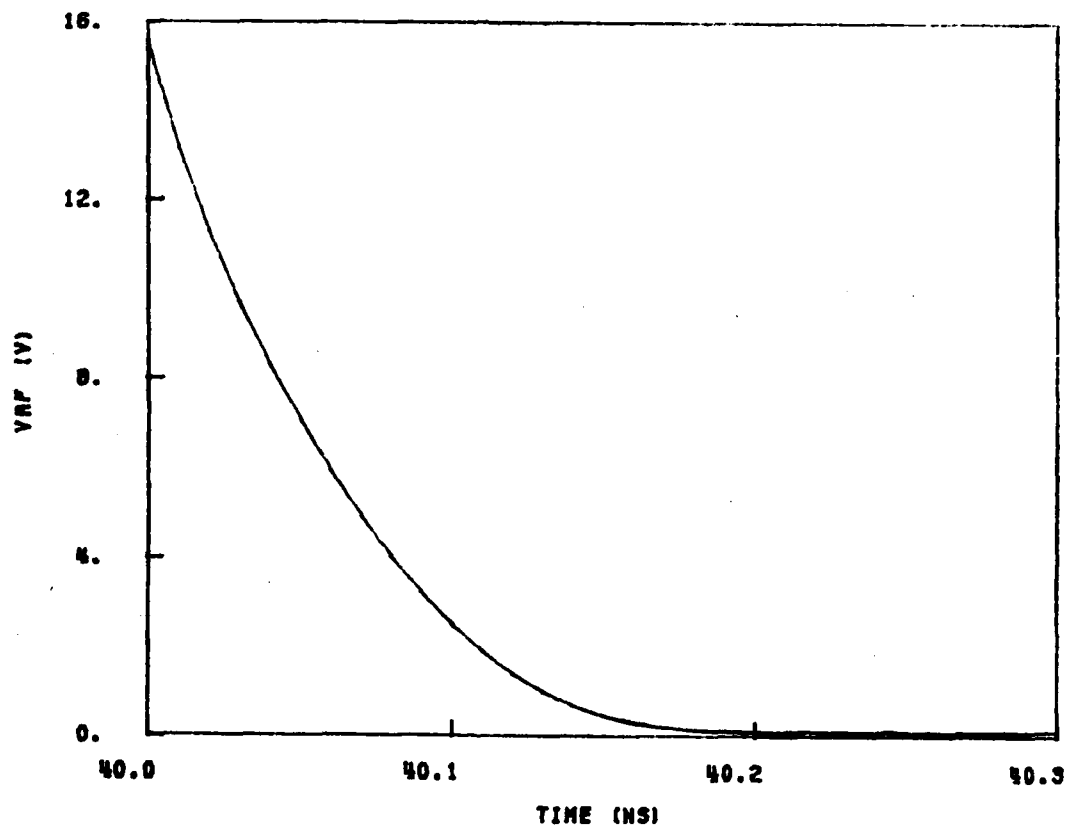
FIG. 2.23 DECREASE OF RF VOLTAGE DURING TURN-OFF.

2.5 Separation of Short- and Long-Term Effects

Short-term (turn-on) and long-term (post turn-on) effects are well separated when the delay time between the applied bias pulse and output power is smaller than the thermal-time constant of the diode as illustrated in Section 2.4. The short-term effect is mainly the result of device-circuit interaction, and the long-term effect is caused by the device temperature rise.

However, in some cases the distinction between short- and long-term effects is not so well defined. Two of them will be described briefly:

1. If the circuit Q is large, as in the cavity stabilized oscillator, a longer time is needed to store the required energy, and the device temperature rises at the same time. When the turn-on time is larger than the pulsewidth, short- and long-term effects cannot be separated.

2. If the magnitude of the device conductance G_d is too small $(G_d + G_c > 0)$ at ambient temperature, the oscillator is not turned on immediately after the bias pulse is applied. Then, the input dc power converts into heat, and the device temperature keeps increasing. After the device temperature increases to a certain value, $|G_d|$ is large enough, and the entire circuit will not be stable. This delay-start phenomenon is a consequence of the temperature increase. Therefore, the short-term effect is not always caused by the sudden increase of bias current, and the long-term effect may not be the consequence of temperature rise.

2.6 Effects of Pulsewidth and Duty Cycle on the Oscillator

Performance

It is the purpose of this section to study the effects of pulsewidth and duty cycle on the pulsed oscillator performance. Limitations on duty cycle, pulsewidth and output power arise from the maximum safe operating temperature of the device. With increased power dissipation, the temperature reaches its limiting value in a shorter time, thereby requiring reduced pulsewidth. Tradeoffs between pulse width, duty cycle and thermal resistance for a thermally limited diode are given in this section.

The thermal resistance caused by the heat sink R_{HS} depends on the pulsewidth, duty cycle and material of the heat sink. Figure 2.24 shows the pulse repetition frequency as a function of pulsewidth with R_{HS} as a parameter. These curves are calculated from Eq. 2.22. These contours indicate, as expected, that for a constant R_{HS}, the pulse repetition frequency PRF must decrease for increasing pulsewidths. For a given pulsewidth, R_{HS} increases with increasing PRF.

For a diamond IIA heat sink, the thermal conductivity k is 20 W/cm°C and thermal diffusivity is 1.0 cm^2/s. Copper has a thermal conductivity of 3.96 W/cm°C and a thermal diffusivity of 1.14 cm^2/s. It can be seen from Eq. 2.22 that R_{HS} for copper is several times larger than that of diamond IIA for a given pulsewidth and duty cycle, since diamond has higher thermal conductivity and the thermal diffusivity is about the same. A diode with diamond heat sink can sustain higher bias current and thereby generate more RF power.
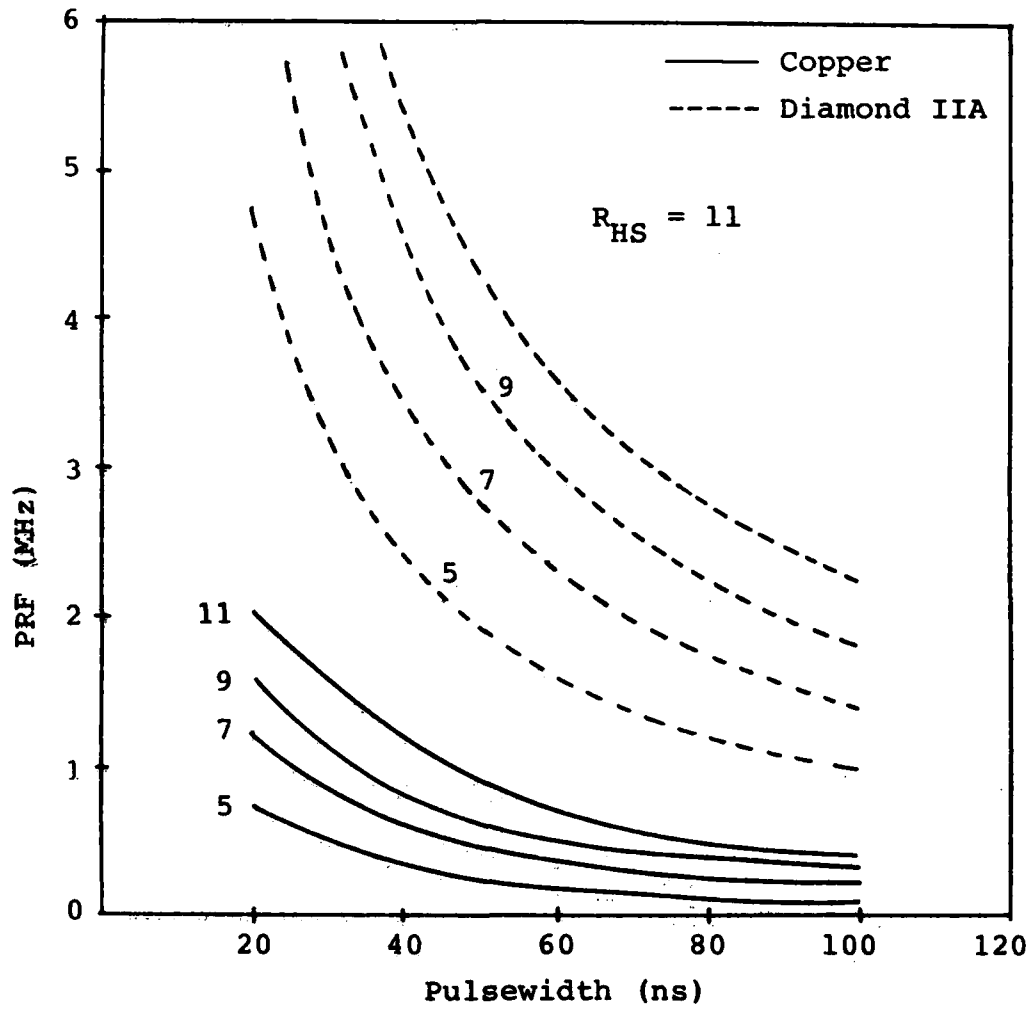
FIG. 2.24   PULSE REPETITION FREQUENCY AS A FUNCTION OF PULSEWIDTH
WITH CONSTANT R_{HS}.

Figure 2.24 shows that a higher PRF can be used with diamond as heat sink.

A family of design curves showing the trades between pulse-width, duty cycle and RF output power are generated in the manner indicated in Fig. 2.25. For a given constant R_{HS}, the total thermal resistance $R_{th} = R_S + R_{HS}$ is constant, and the time required for temperature T to reach T_{max} (500°K) for different current pulse amplitudes is calculated. This time then represents the pulsewidth, with the duty cycle or PRF obtained from Fig. 2.24 for the given value of RHS. The higher the bias current, the shorter the pulse-width needed, but the higher the RF power generated. Typical output power responses for $R_{HS} = 11$ and various bias current densities are shown in Fig. 2.26. Since the power varies substantially over the pulse, the total RF energy, or average power defined as

$$P_{av} = \frac{1}{t_1} \int_0^{t_1} P_{RF}(t) \, dt$$

is used for purposes of comparison.

The average power as a function of pulsewidth for various values of R_{HS} is shown in Fig. 2.27. Again, the PRF associated with a given point is obtained from Fig. 2.24. Values of PRF for inter-mediate R_{HS} can be easily obtained by interpolation.

The curves generated are representative of the fixed-tuned circuit situation, i.e., the circuit impedance is held constant for all calculations. This is the situation occurring for a given oscillator operating under a variety of duty cycles, pulsewidths, and dc input power.
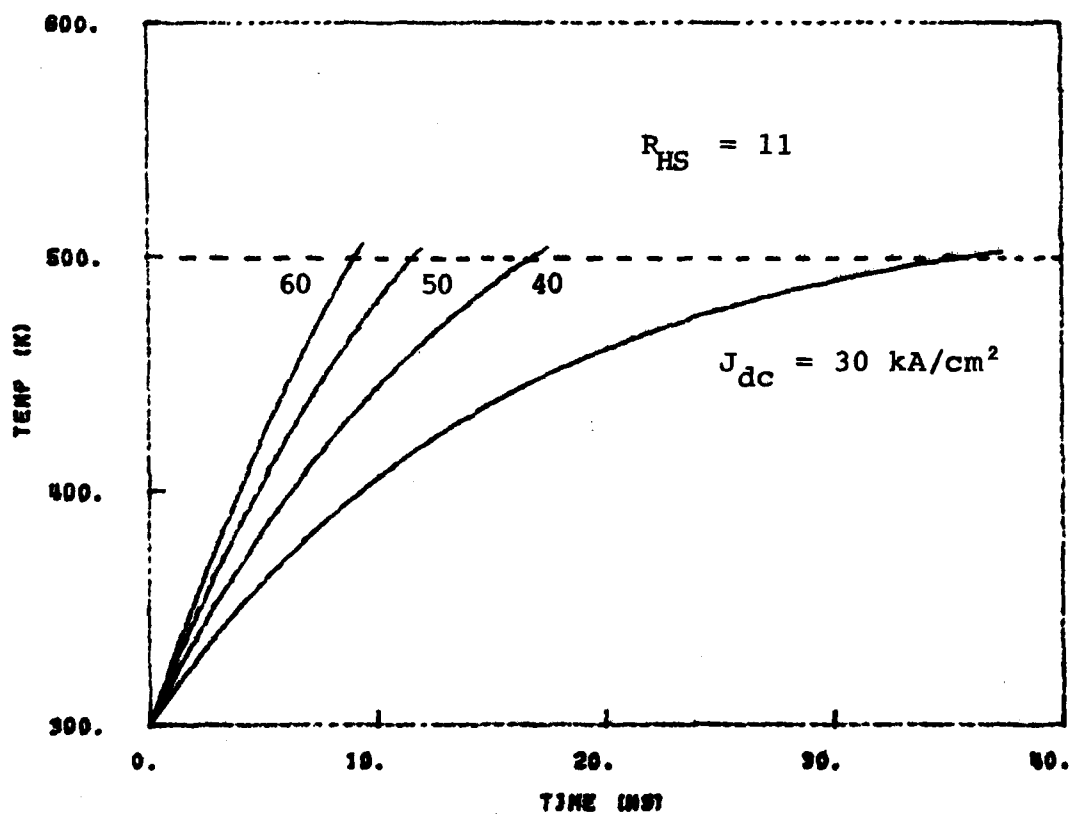
FIG. 2.25   TEMPERATURE RESPONSES OF THE PULSED OSCILLATOR WITH

VARIOUS BIAS CURRENT LEVELS.
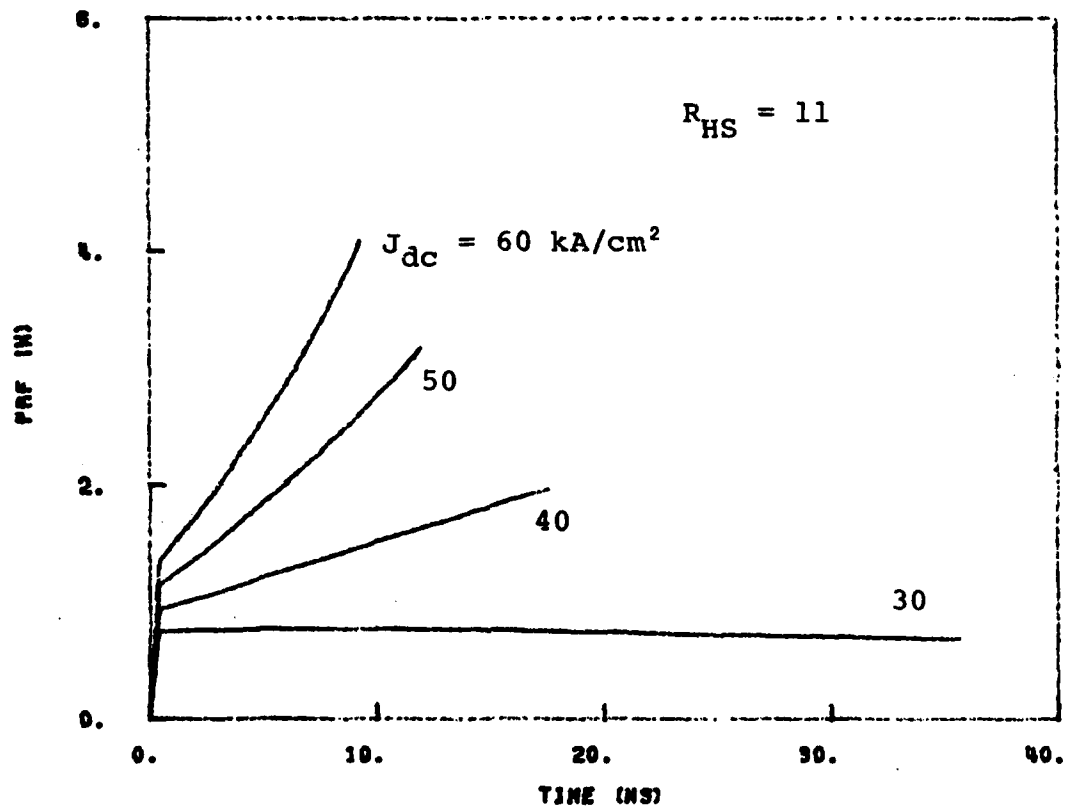
FIG. 2.26 OUTPUT POWER RESPONSES FOR VARIOUS BIAS CURRENT LEVELS.
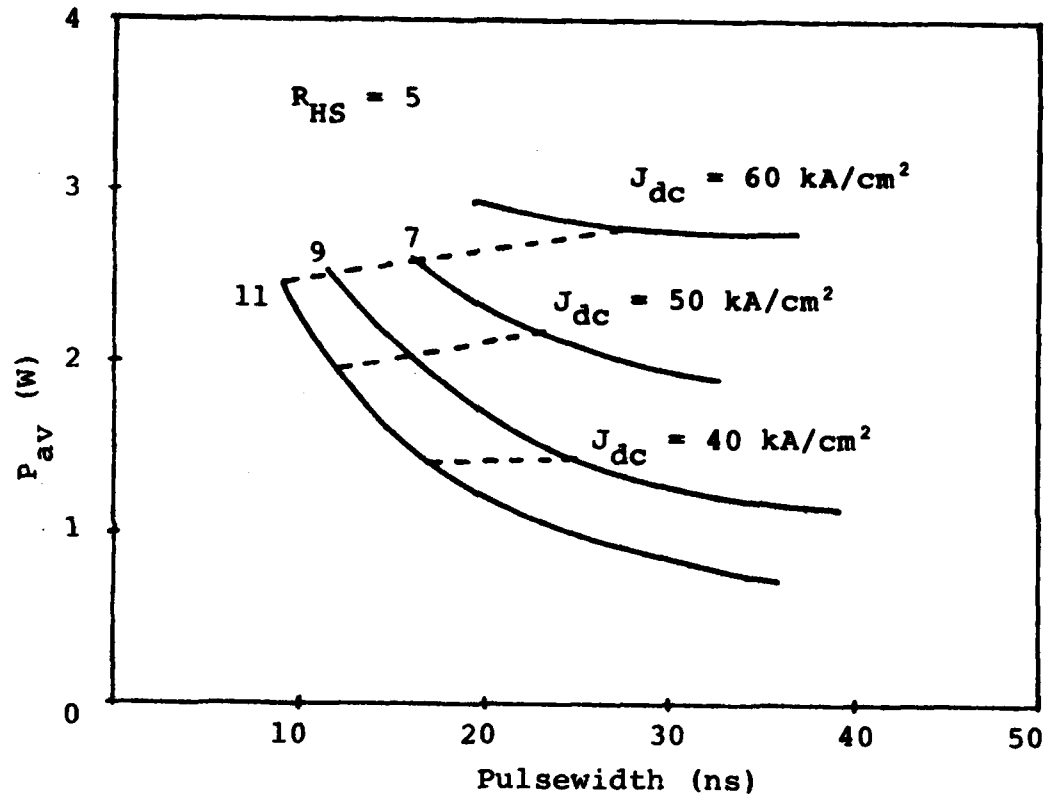
FIG. 2.27 THE AVERAGE POWER AS A FUNCTION OF PULSEWIDTH.

Figure 2.28 shows the mean power as a function of pulsewidth for various values of R_{HS}. The mean power is defined as

$$P_{mean} = \frac{1}{T} \int_{o}^{t_1} P_{RF}(t) \, dt$$

$$= P_{av} \times \text{duty cycle} \quad ,$$

where t_1 is the pulsewidth and T is the period.

To illustrate the influence of heat sink on pulsed oscillator performance, a pulsed oscillator with R_{HS} of 9 °C/W and pulsewidth of 39.6 ns is used as an example. With a copper heat sink, P_{av} is 1.13 W, PRF is 826 kHz, the duty cycle is 3.27 percent and P_{mean} is 0.037 W as shown in Figs. 2.27 and 2.28. With diamond IIA heat sink, P_{av} is the same (1.13 W). However, the duty cycle is 17.9 percent, since PRF of 4.5 MHz can be used and P_{mean} of 0.2 W is obtained.

2.7 Conclusions

In this chapter a simple oscillator model was developed, and various parameter state equations governing its behavior were presented. Usefulness and limitations of this oscillator model were discussed, and the model was applied to a simple RLC oscillator circuit to indicate its response to an applied bias pulse. Immediately after application of the bias pulse, a high growth rate occurred while the RF voltage was small. As the RF voltage increased, the growth rate decreased as expected in a stable oscillator circuit. In addition, the device susceptance B_d increased with increasing RF voltage, resulting in a decrease of oscillation frequency during turn-on. After the initial turn-on of the oscillator stabilized, the junction
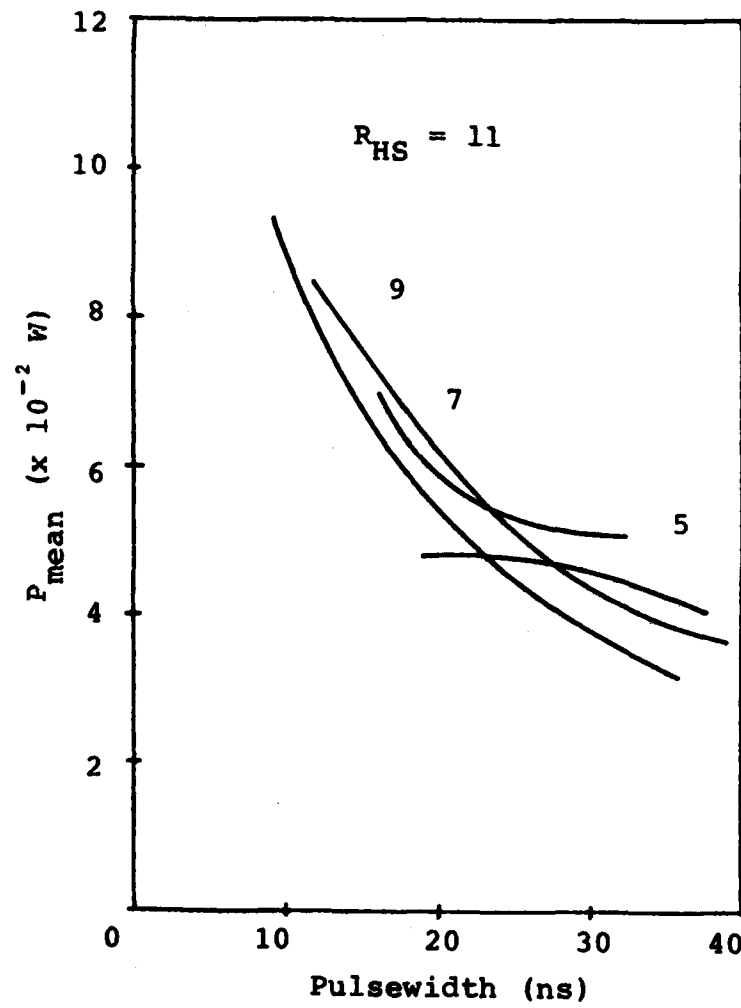
FIG. 2.28 MEAN POWER AS A FUNCTION OF PULSEWIDTH.

temperature continued to increase, and the device properties varied accordingly. The frequency drifted downward, and the output power increased as the temperature increased. When the bias pulse was turned off, the RF voltage decreased rapidly to a small value, and junction temperature decreased to ambient temperature in the expected manner. The separation of turn-on and post turn-on effects in this circuit were readily apparent because the thermal-time constant was long compared to the growth time of the oscillator RF voltage. These results illustrate the several important effects in pulsed oscillator behavior, pointing out both circuit and temperature dependence of oscillator dynamics and demonstrating the use of the quasi-static model.

CHAPTER III. DEPENDENCE OF OSCILLATOR TURN-ON TRANSIENTS

ON DEVICE AND CIRCUIT PARAMETERS

3.1 Introduction

The turn-on transient of a free-running or injection-locked IMPATT oscillator can be analyzed by solving for the RF voltage $V_{RF}(t)$ and phase $\theta(t)$, given the initial RF voltage $V_{RF}(0)$ and phase $\theta(0)$. Detailed analysis has shown that the transient response is sensitive to many device and circuit parameters.

From the condition for free-running oscillation $Y_d(s) = - Y_c(s)$, a great deal of insight into oscillator turn-on transients can be obtained from a complex plane representation (device-circuit diagram) of the device admittance Y_d together with the negative locus of the circuit admittance vs. frequency, $- Y_c(f)$. Y_d is a function of RF voltage, frequency, junction temperature, bias current and photon injection, while $Y_c(f)$ is the frequency response of the circuit seen from the device terminals.

The approximate magnitude of the initial growth rate at $t = 0$ is proportional to the distance between the device admittance curve and the circuit (negative) curve, while the imaginary parts of the device and the circuit admittance determine the frequency response of the free-running oscillator. Details of the turn-on transient can be obtained through a simulation program.

In this chapter the turn-on transients (growth rate decrease, RF voltage buildup, output power increase, dc voltage decrease, oscillation frequency decrease, device admittance change, etc.) and

-64-

their dependence on device and circuit parameters are obtained from the oscillator model developed in the previous chapter. This oscillator model is used to predict many important turn-on transients of millimeter-wave IMPATT oscillators including the following:

1. Turn-on time and oscillation frequency as a function of bias current.

2. Turn-on time and frequency response as a function of circuit Q.

3. Effects of various bias circuits.

4. Influence of injection locking.

5. Effects of photon injection under different bias conditions.

6. Starting jitter in the leading edge envelope of the output power.

7. Turn-on time as a function of ambient temperature.

3.2 Effect of Bias Current

In this section simulation results of the turn-on transient of an IMPATT oscillator at various bias current densities are demonstrated. In order to understand the bias current dependence of turn-on transients, it is essential to know the device properties as a function of bias current. At the start of oscillation, the RF voltage across the device terminals is small. Thus, the small-signal device admittance is very important at the beginning of turn-on (t = 0). The small-signal properties of IMPATT diodes studied by Misawa[18] can be summarized as follows:

1. The avalanche frequency is proportional to the square root of the dc bias current [$f_a \propto (I_{dc})^{\frac{1}{2}}$].

2. The magnitude of the device conductance $|G_d|$ increases with bias current at most frequencies.

3. The device susceptance B_d decreases with bias current.

4. The magnitude of the device Q decreases with bias current where the device Q is negative and has a value determined by the ratio of device susceptance to device conductance. Since power is generated by an IMPATT diode, the device Q is negative.

In addition to the small-signal device properties, the large-signal device properties which determine the efficiency and output power of an oscillator are also important. Efficiency and output power increase with bias current before space-charge effects become important. From the small- and large-signal device properties, turn-on transients of the IMPATT oscillators can be predicted qualitatively.

The small-signal Q of the device gives information about the threshold condition and the initial growth rate of a pulsed oscillator. Since the magnitude of the device Q decreases with bias current, there exists a threshold current for the onset of oscillation. Therefore, higher initial growth rate, larger output power, and increased oscillation frequency at steady state can generally be obtained by operating the device at a higher bias current.

To illustrate the bias current dependence of turn-on transients, a fixed tuned oscillator in which the microwave circuit is represented by a simple RLC parallel network (G = 24.9 mmho, L = 9.39 x 10^{-13} H, and C = 1.4522 pF) is assumed, and the current density J_{dc} varies from 20 to 60 kA/cm^2. Figure 3.1 shows the variation of output power of this fixed tuned oscillator at various bias current levels.
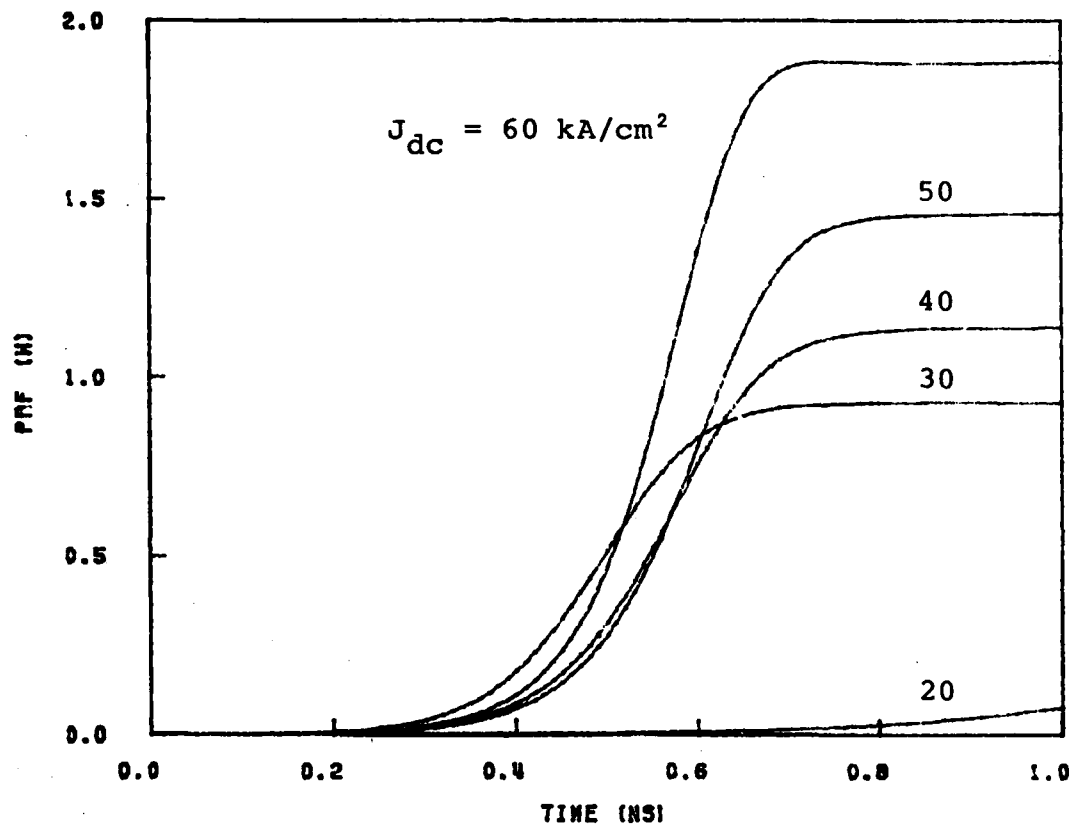
FIG. 3.1 OUTPUT POWER BUILDUP OF A FIXED TUNED OSCILLATOR AT VARIOUS
CURRENT DENSITIES.

When the current density is smaller than the threshold value
($\cong 20$ kA/cm^2), the output power does not build up within 1 ns. When
the current density is 30 kA/cm^2 or more, the output power and RF
voltage at steady state increase as the bias current increases. Turn-
on time remains approximately the same (0.7 ns), although the initial
growth rate may be larger at a higher current. Figure 3.2 shows the
frequency response during turn-on at various current levels. Oscillation
frequency at steady state increases with current density as expected.
Since the RF voltage swing increases with bias current, the amount of
frequency change during turn-on increases accordingly.

3.3 RF Circuit Dependence

During the turn-on, the amplitude of the RF oscillation increases
exponentially, and the growth rate of RF voltage is related to the
circuit Q. Thus, if the diode is placed in a low Q circuit, substan-
tial frequency decrease and faster turn-on would be expected. However,
in a high Q circuit smaller frequency decrease and slower turn-on
would be obtained. Of course, to predict the turn-on of a given
oscillator, the impedance presented to the diode by the circuit must
be known.

To study the RF circuit dependence of the turn-on transient,
it is essential to have a model for the external circuit of an IMPATT
oscillator. The most straightforward method of modeling is by means
of a lumped equivalent network representing the microwave circuit.
In this section, a simple parallel RLC network representing the
circuit seen from the device terminals as shown in Fig. 2.5 is
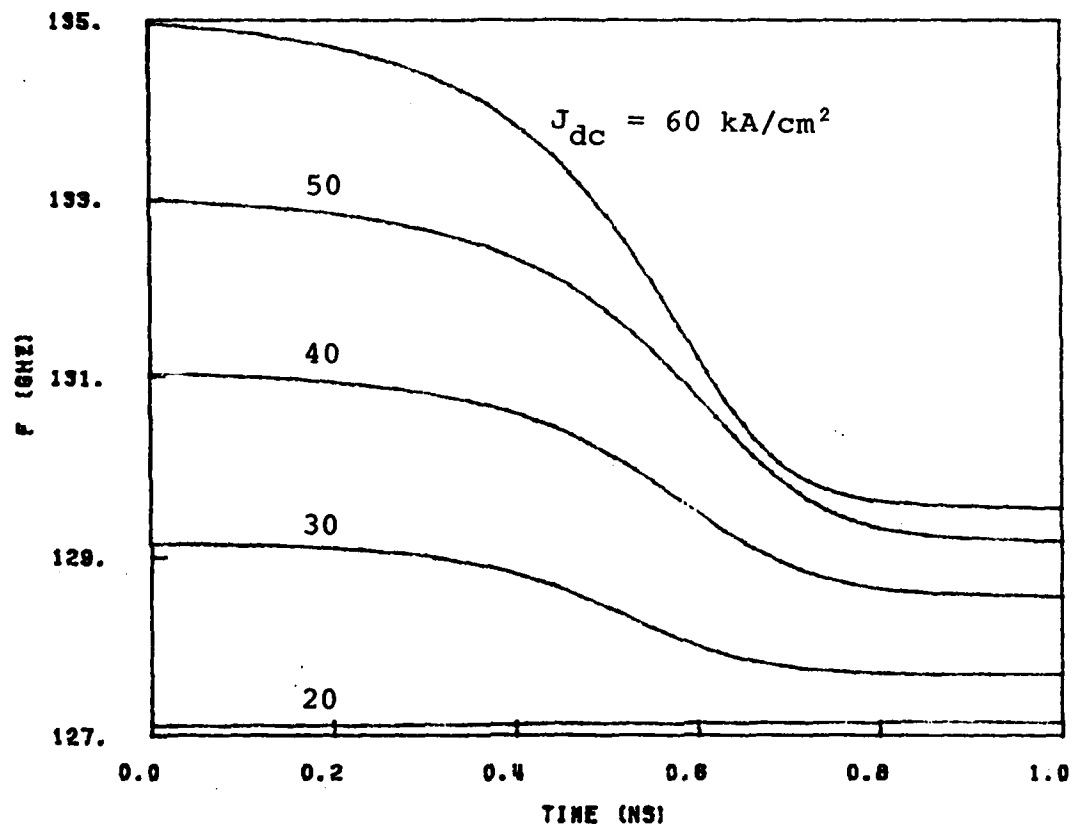
FIG. 3.2 FREQUENCY RESPONSE DURING TURN-ON AT VARIOUS CURRENT DENSITIES.

combined with the device to study the RF circuit dependence of the turn-on transient.

Turn-on time and output power at steady state of an oscillator are very sensitive functions of the circuit conductance. Circuit conductance G is chosen to be equal to $- G_d(V_o,f)$ where V_o is the RF voltage at steady state, and f is the oscillation frequency at steady state. L and C are chosen such that

$$B_d(V_o,f) + B_c(f) = 0 \quad , \quad \text{i.e.,} \quad \omega C - \frac{1}{\omega L} = - B_d(V_o,f) \qquad (3.1)$$

and

$$Q_{L,C} = \frac{\omega}{2G} \frac{\partial B_c}{\partial \omega} = \frac{\omega}{2G}\left(C + \frac{1}{\omega^2 L}\right) \quad . \qquad (3.2)$$

Given the frequency f, $G_d(V_o,f)$, $B_d(V_o,f)$, and loaded circuit quality factor $Q_{L,C}$, then G, L and C can be determined from Eqs. 3.1 and 3.2. To illustrate the RF circuit dependence of the turn-on transient, the following device parameters are used: current density $J_{dc} = 60$ kA/cm^2, frequency f = 130 GHz, RF voltage $V_o = 12$ V, device conductance $G_d(V_o,f) = - 24.9$ mmho, and device susceptance $B_d(V_o,f) = 117.6$ mmho.

From Eqs. 3.1 and 3.2, L and C are

$$L = \frac{2}{\omega} \frac{1}{2|G_d|Q_{L,C} + B_d} \qquad (3.3)$$

and

$$C = \frac{- B_d + 2|G_d|Q_{L,C}}{2\omega} \quad . \qquad (3.4)$$

In this section G equals 24.9 mmho, and L and C for different $Q_{L,C}$ are as follows:

$Q_{L,C}$	L (H)	C (pF)
25	1.7970×10^{-12}	0.69012
50	9.3900×10^{-13}	1.4522
75	6.3555×10^{-13}	2.2143
100	4.8033×10^{-13}	2.9764
125	3.8605×10^{-13}	3.7385

Threshold current, which is defined as the minimum current to trigger the oscillation, increases with increasing circuit conductance. Various circuit parameters with different $Q_{L,C}$ have been used to demonstrate the RF circuit dependence of the turn-on transient. In the calculation, a current density $J_{dc} = 60$ kA/cm^2 is applied to the diode. The output power buildup of an IMPATT oscillator shortly after the bias pulse is applied is shown in Fig. 3.3. The output power builds up within 0.4 ns for the RF circuit with $Q_{L,C} = 25$, while the turn-on time is more than 1 ns for the circuit with $Q_{L,C} = 75$. Growth rate at t = 0 varies from 1.88×10^{10} ($Q_{L,C} = 25$) to 4.81×10^{9} ($Q_{L,C} = 75$). Figure 3.4 shows that a 9-GHz frequency decrease (138.2 to 129.2 GHz) is obtained with $Q_{L,C} = 25$, while a 5.5-GHz frequency decrease (135.0 to 129.5 GHz) is obtained with $Q_{L,C} = 50$.

3.4 Bias Circuit Dependence

An IMPATT diode is a current-controlled device, and the waveform of the bias current passing through the diode is heavily
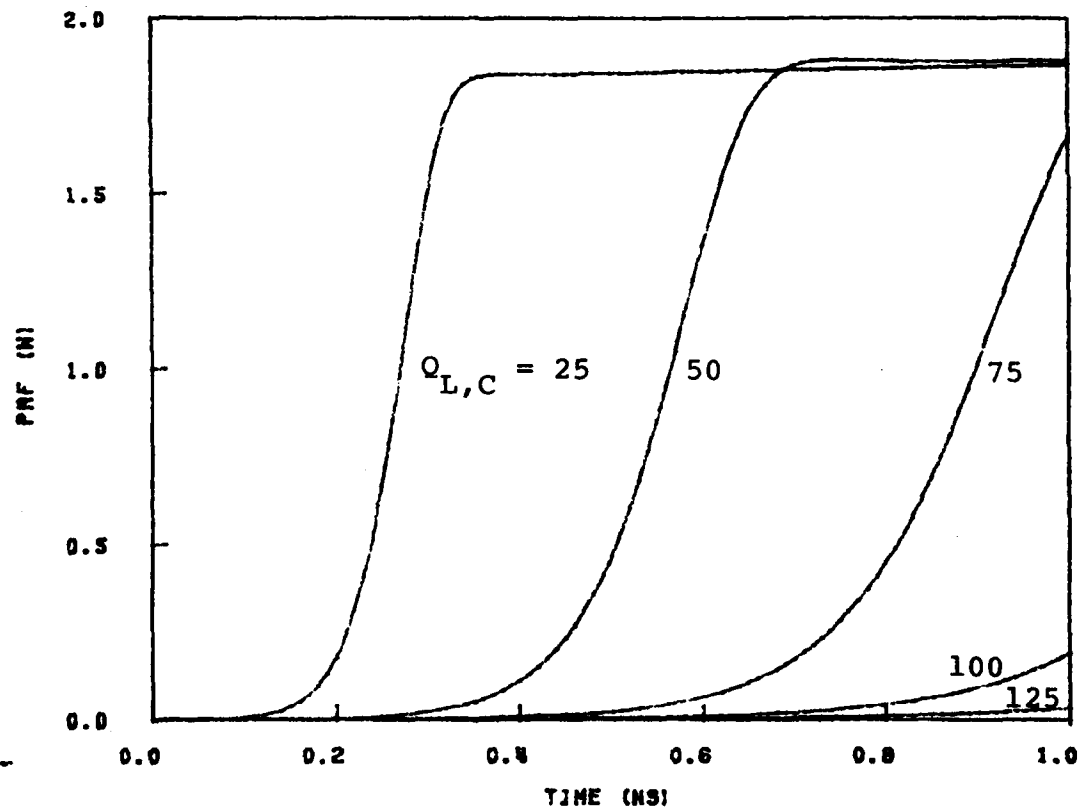
FIG. 3.3 OUTPUT POWER BUILDUP OF IMPATT OSCILLATOR FOR DIFFERENT
LOADED Q CIRCUITS.
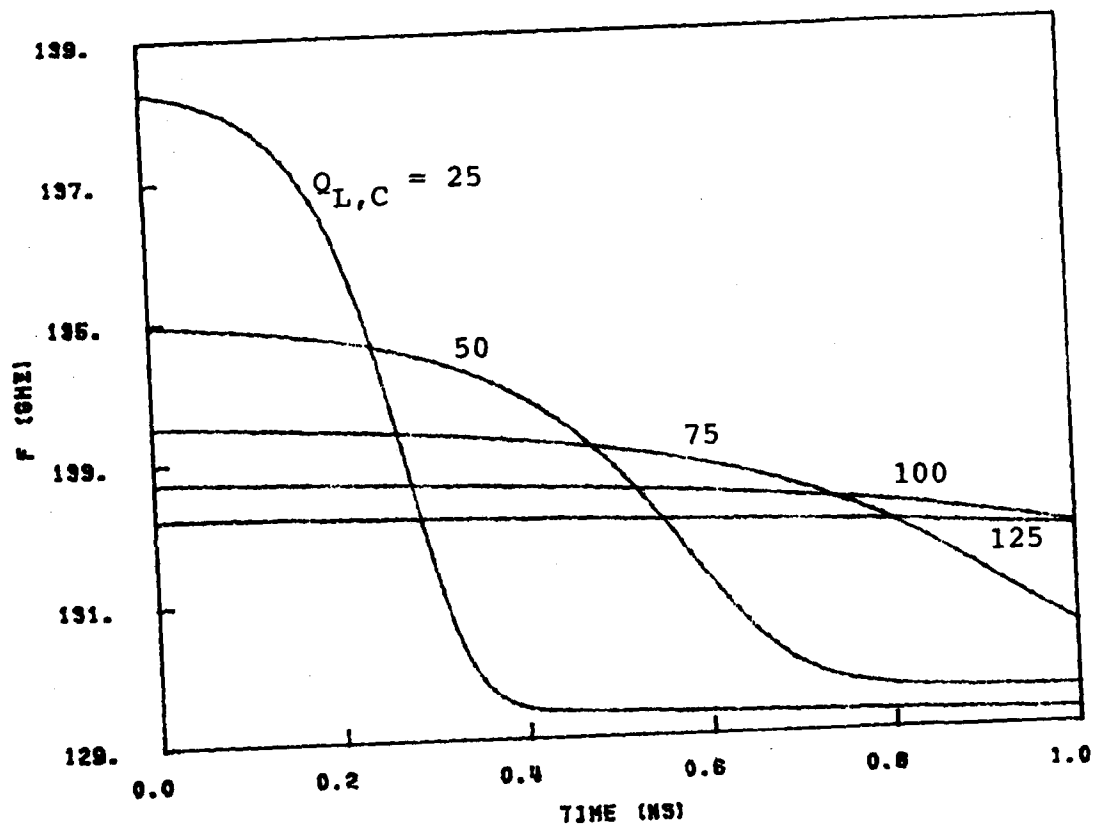
FIG. 3.4 FREQUENCY RESPONSE DURING TURN-ON FOR DIFFERENT LOADED Q CIRCUITS.

dependent on the device properties and the bias circuit. This section

presents the results of an investigation of the effects of the bias

circuit on the turn-on transient. Constant current source, constant

voltage source, and constant voltage source with finite internal

impedance have been used to represent the different bias circuits.

The source impedance is represented by a series of combinations of

a resistor R and an inductor L. The rise time of the bias source

is adjusted by varying the values of R and L.

Normally under constant current operation, the dc voltage

across the diode will drop with increasing RF voltage amplitude. The

turn-on transient for the constant current source case has been des-

cribed in the example in Chapter II. Only the constant voltage source

and constant voltage source with finite impedance will be discussed

in this section. If the voltage across the diode is held constant,

the bias current passing through the diode will increase as the RF

voltage increases. When the constant voltage source with finite

impedance is used as a bias circuit, the dc voltage and the bias

current are not held constant. The dc voltage decreases and the

bias current increases as the RF oscillation builds up. This may

cause low-frequency oscillation.[19]

Low-frequency instabilities are serious in millimeter-wave

IMPATT diodes, especially DDR diodes which produce the required

higher power and efficiency in the millimeter-wave range. The

maximum frequency for which low-frequency negative resistance exists

in millimeter-wave diodes is larger than that in

microwave diodes. Thus, the suppression of instabilities in higher

frequency diodes is more difficult than in lower frequency diodes.

Output power will be reduced by low-frequency oscillations, and the elimination of the low-frequency instabilities is essential in the oscillator design.

To illustrate the bias circuit dependence of turn-on transients, a constant voltage source with finite impedance ($V_s = 83$ V, R = 50 Ω, and L = 10 nH) as shown in Fig. 2.3 is used as a bias circuit. Figure 3.5 shows that the current density J_{dc} increases from 0 to 62.8 kA/cm^2 after the step increase of the constant voltage source V_s. Bias current continues to increase until the increase of the junction temperature is significant enough to offset the back-bias effect.

The growth rate σ is negative, and the output power is zero until the current density is greater than 15 kA/cm^2. Then, the rapid increase of bias current causes the growth rate to increase drastically. Consequently, the RF voltage and the output power start to increase. Figure 3.6 shows the increase of output power. The output power builds up to 2 W within 1 ns. The bias current increase and junction temperature rise contribute to the continuous increase of output power after the oscillator is turned on.

Low-frequency negative resistance is determined[20] by the large-signal back-bias effect, the dependence of the device admittance on the RF voltage and dc current, and the oscillator circuit constraint $Y_d(s) + Y_c(s) = 0$. The load for the low-frequency negative resistance is the bias circuit impedance seen from the diode. A low-frequency bias circuit is stable when

$$R_{sc} + R_{ind} + R > 0 , \qquad (3.5)$$

where R_{sc} is the space-charge resistance of the diode, R_{ind} is the
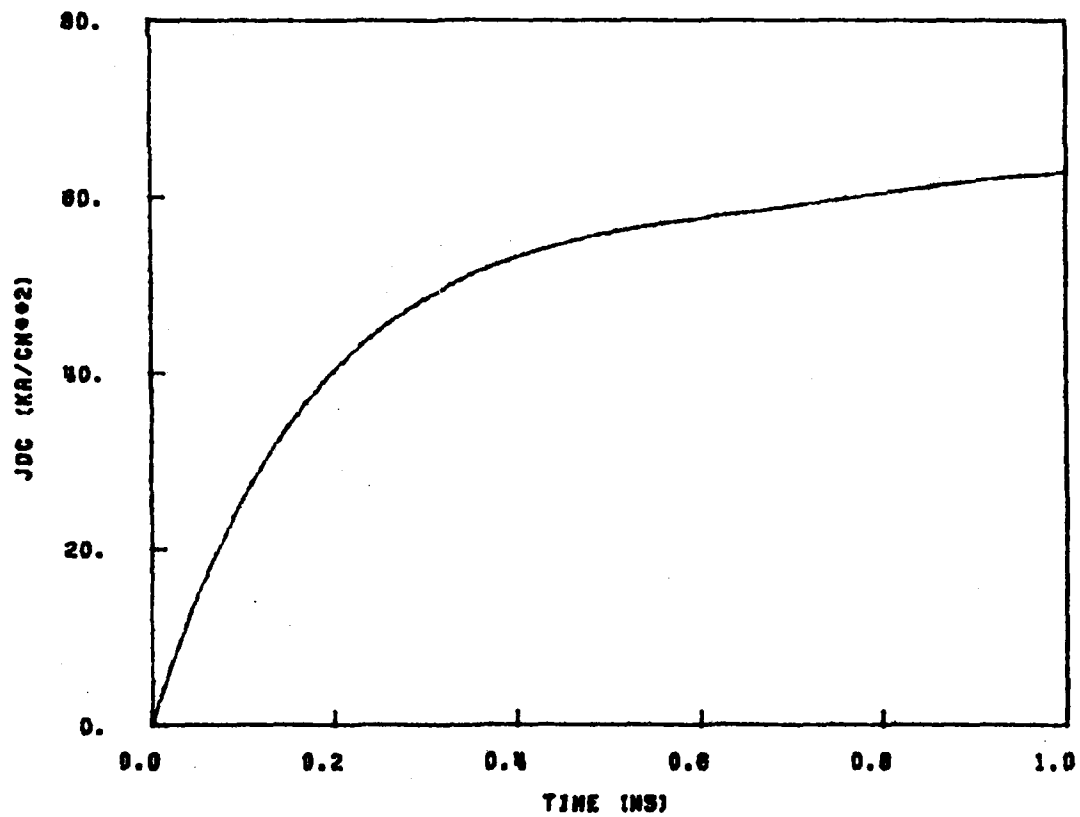
FIG. 3.5   INCREASE OF CURRENT DENSITY FOR CONSTANT VOLTAGE SOURCE
WITH FINITE IMPEDANCE.
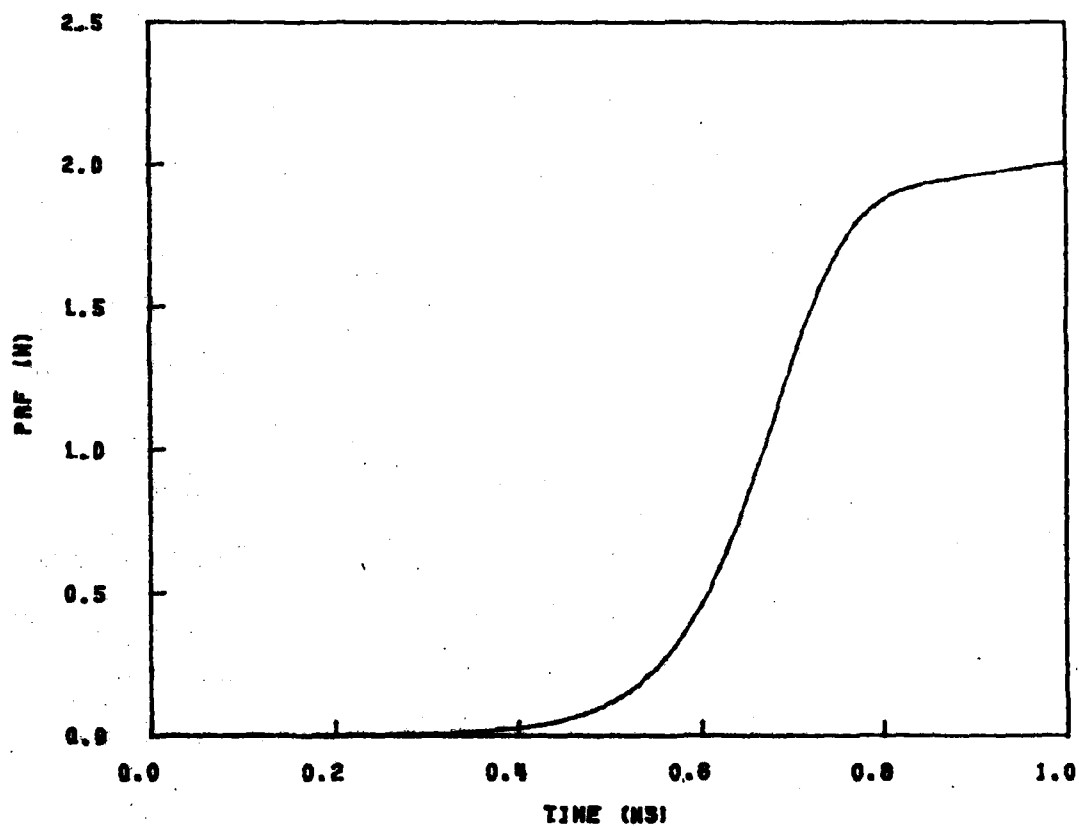
FIG. 3.6 BUILDUP OF OUTPUT POWER FOR CONSTANT VOLTAGE SOURCE WITH
FINITE IMPEDANCE.

negative resistance induced by back-bias effect, and R is the bias source resistance.

It can be seen from Eq. 3.5 that low-frequency oscillations can be eliminated by making the bias source resistance R large or by biasing the diode with a constant current source ($R = \infty$). However, at higher frequencies the unavoidable circuit reactances, such as blocking capacitors and bias chokes, introduce time constant that will prevent either constant-current or constant-voltage operation of the diode. Although the space-charge resistance has some stabilizing effect, it usually cannot prevent the stable condition from being violated at large RF voltages, and low-frequency oscillations may then appear.

Figure 3.7 shows the behavior of dc voltage across the diode V_{dc} and dc current passing through the diode I_{dc} during turn-on. I_{dc} and V_{dc} increase when the RF voltage is small, while I_{dc} increases and V_{dc} decreases when the RF voltage is building up. From positive- and negative-resistance regions of the dc response, R_{sc} and R_{ind} can be estimated:

$$R_{sc} \approx 4.8 \ \Omega \tag{3.6}$$

and

$$R_{ind} + R_{sc} \approx -53.9 \ \Omega \ . \tag{3.7}$$

From Eqs. 3.6 and 3.7, it can be seen that the magnitude of R_{sc} is much smaller than that of R_{ind}. To achieve a stable condition at low frequency, $R > 53.9 \ \Omega$ is desired. The 50-Ω bias source resistance used here is not large enough to eliminate the low-frequency oscillation.
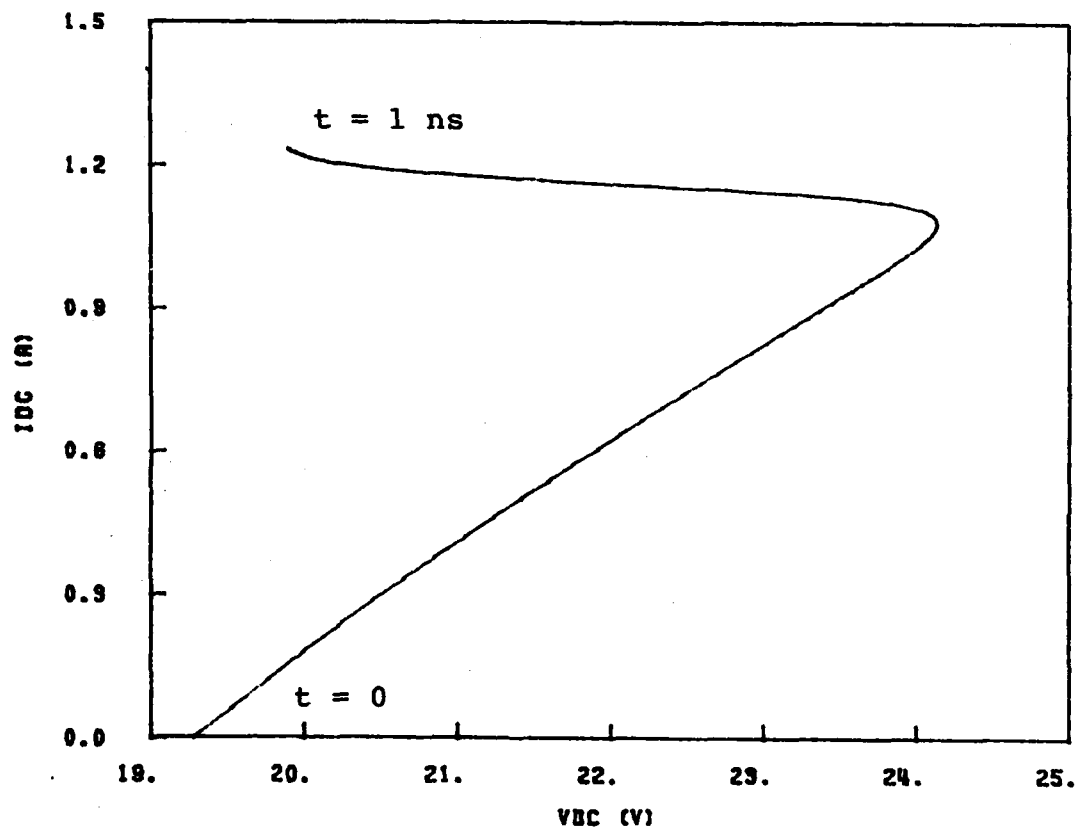
FIG. 3.7 BEHAVIOR OF DC VOLTAGE AND DC CURRENT FOR CONSTANT VOLTAGE
SOURCE WITH FINITE IMPEDANCE.

3.5 Effect of Injection Locking on the Turn-On Transient

Millimeter-wave oscillators can achieve pulse-to-pulse coherency by injection locking to low level stable oscillators. At t = 0, the bias current is negligible, and the IMPATT diode behaves as a capacitor. The device capacitance C_d at t = 0 is given by

$$C_d = \frac{\varepsilon A}{d} , \tag{3.8}$$

where ε is the dielectric constant of the semiconductor, A is the device area, and d is the device width.

For the Si DDR IMPATT diode used in the calculation, the values are d = 1 μm, A = 1.9635 x 10^{-5} cm^2, and ε = 1.06 x 10^{-12} F/cm^2, which gives C_d = 0.208 pF. $V_{RF}(0)$, which is the RF voltage at t = 0, depends on the frequency of the locking signal f_i, device admittance $Y_d(j\omega_i C_d)$, RF circuit admittance $(G + jB_c)$, and the injection current I_i:

$$V_{RF}(0) = \frac{I_i}{\sqrt{(\omega_i C_d)^2 + (G^2 + B_c^2)}} \tag{3.9}$$

and

$$I_i = \sqrt{8 \, GP_{in}} , \tag{3.10}$$

where ω_i is the angular frequency of the locking signal and P_{in} is the injection power of the locking signal.

The initial phase angle $\theta(0)$ at t = 0 depends on device admittance, circuit admittance and injection frequency:

$$\theta(0) = -\tan^{-1}\left[\frac{\omega_i C_d + B_c}{G}\right] . \tag{3.11}$$

In this section the effects of the injection locking on the turn-on transient are described. All the other conditions (bias circuit, RF circuit, bias current, etc.) are the same; only the injection frequency and injection power are varied. The injection power of the locking signal P_{in} = 0.2 W is approximately 10 dB below the output power of the free-running oscillator. The oscillator is simulated with the circuit conductance G = 24.9 mmho, inductor L = 9.39 x 10^{-13} H, and capacitor C = 1.4522 pF as shown in Fig. 2.5. From Eq. 3.10 the injection current I_i for the preceeding parameters is I_i = 0.2 A.

To study the effects of injection locking on the pulsed oscillator behavior, the following dynamic equations are used:

$$\sigma = \frac{1}{V_{RF}} \frac{dV_{RF}}{dt} \tag{3.12}$$

and

$$\dot{\theta} = \omega - \omega_i . \tag{3.13}$$

Therefore, the RF voltage and phase at different times can be calculated:

$$V_{RF}(t + dt) = V_{RF}(t) + dV_{RF} \tag{3.14}$$

and

$$\theta(t + dt) = \theta(t) + d\theta , \tag{3.15}$$

where dV_{RF} equals $(\sigma V_{RF})dt$, $d\theta$ equals $(\omega - \omega_i)dt$, and dt is the time step used in the calculation. The current values of σ and ω are obtained by solving the oscillator equation in the presence of the locking signal as described in Chapter II.

END

FILMED

DTIC
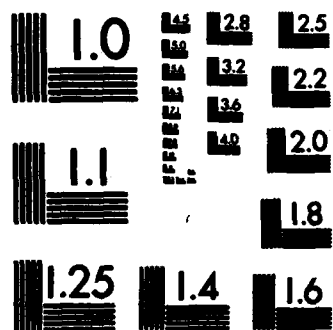
MICROCOPY RESOLUTION TEST CHART

NATIONAL BUREAU OF STANDARDS-1963-A

3.5.1 Effect of Injection Current on the Turn-On Transient.

The effects of the injection current on the turn-on transient

will be studied first while the injection frequency is unchanged. An

injection frequency of f_i = 129 GHz is used, and the initial conditions

for the phase and RF voltage are

$$\theta(0) \approx -0.91 \text{ rad}, \tag{3.16}$$

and

$$V_{RF}(0) = I_i (4.58). \tag{3.17}$$

The free-running oscillator (FRO) was found to have a fast growth

rate and a turn-on time of less than 1 ns with $V_{RF}(0) = 0.1$ V. The

dynamics of the pulsed injection locked oscillator (PILO) have been

studied. Figure 3.8 shows the RF voltage response of the PILO in the

time domain for different injection current levels I_i. I_i varies from

0.04 to 0.1, i.e., $V_{RF}(0)$ varies from 0.183 to 0.458. As the injection

current I_i is increased, the level from which RF oscillation is

initiated, $V_{RF}(0)$, increases. The turn-on time increases or decreases

depending on the initial phase angle and injection frequency. For

a given initial phase angle $\theta(0)$ = - 0.91 rad and injection frequency

f_i = 129 GHz, the initial growth rate of the PILO remains the same

(5.4×10^{10}) for different injection currents and is much larger than

that of the FRO (8×10^9). Thus, the RF voltage builds up faster with

injection locking, and the decrease of turn-on time as the injection

current is increased is mainly caused by the increase of $V_{RF}(0)$ as

demonstrated in Figure 3.8.

Phase response of the PILO is determined by Eq. 3.13. The

large frequency decrease of the free-running oscillator during turn-on
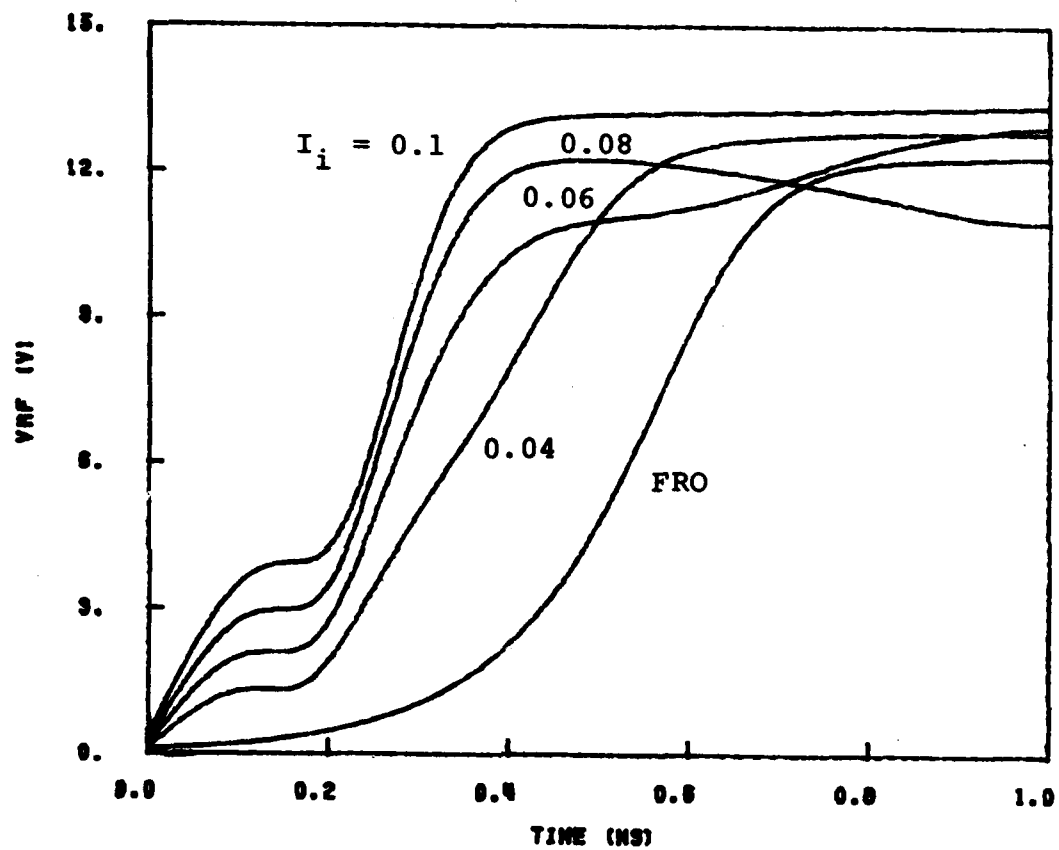
FIG. 3.8 RF VOLTAGE RESPONSE FOR DIFFERENT INJECTION CURRENT I_i.

has been described. This large frequency decrease causes the phase angle to vary drastically. Figure 3.9 shows the phase response of the PILO in a time domain for different injection current levels. It can be seen that phase variation is maximum (phase angle increases from - 0.91 to 12.9 rad) when I_i = 0.04. For I_i = 0.1, the phase angle increases from - 0.91 to 6.94 and then decreases to 6.81 rad in 1 ns. RF voltage of the PILO can increase or decrease depending on the value of the phase angle. The large variation of the phase angle when an injection signal is present causes the RF voltage to remain constant or even decrease during a portion of the 1 ns as shown in Figure 3.8.

The response of the PILO on the GB plane is shown in Fig. 3.10 when the injection current I_i = 0.04 and the injection frequency f_i = 129 GHz. At t = 0, RF voltage is small, and the injection vector $I_i e^{-j\theta}/V_{RF}$ (= Y_d + Y_c) is large. Y_d (t = 0) is the device admittance when bias current is zero. The device admittance Y_d (t = 1 ns) at steady state, the circuit line - Y_c as a function of frequency, and the device line Y_d as a function of RF voltage with f = f_i are also shown. It can be seen that the RF voltage is large, and the injection vector is small at steady state. Figure 3.11 shows the behavior of $V_{RF}e^{j\theta}$ during turn-on under the same locking conditions (I_i = 0.04 and f_i = 129 GHz). The RF voltage increases from 0.18 to 12.8 V, and the phase angle increases from - 0.91 to 12.9 rad in 1 ns.

In the previous calculation, a step increase of bias current (zero rise time) is assumed. To investigate the effect of bias current rise time on the turn-on transient of PILO, a rise time of 0.5 ns (current density J_{dc} increases linearly from 0 to 60 kA/cm^2 in 0.5 ns and remains at 60 kA/cm^2 for the rest of the pulsewidth), with
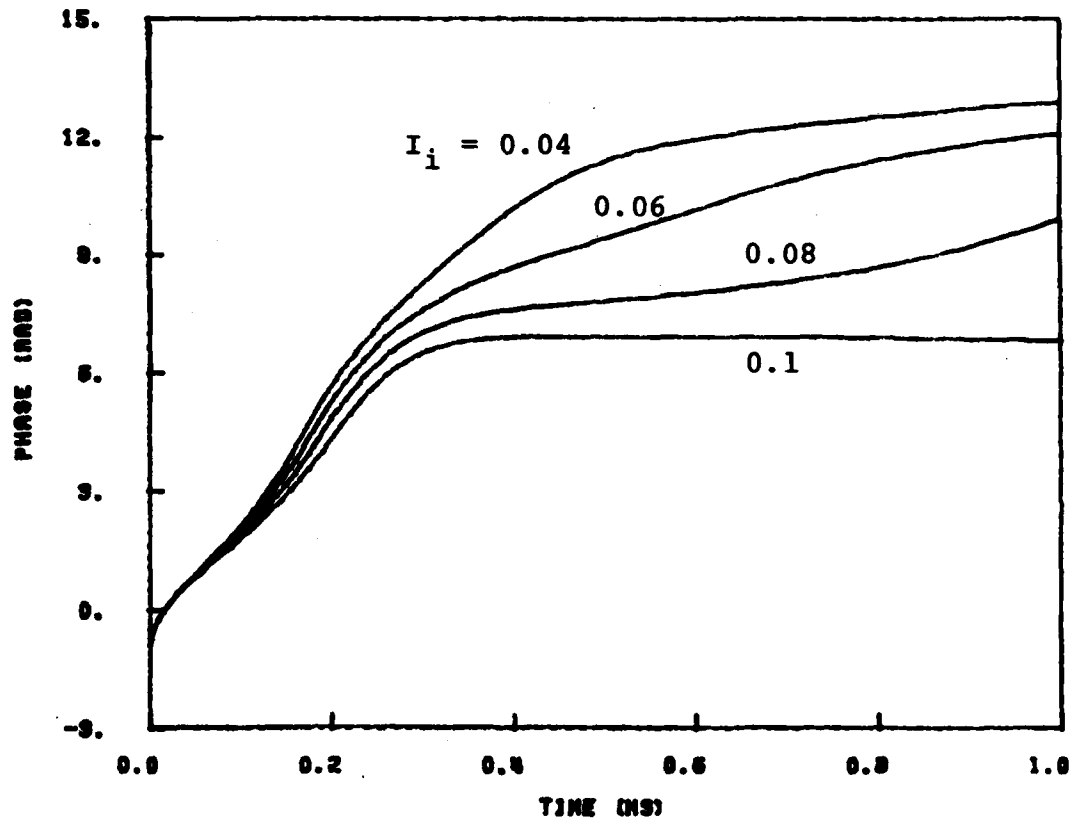
FIG. 3.9 PHASE RESPONSE FOR DIFFERENT INJECTION CURRENT I_i.
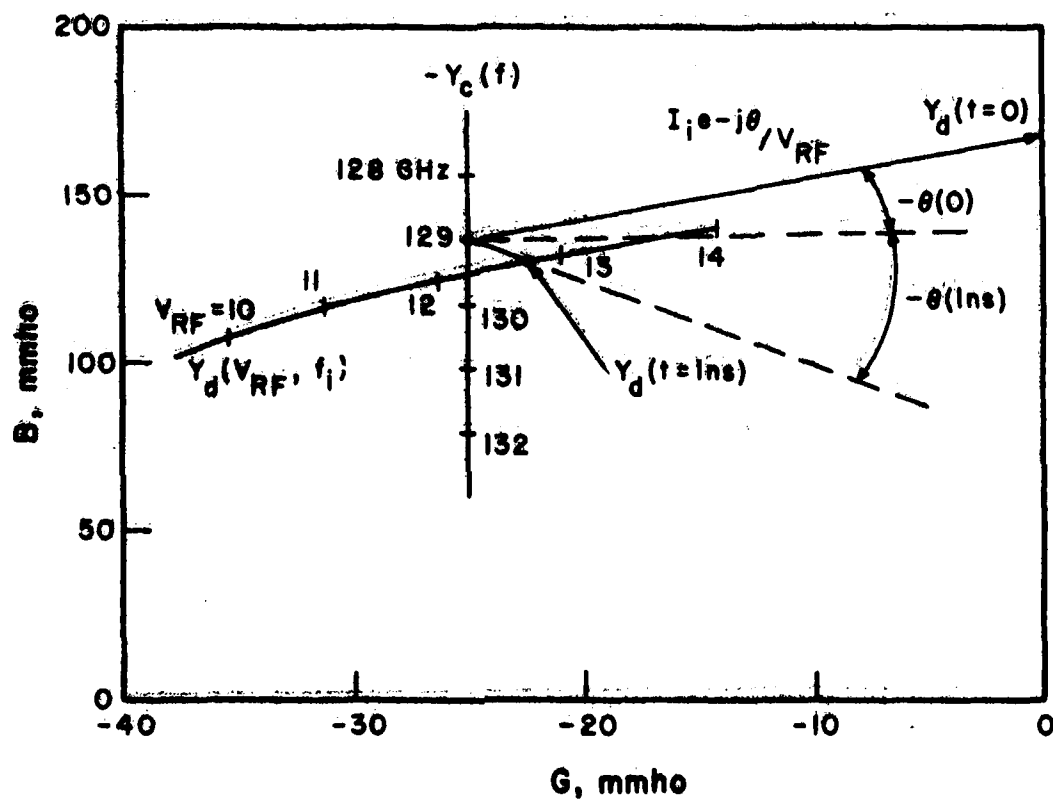
FIG. 3.10   RESPONSE OF THE PILO ON GB PLANE WHEN INJECTION CURRENT

I_i = 0.04 AND INJECTION FREQUENCY f_i = 129 GHz.
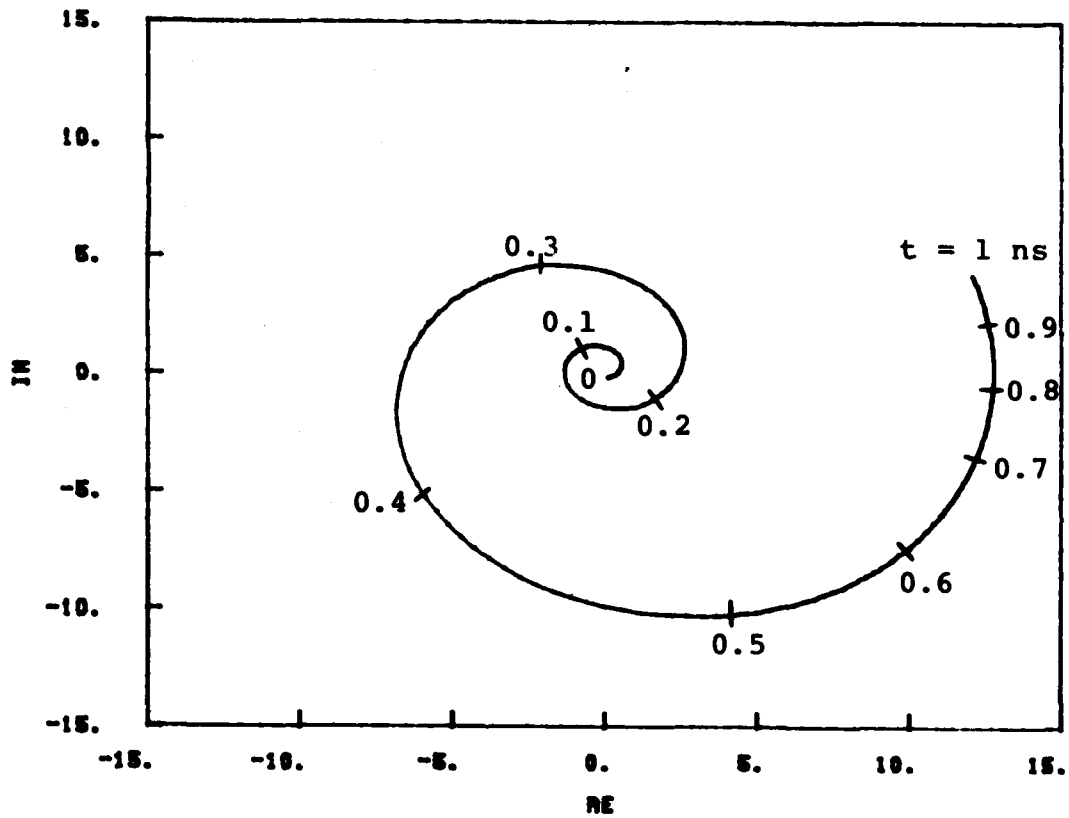
FIG. 3.11 BEHAVIOR OF $V_{RF} e^{j\theta(t)}$ DURING TURN-ON WHEN $I_i = 0.04$ AND $f_i = 129$ GHz.

I_i = 0.04 and f_i = 129 GHz were used. The turn-on time of the PILO increases as expected when the bias current with finite rise time is present. The phase angle decreases from - 0.91 to - 1.4 and then increases to 3.3 rad as shown in Fig. 3.12. Phase response of the PILO with a step increase bias current is also shown for comparison.

3.5.2 Effect of Injection Frequency on the Turn-On Transient.

The effect of injection frequency on the turn-on transient of

a PILO was investigated using an injection current of I_i = 0.06 A. Injection frequency f_i, calculated initial RF voltage $V_{RF}(0)$, and phase angle $\theta(0)$ are as follows:

f_i (GHz)	$V_{RF}(0)$	$\theta(0)$
129	0.275	- 0.91
129.5	0.282	- 1.04
130	0.288	- 1.13
131	0.301	- 1.24

A major influence of the injection signal on the turn-on transient is in the response of the phase angle. When there is no injection signal, frequency decreases from 135 to 129.5 GHz during turn-on. The variation of the phase angle is maximum [$\theta(0)$ varies from - 0.91 to 12.1 rad] for f_i = 129 GHz since the frequency difference between the injection signal and the free-running oscillator is maximum. Figure 3.13 shows the phase response of a PILO for various injection frequencies. The injection frequency varies from 129 to 131 GHz.
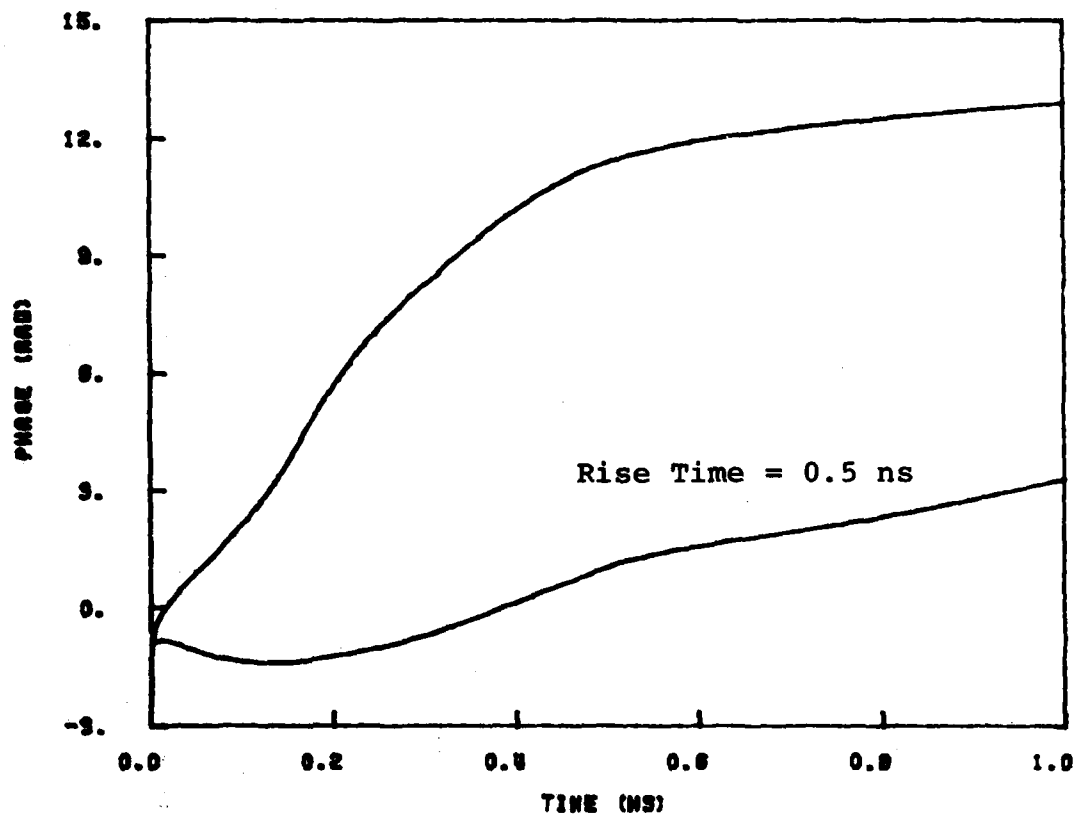
FIG. 3.12   PHASE RESPONSE OF THE PILO WITH FINITE BIAS CURRENT
RISE TIME.
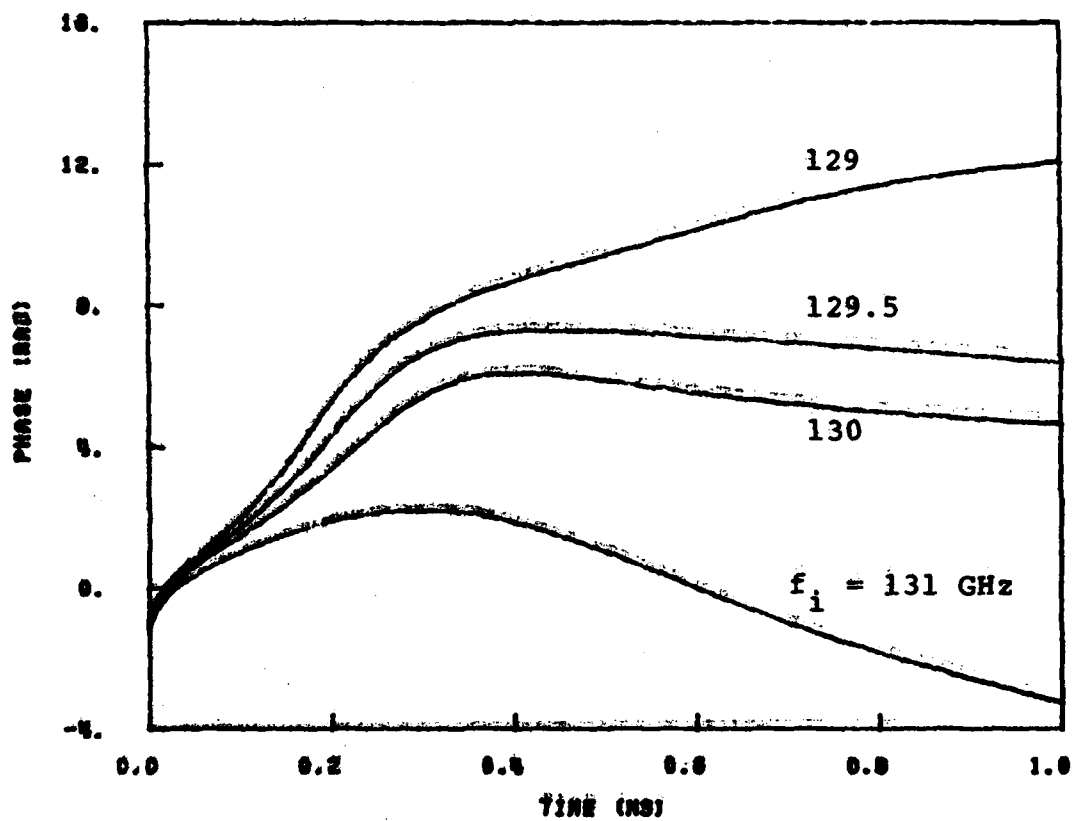
FIG. 3.13 PHASE RESPONSES OF PILO FOR VARIOUS INJECTION FREQUENCIES.

3.6 Effect of Photon Injection on the Turn-On Transient

The influence of the photon injection on IMPATT oscillators can be understood in terms of the effect photon injection has on the device admittance Y_d, assuming negligible optical dependence of the microwave circuit admittance. Photon injection effectively increases reverse saturation current I_o, and this increase results in the variation of device properties. Misawa[18] has shown that an increase in reverse saturation current leads to a premature buildup of the avalanche current and reduces the phase delay associated with the avalanche process, which in turn severely reduces the generated output power and efficiency. If the phase delay is reduced sufficiently, the negative conductance will be insufficient to overcome the circuit losses, and RF oscillation will cease at high level photon injection.

Figure 3.14 shows the buildup of output power at various optical current densities (J_{op} varies from 0 to 875 A/cm^2) when the diode is biased with a constant current source (J_{dc} = 60 kA/cm^2). It can be seen that output power decreases with increasing optical current. Output power decreases from 1.9 to 1.5 W when J_{op} = 500 A/cm^2. The small-signal negative conductance, and hence the initial growth rate of the RF oscillation, are changed by photon injection. The initial growth rate of the IMPATT oscillator decreases, and the turn-on time increases with photon injection. The oscillator is turned on within 0.7 ns when there is no photon injection, and the buildup is not completed in 1 ns when J_{op} = 875 A/cm^2. Initial growth rate at the start of turn-on is maximum (6... , 1(when J_{op} = 0 and is minimum (5 x 10^9) when J_{op} = 875 A/cm^2.
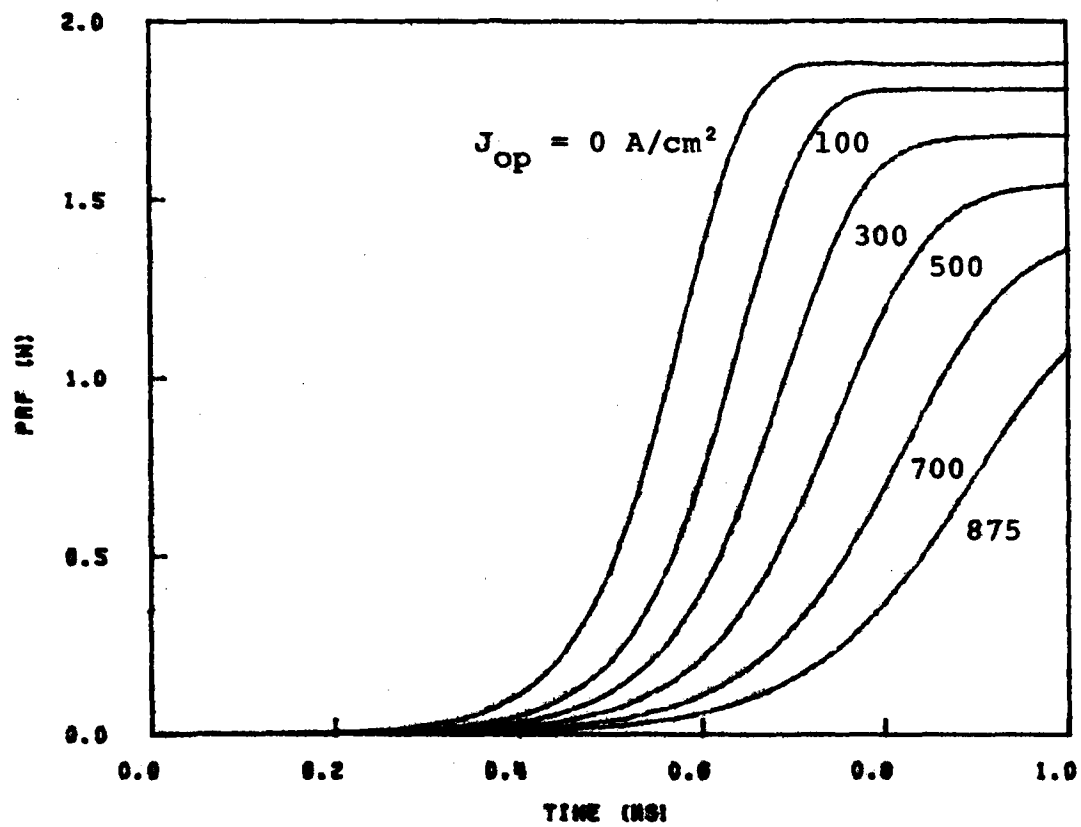
$J_{dc} = 60$ kA/cm^2

FIG. 3.14 BUILDUP OF OUTPUT POWER AT VARIOUS OPTICAL CURRENT

DENSITIES WHEN THE DIODE IS BIASED WITH A CONSTANT

CURRENT SOURCE.

Another important parameter is the oscillator frequency determined by the resonance of the circuit-supplied inductive suscep- tance with the diode-supplied capacitive susceptance. The capacitive susceptance of the diode decreases with photon injection level. This in turn leads to an increase in operating frequency. The simulation result shows that the operating frequency f_o at steady state increases with increasing optical current. The operating frequency f_o increases from 129.5 GHz (J_{op} = 0) to 130 GHz (J_{op} = 500 A/cm^2). This resulting frequency shift, which depends heavily on the circuit Q, is less than 0.5 percent with J_{op} = 500 A/cm^2. RF voltage at steady state, and hence the amount of frequency decrease during turn-on, decreases with increasing optical current.

With an appropriate bias circuit, photon injection can be used to trigger RF oscillation. To illustrate this phenomenon, a constant voltage source (20.6 V) with finite impedance (0.5-Ω bias resistor and 0.2-nH bias inductor) is used as the bias circuit. The microwave circuit parameters are G = 22.4 mmho, L = 3.04 x 10^{-12} H, and C = 0.22 pF. Figures 3.15 and 3.16 show the bias current and output power responses in the time domain when the diode is exposed to various photon injection levels at t = 0.1 ns. Without photon injection, the IMPATT diode cannot generate RF power since the bias current is below the threshold value (J_{dc} = 15 kA/cm^2). When the diode is exposed to an external optical source, the breakdown voltage and the dc voltage across the diode decrease. To offset this decrease of dc voltage, the bias current increases. The degree of current increase depends on the injection level and bias circuit configuration. Bias current and output power increase with increasing optical current. With
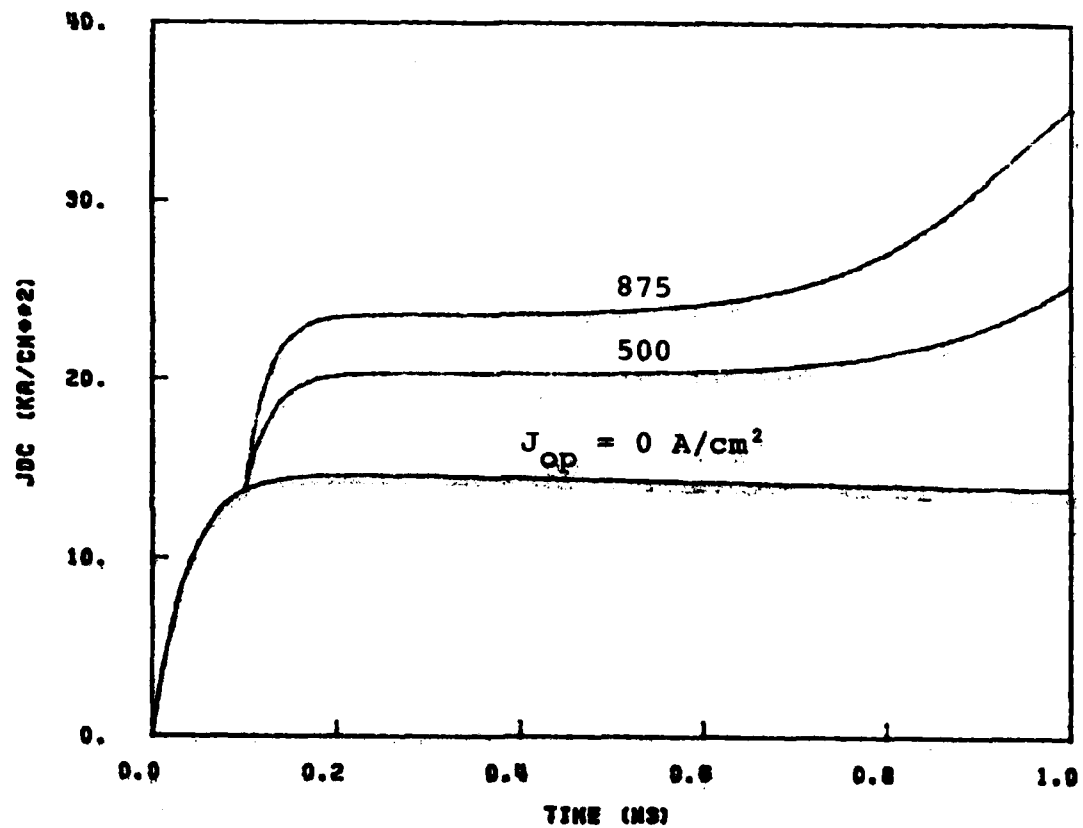
FIG. 3.15 BIAS CURRENT RESPONSE WITH VARIOUS PHOTON INJECTION LEVELS
APPLIED AT TIME = 0.1 ns.
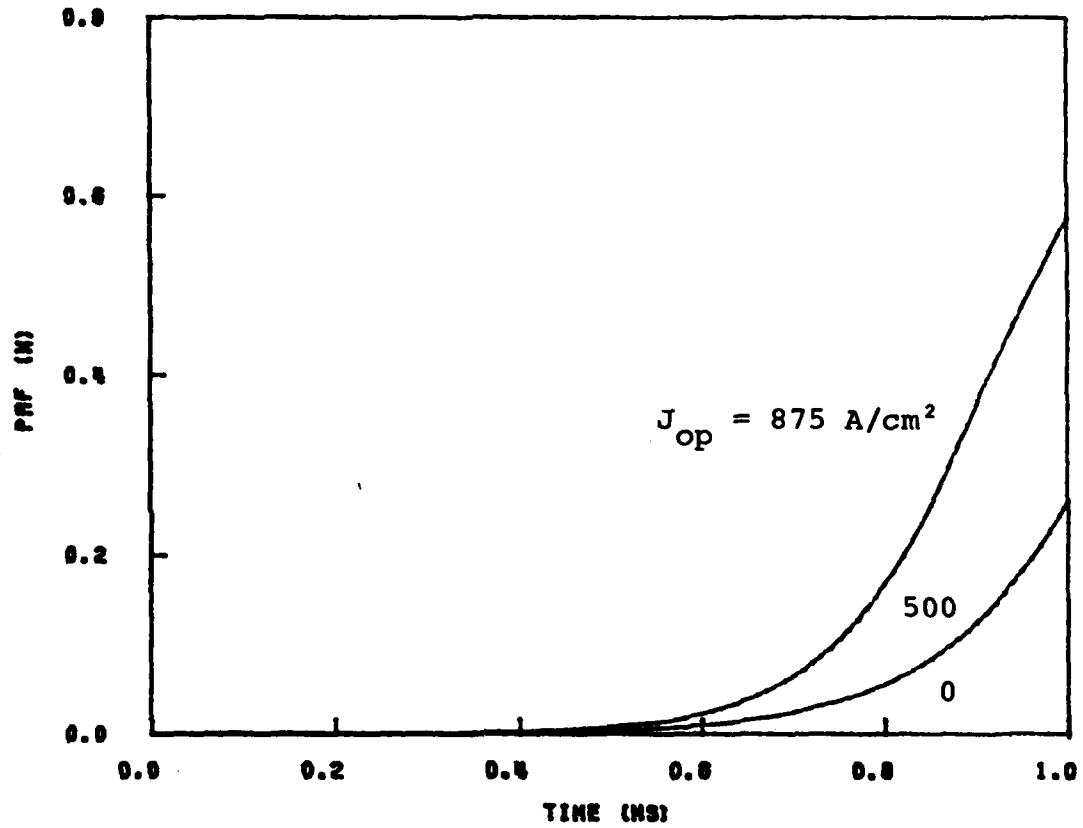
FIG. 3.16 OSCILLATOR TURN-ON BY PHOTON INJECTION. VARIOUS PHOTON
INJECTION LEVELS APPLIED AT TIME = 0.1 ns.

J_{op} = 875 A/cm^2, J_{dc} increases to 35 kA/cm^2, and 0.6 W output power is obtained at t = 0.1 ns. Low bias resistance is required to trigger RF oscillation by photon injection. When the bias resistance is large, the current increase is too small to turn on the oscillator.

Figures 3.17, 3.18 and 3.19 show the responses of the bias current density, J_{dc}, output power P_{RF} and junction temperature T_J to various optical current levels applied at t = 0.1 ns. With J_{op} = 500 A/cm^2, J_{dc} increases to 90 kA/cm^2 at t = 1.75 ns. The bias current keeps increasing until the temperature rise of the device is significant enough to offset this current increase. The device dc and ac properties used in the simulation program were generated by Burmawi,[8] and the maximum bias current density is 60 kA/cm^2. The device admittance of J_{dc} = 90 kA/cm^2 was not available. With J_{op} = 875 A/cm^2, J_{dc} increases to 49 kA/cm^2, 1.1 W output power is obtained and the junction temperatur. increases to 312°K at t = 1.8 ns. This temperature rise causes the dc voltage across the diode to increase and the bias current to decrease accordingly. J_{dc} decreases to 19 kA/cm^2, output power drops to zero and the junction temperature increases to 326°K at t = 5 ns. It can be seen that the photon injection can be used to trigger the RF oscillation. This RF oscillation can be short pulse or long pulse depending on the photon injection level, temperature behavior and the bias circuit configuration. It is apparent that a thermal instability occurs for J_{op} = 500 A/cm^2, and that the response is _very_ sensitive to the value of J_{op}.
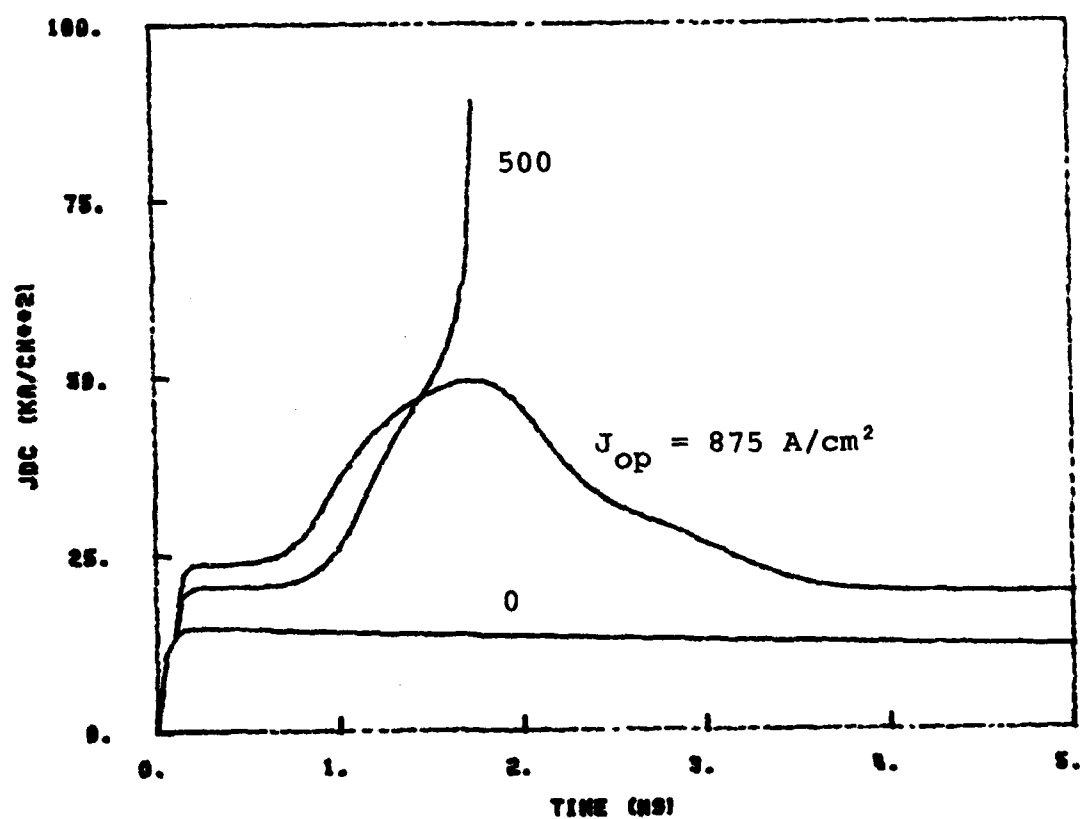
FIG. 3.17 RESPONSES OF THE BIAS CURRENT DENSITY WITH VARIOUS OPTICAL
CURRENT LEVELS APPLIED AT TIME = 0.1 ns.
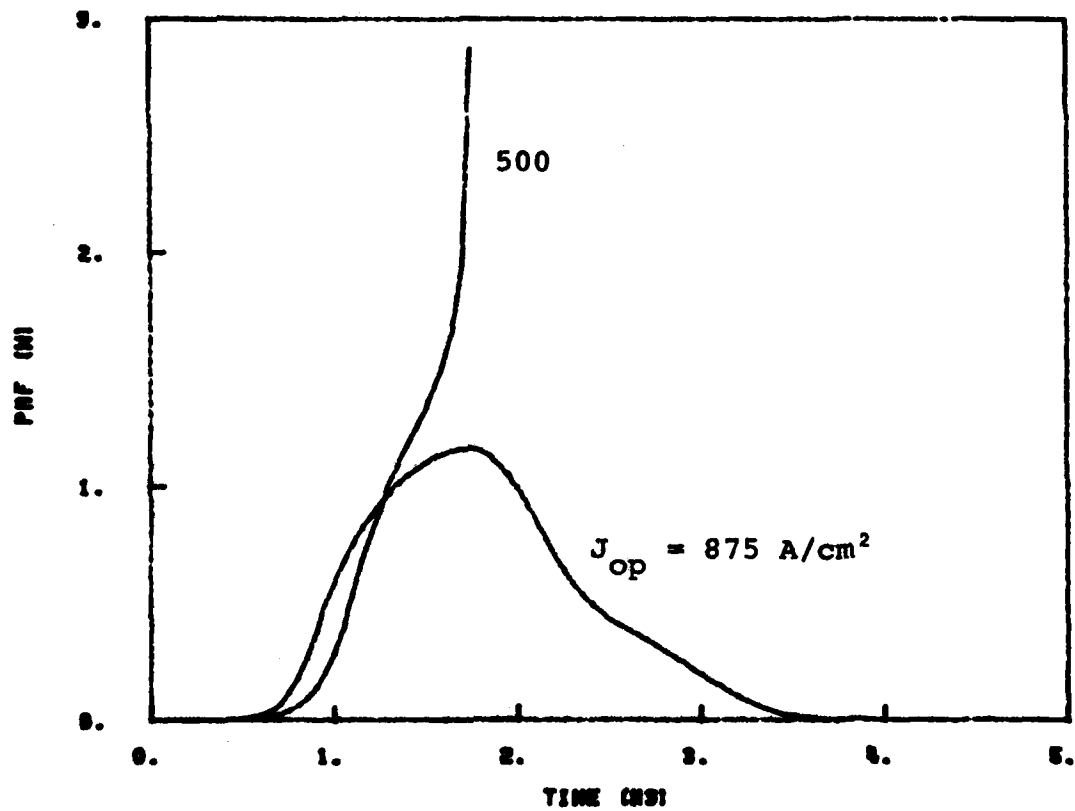
FIG. 3.18 RESPONSES OF THE OUTPUT POWER WITH VARIOUS OPTICAL CURRENT
LEVELS APPLIED AT TIME = 0.1 ns.
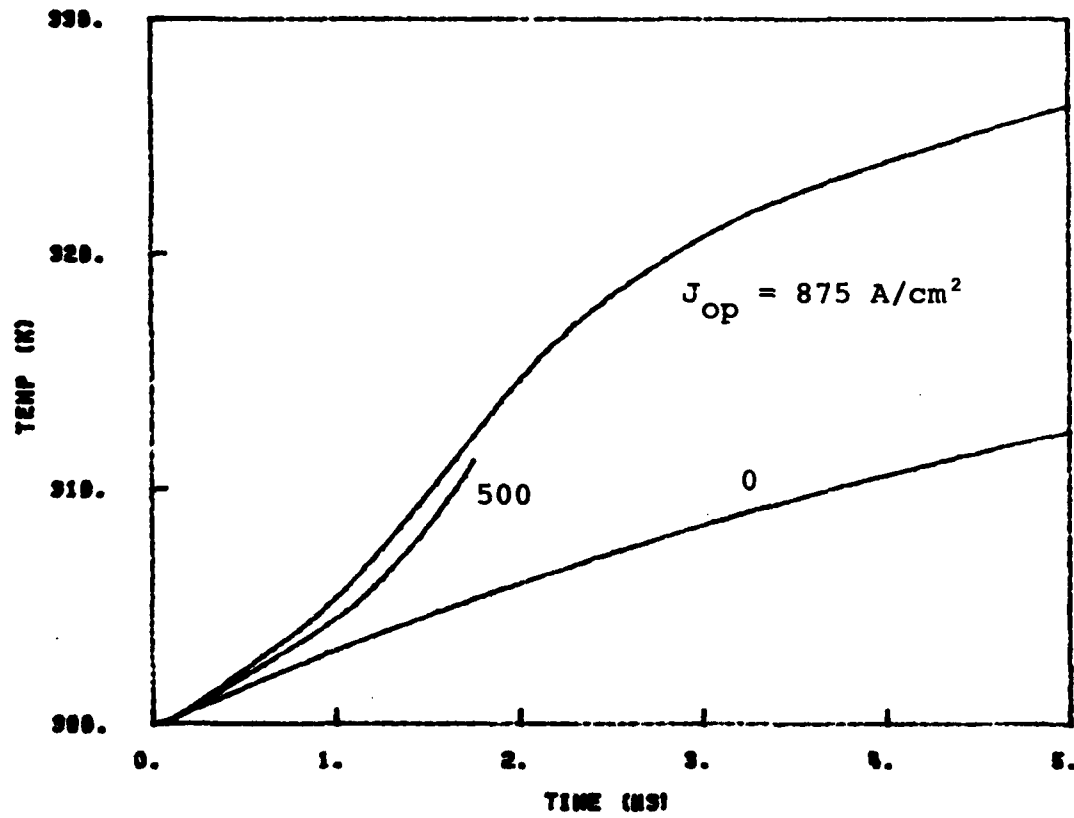
FIG. 3.19   RESPONSES OF THE JUNCTION TEMPERATURE WITH VARIOUS OPTICAL CURRENT LEVELS APPLIED AT TIME = 0.1 ns.

3.7 Turn-On Jitter

Turn-on jitter is the variation of the leading edge of
the output power with respect to the time the bias current pulse is
applied to the diode. Pulsed IMPATT oscillators show detectable
turn-on jitter. RF power displayed on an oscilloscope shows a
blurred front edge jitter. All exponentially growing systems
including pulsed oscillators must start from a finite amplitude
if they are to build up to a larger amplitude in a finite time.
In the case of the free-running IMPATT oscillator, the starting
level is generated by the high frequency component of the noise
voltage. The time-dependent RF voltage of the oscillator has an
amplitude which can be described by[21]

$$V_{RF}(t) = V_{RF}(0) \, e^{\sigma(t)t} \quad , \tag{3.18}$$

where $\sigma(t)$ is the time-dependent growth rate of the RF voltage,
and $V_{RF}(0)$ is the initial amplitude of the RF voltage at $t = 0$,
when the bias pulse is applied to the diode.

Since $V_{RF}(0)$ is noise generated, its amplitude may vary
from pulse to pulse. If the noise is purely random, it will
have Rayleigh probability distribution which has the form

$$P_r(x) = \begin{cases} \dfrac{x}{b} \, e^{-x^2/2b} & \text{for } x \geq 0 \\ 0 & \text{for all other cases} \end{cases} \quad , \tag{3.19}$$

where $b > 0$ and $x = V_{RF}(0)$.

The mean and the variance of this distribution are, respectively $u = \sqrt{b\pi/2}$ and $\sigma^2_{V_{RF}}(0) = (2 - \pi/2)b$ as is easily verified by direct integration. Figure 3.20 shows the Rayleigh probability distribution with $\sigma_{V_{RF}}(0) = 0.1$.

V_{ss} is the RF voltage at steady state, and t_{on} is defined as the time when V_{RF} increases to one half of V_{ss}. Figure 3.21 shows the decrease of t_{on} as initial RF voltage increases. All other devices ($J_{dc} = 60$ kA/cm^2) and circuit parameters are unchanged in the calculation. The mean of t_{on} is

$$\langle t_{on} \rangle = \int_0^\infty t_{on}(x) P_r(x) \, dx \quad . \tag{3.20}$$

The variance of t_{on} is

$$\int_0^\infty [t_{on}(x) - \langle t_{on} \rangle]^2 P_r(x) \, dx \quad . \tag{3.21}$$

The mean of t_{on} is 0.57 ns and σ_{jitter}, the standard deviation (square root of the variance) of t_{on}, is 6.55×10^{-2} ns with $\sigma_{V_{RF}}(0) = 0.1$ Figure 3.22 shows that σ_{jitter} increases with $\sigma_{V_{RF}}(0)$ as expected.

For a given diode and pulse generator, the bias circuit and microwave circuit can be optimized to achieve the minimum turn-on jitter of a free-running oscillator. With an external injection signal or optical injection, the successive pulses start from relatively constant $V_{RF}(0)$. Thus the jitter can be greatly reduced.
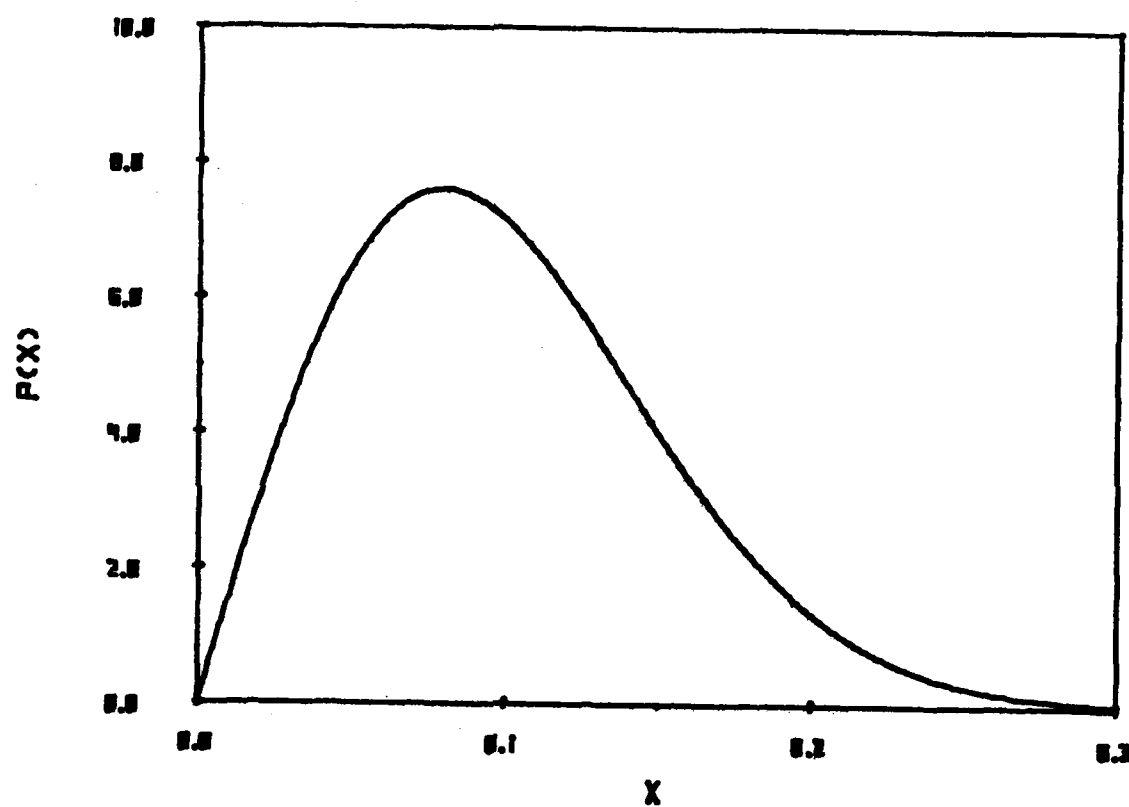
FIG. 3.20 RAYLEIGH PROBABILITY DISTRIBUTION.
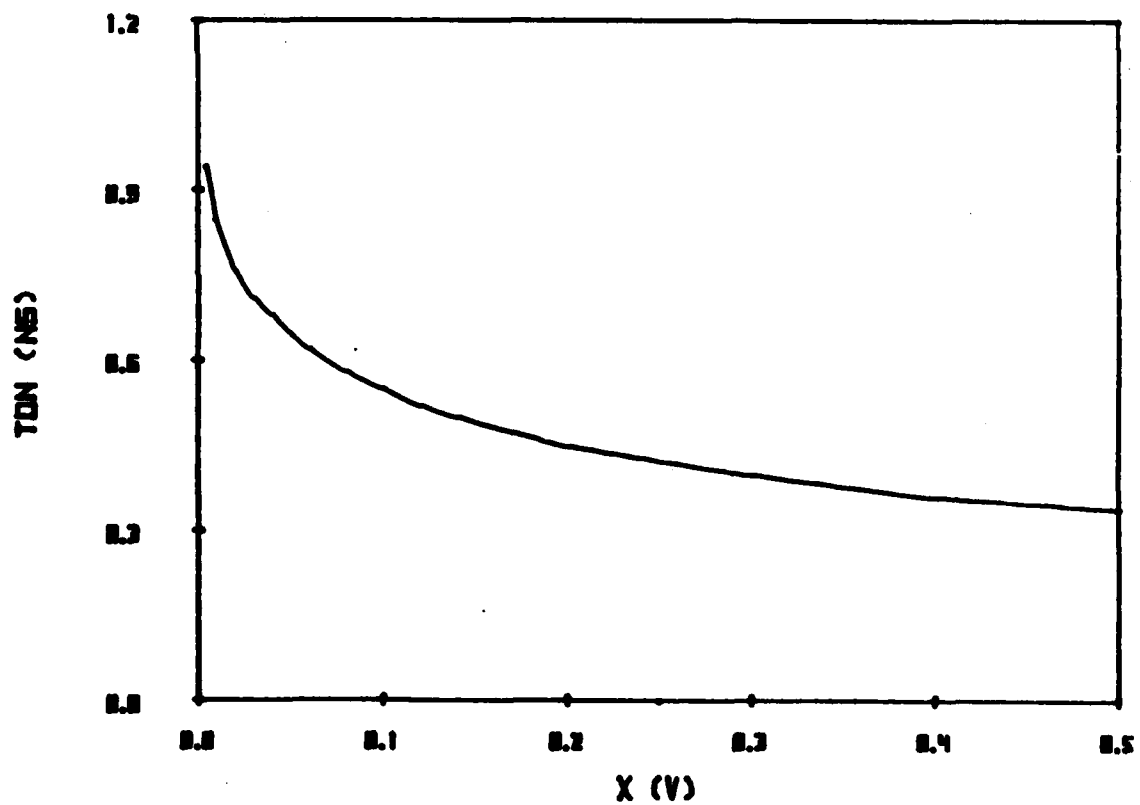
FIG. 3.21 DECREASE OF TURN-ON TIME AS INITIAL RF VOLTAGE INCREASES.
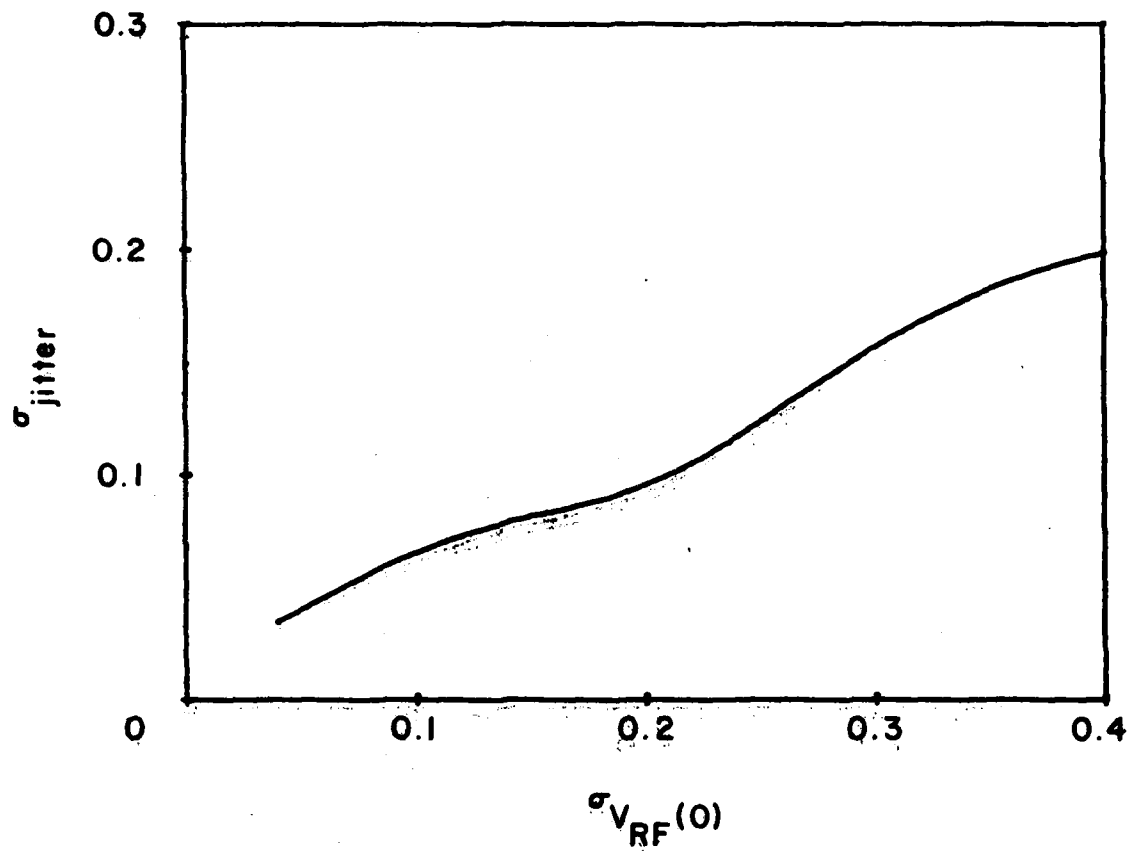
FIG. 3.22   INCREASE OF σ_{jitter} WITH INCREASING $\sigma_{V_{RF}(0)}$.

3.8 Effect of Ambient Temperature

In this section the effect of ambient temperature on the turn-on transient will be described. Reliability of a semiconductor device is a function of its operating junction temperature T_j. In order to maintain the desired reliability, the maximum junction temperature $T_{j,max}$ is constrained, as is the allowed junction temperature increase $\Delta T = T_{j,max} - T_a$, where T_a is the ambient temperature. An oscillator operated under high ambient temperature (smaller ΔT) generates less output power since the bias current is limited by ΔT. IMPATT diodes can be operated at lower bias current to improve reliability at the expense of reduced output power. Devices operated at a lower T_a may generate additional power by application of higher bias current.

For $J_{dc} = 60$ kA/cm^2, the magnitude of the small-signal G_d at 300°K is larger or smaller than the magnitude at 500°K depending on whether oscillation frequency f is greater or less than 134 GHz, respectively. Figure 3.23 shows the buildup of RF power as a function of ambient temperature. T_a varies from 270 to 330°K. Since oscillation frequency at t = 0 is 135 GHz, the initial growth rate decreases, and the turn-on time increases with increasing ambient temperature. Output power at steady state increases with ambient temperature as expected.

3.9 Conclusions

In this chapter the oscillator model developed in Chapter II was used to study the dependence of oscillator turn-on transients
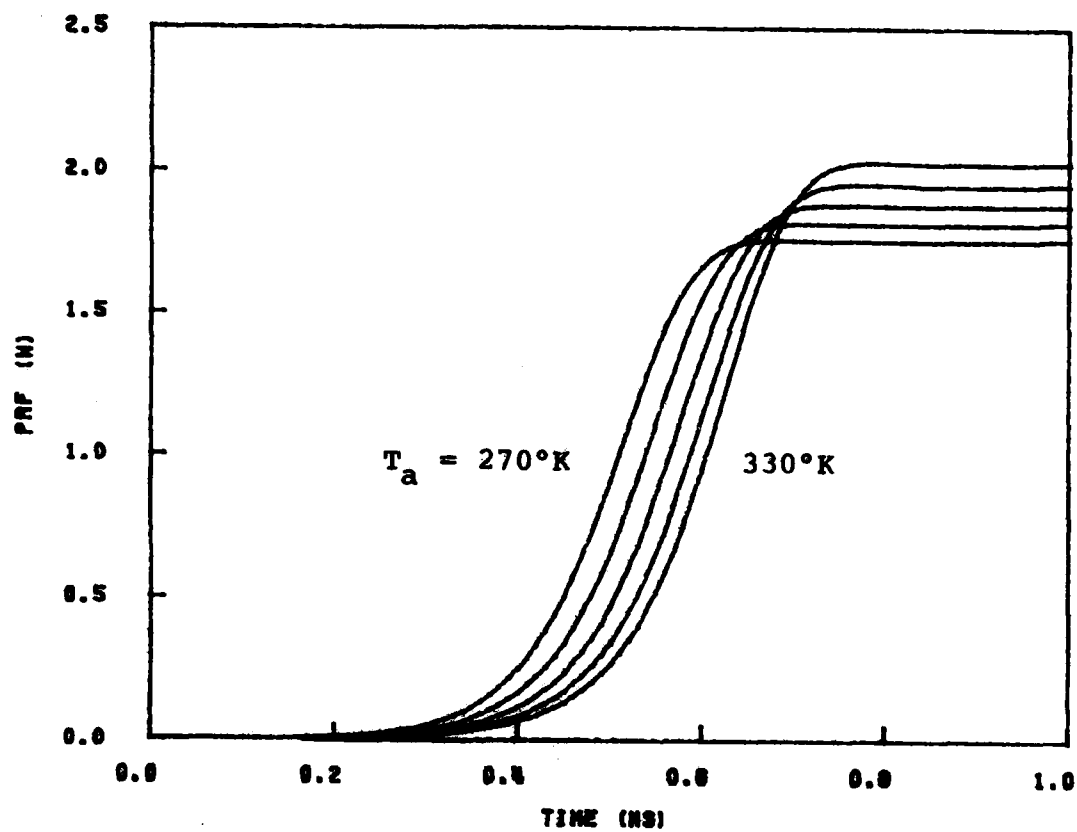
FIG. 3.23 BUILDUP OF OUTPUT POWER AS A FUNCTION OF AMBIENT TEMPERATURE.

on bias current, RF circuit characteristics, bias circuit
characteristics, injection locking, photon injection and ambient
temperature. As the bias current increased, the output power and
oscillation frequency increased at steady state. With increasing RF
circuit Q, the delay time between the bias pulse and output power
increased while the frequency drift during turn-on decreased. When
a constant voltage source with finite impedance was used as bias cir-
cuit, the bias current increased, and the output power built up after
the step increase of the voltage source. As the injection current
increased, the initial RF voltage increased, and the output power built
up faster. With increasing optical current, turn-on time increased,
output power decreased and operating frequency increased at steady
state when the diode was biased with a constant current source. Photon
injection was used to trigger RF oscillation when a constant voltage
source with finite impedance was used as bias circuit. Increase of
σ_{jitter} of a free-running oscillator with increased $\sigma_{V_{RF}(0)}$ was
illustrated. The effect of ambient temperature on the turn-on transient
was also described. The information obtained in this chapter can be
used to improve the performance of pulsed IMPATT oscillators. The
RF circuit can be designed to achieve minimal turn-on time. Injection
locking and photon injection can be used to reduce the turn-on jitter
and tune the oscillation frequency.

CHAPTER IV.   CONTROL OF THE POST TURN-ON TRANSIENT

4.1   Introduction

Millimeter-wave oscillators can have a wide range of duty cycles (continuous wave, short pulse, and long pulse). One of the problems in millimeter-wave pulsed IMPATT oscillators is the frequency drift caused by the temperature rise of the diode during the bias pulse. The high bias current required for high power oscillation results in a negative frequency drift of several percent during the pulse as described in Chapter II.

For some systems, post turn-on frequency drift is acceptable. For others the combination of frequency drifts caused by device temperature rise and ambient temperature variation may take the oscillation frequency out of the receiver bandwidth or compromise some other system parameters. It is, therefore, often desirable to reduce or eliminate the post turn-on frequency drift. To improve the post turn-on frequency drift of pulsed oscillator, a number of techniques are available[22,23] including the following: (1) varying the dc bias voltage of a varactor diode located near the IMPATT diode; (2) high Q circuit; (3) using a CW oscillator followed by a microwave switch (such as a PIN diode); (4) use of a capacitor with negative temperature coefficient; (5) shaping the bias current waveform; (6) applying a time-dependent optical injection while the bias current remains constant, and (7) injection locking. These techniques have various advantages and disadvantages. The first four techniques are discussed briefly here, and the others are described in the following sections.

4.1.1 Varactor Compensation. By inserting a varactor diode $n\lambda_g/2$ away from the diode, a small but useful amount of electronic tuning can be obtained. The frequency in a pulsed solid-state oscillator has an almost exponential dependence with time as shown in Chapter II. By applying a nonlinear upward voltage biasing $V(t)$ to the varactor [$V(t)$ increases with time during the pulse], the susceptance of the varactor decreases with time. Therefore, the frequency of the oscillator can be adjusted to increase during the pulse by almost the same magnitude as the frequency drop caused by device heating.

4.1.2 High Q Circuit. Post turn-on frequency drift can be improved by using a high Q circuit as shown in Chapter 11. A smaller drift value ($\Delta f/\Delta t$) can be achieved by this method. However, the delay time between the output power and the bias pulse increases with circuit Q.

4.1.3 Microwave Switch. When a CW oscillator is followed by a microwave switch, the low drift pulsed oscillator can be realized, and the problem of turn-on transient may also be avoided by turning on and off the microwave switch appropriately. This technique reduces the frequency drift during the pulse but at the expense of less peak power and an extra component (microwave switch). The peak power of the oscillator is limited to the maximum output power under CW condition.

4.1.4 Capacitor with Negative Temperature Coefficient. A simple frequency stabilization method using a ceramic dielectric has been demonstrated by Kondo.[24] The increase of diode capacitance causes the oscillation frequency to shift lower when the bias current is held constant, and the cavity expansion due to the temperature rise also

invites the same result on frequency response. When a ceramic capacitor C with a negative temperature coefficient (C decreases with temperature) is loaded in parallel with the diode package, the susceptance changes of the diode and cavity are compensated, and the oscillator would have less post turn-on frequency drift. Advantages of this technique are simplicity and low cost.

4.2 Bias Current Compensation

Since the device admittance is dependent on the bias current, the amount of post turn-on frequency drift can be controlled by shaping the waveform of bias current pulse applied to the diode. Device conductance G_d and susceptance B_d of the IMPATT diode both decrease with an increase of the bias current. The influence of the bias current shaping on the frequency drift can be understood qualitatively from Eq. 4.1 which has been derived in Chapter II:

$$\frac{\partial(B_d + B_c)}{\partial f} \Delta f = A_1 \Delta T + A_2 \Delta I_{dc} , \qquad (4.1)$$

where

$$A_2 = \frac{\partial B_d}{\partial V_{RF}} \frac{1}{\partial G_d / \partial V_{RF}} \frac{\partial G_d}{\partial I_{dc}} - \frac{\partial B_d}{\partial I_{dc}} . \qquad (4.2)$$

Both the first and the second terms $(\partial B_d / \partial I_{dc})$ of Eq. 4.2 are negative, so that the sign of A_2 has to be determined quantitatively. To evaluate the current coefficient A_2, the following parameters estimated at the operating point when $T_j = 300°K$ and $J_{dc} = 60$ kA/cm^2 are used for the millimeter-wave IMPATT diode: $\partial B_d / \partial V_{RF} = 1.09 \times 10^{-2}$ mho/V, $\partial G_d / \partial V_{RF} = 2.1 \times 10^{-3}$ mho/V, $\partial G_d / \partial I_{dc} = -1.83 \times 10^{-2}$ mho/A, and $\partial B_d / \partial I_{dc} = -1.14 \times 10^{-1}$ mho/A.

When these parameters are substituted into Eq. 4.2, the value of A_2 is obtained as

$$A_2 = -9.5 \times 10^{-2} + 1.14 \times 10^{-1} = 1.9 \times 10^{-2} \text{ mho/A} \quad .$$

It has been demonstrated that frequency decreases with temperature ($A_1 < 0$). The calculated result ($A_2 > 0$) suggests that an appropriate bias current waveform can be used to compensate the variation of the device admittance due to the thermal effect and provide an improvement of the frequency drift produced in the pulsed oscillator. In this chapter a post-in-waveguide circuit is used as the circuit model. The circuit and package parameters are described in the appendix.

An increase of dc current results in more dissipated power and accordingly more temperature rise. To compare the effects of various bias current waveforms on the frequency drift, the temperature rise during the pulse has to be taken into consideration. Figure 4.1 shows the various bias current density waveforms used to study the effects of current shaping on the frequency drift and power variation of pulsed IMPATT oscillators. For curve E, current density J_{dc} increases from 45 to 75 kA/cm² linearly during the 40-ns pulsewidth. The current waveforms are chosen to give roughly the same junction temperature rise ΔT.

Figure 4.2 shows the frequency responses of the pulsed oscillator under various current waveforms. When there is no current compensation (curve B), the junction temperature rise is 167.5°C, and the frequency decrease caused by the temperature rise is 3.7 GHz (frequency decreases from 119.1 to 115.4 GHz). The temperature coefficient ($f_d/\Delta T$) is
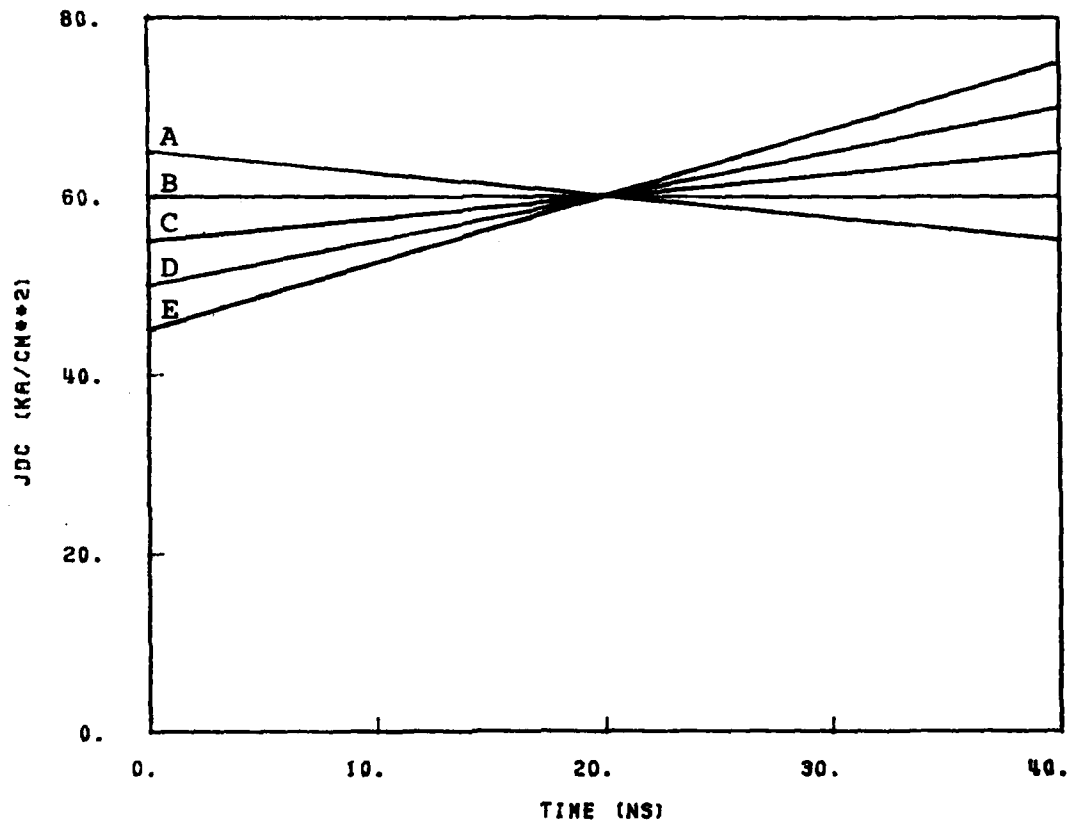
FIG. 4.1 VARIOUS BIAS CURRENT WAVEFORMS USED TO STUDY THE EFFECTS OF
CURRENT SHAPING ON THE FREQUENCY DRIFT AND POWER VARIATION
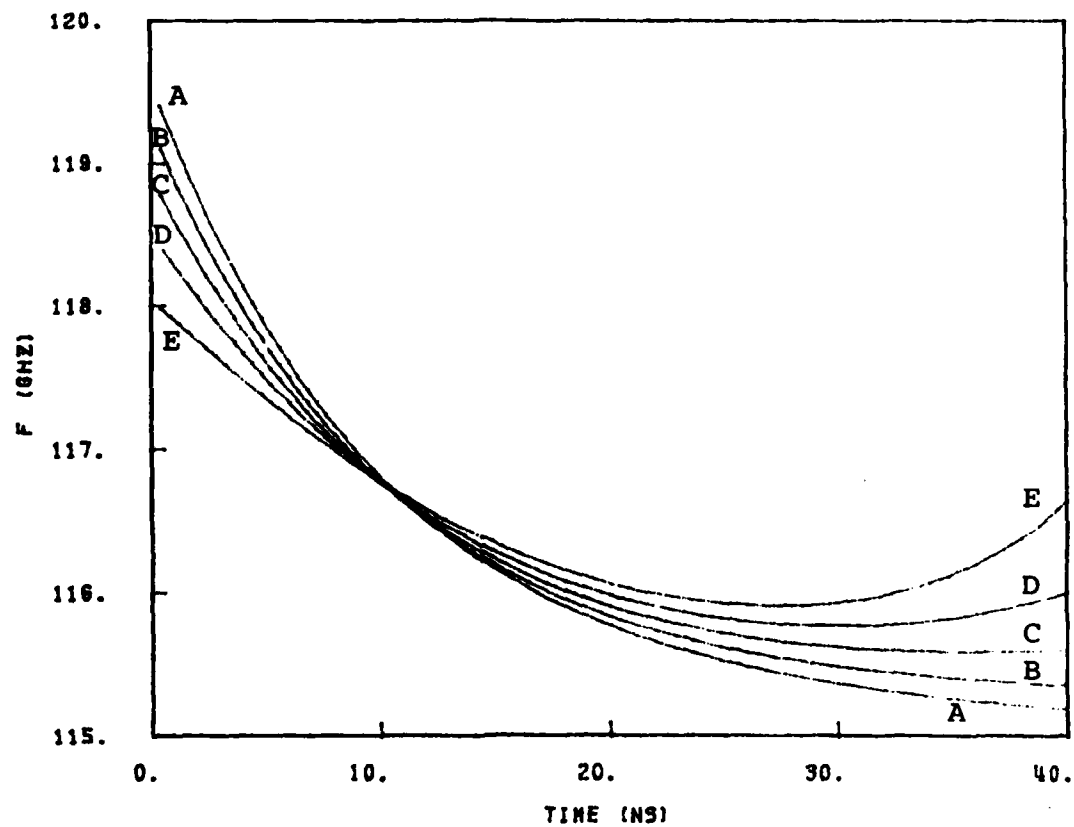OF PULSED OSCILLATOR.

FIG. 4.2 FREQUENCY RESPONSES OF THE PULSED OSCILLATOR UNDER VARIOUS
BIAS CURRENT WAVEFORMS.

22.1 MHz/°C, where f_d is defined as the difference between the maximum frequency f_{max} and the minimum frequency f_{min}. The temperature rise of the oscillator with current compensation (curve E) is 187.7°C, and f_d is 2.1 GHz (f_{max} = 118.0 GHz, f_{min} = 115.9 GHz). The temperature coefficient 11.2 MHz/°C is only one-half of that due to the flat current. It can be seen that the frequency drift is varied by biasing the diode with a current pulse having a time-dependent amplitude, and the amount of frequency drift f_d decreases with upward current compensation. For curve E, the oscillation frequency decreases from 118.0 to 115.9 GHz and then increases to 116.6 GHz. The reason for this frequency increase is that the frequency drop caused by the thermal effect is over-compensated by the current increase.

Figure 4.3 shows the power variation of the pulsed oscillator under various bias current waveforms. When there is no current compensation, output power increases from 1.3 to 3.27 W. With upward current compensation (curve E), output power increases from 1.03 to 4.15 W. It can be seen that the amount of power variation increases with an upward current waveform although the frequency drift is improved.

Since the temperature increases and frequency decreases exponentially in the time domain, an exponentially increasing current waveform may achieve less frequency drift than that due to a linearly increasing current waveform. Figure 4.4 shows the exponentially increasing current waveforms used to study the effects of exponentially and linearly increasing current waveforms on the frequency drift. For curve I, current density J_{dc} = 75 + (45 - 75) $e^{-t/\tau_{th}}$ kA/cm^2, where τ_{th} (11.24 ns) is the thermal time constant. Figure 4.5 shows the
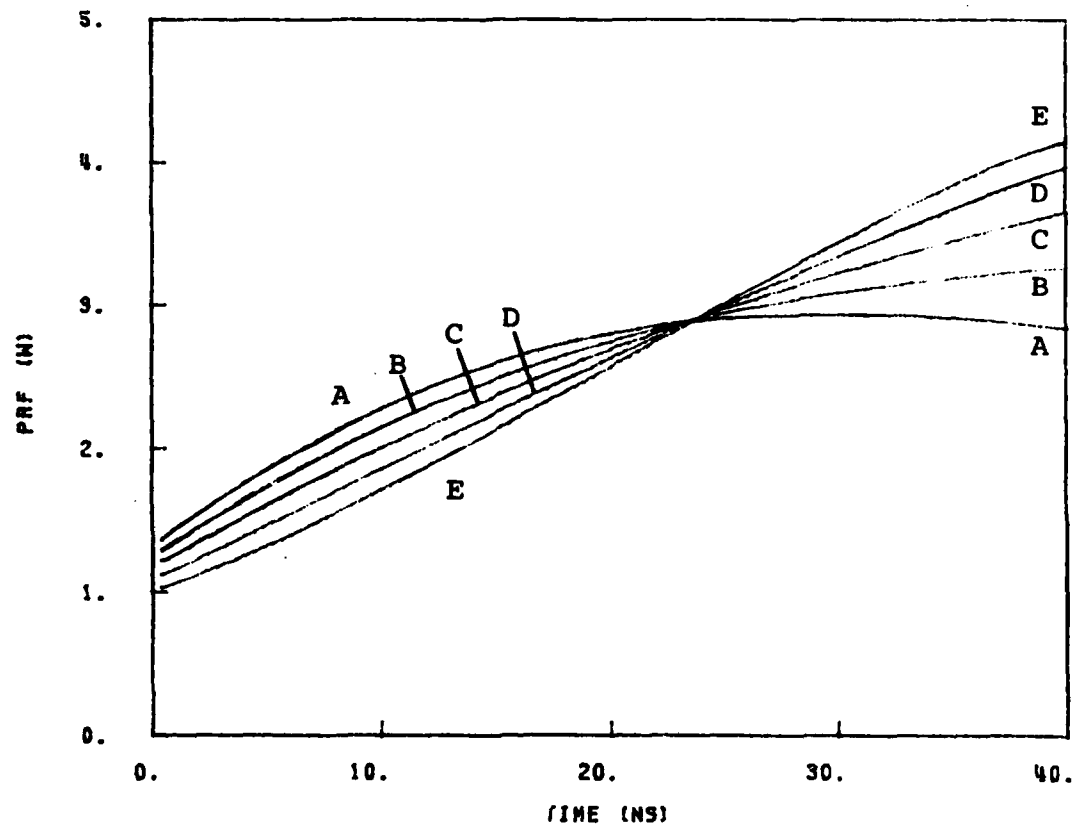
FIG. 4.3 POWER VARIATIONS OF THE PULSED OSCILLATOR UNDER VARIOUS

BIAS CURRENT WAVEFORMS.
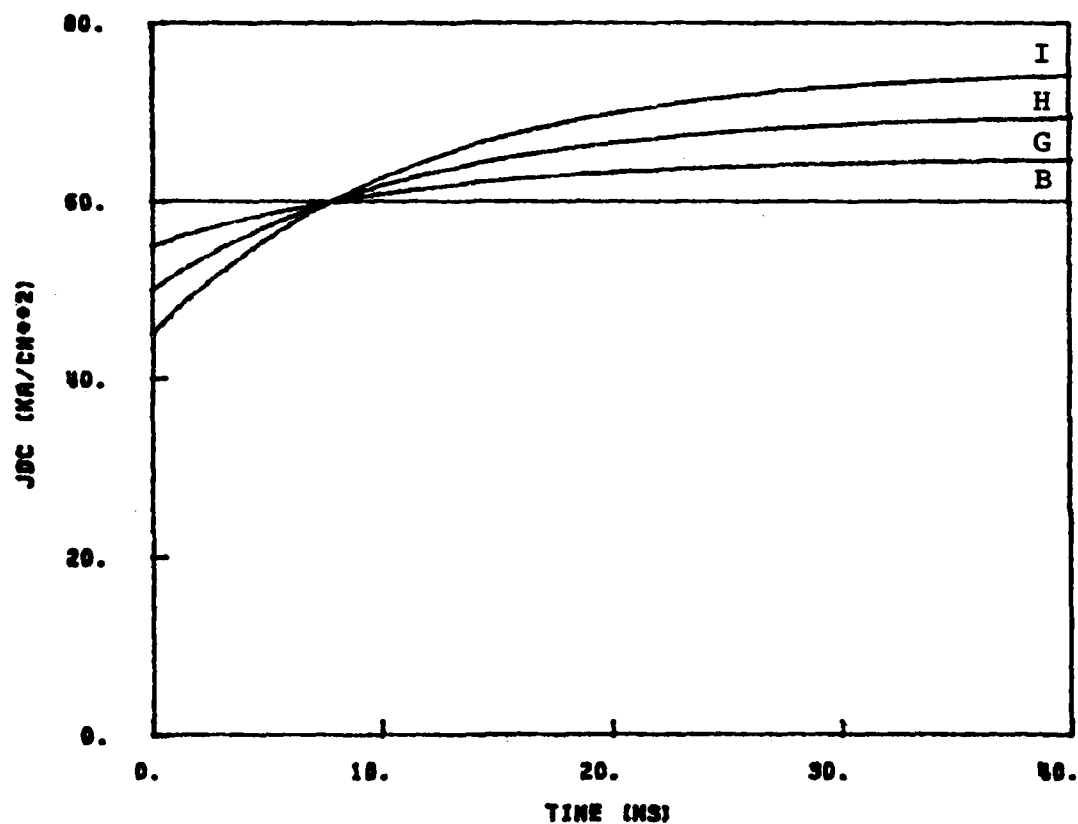
FIG. 4.4 EXPONENTIALLY INCREASING CURRENT WAVEFORMS USED TO STUDY THE
EFFECTS OF EXPONENTIALLY AND LINEARLY INCREASING CURRENT
WAVEFORMS ON THE FREQUENCY DRIFT.
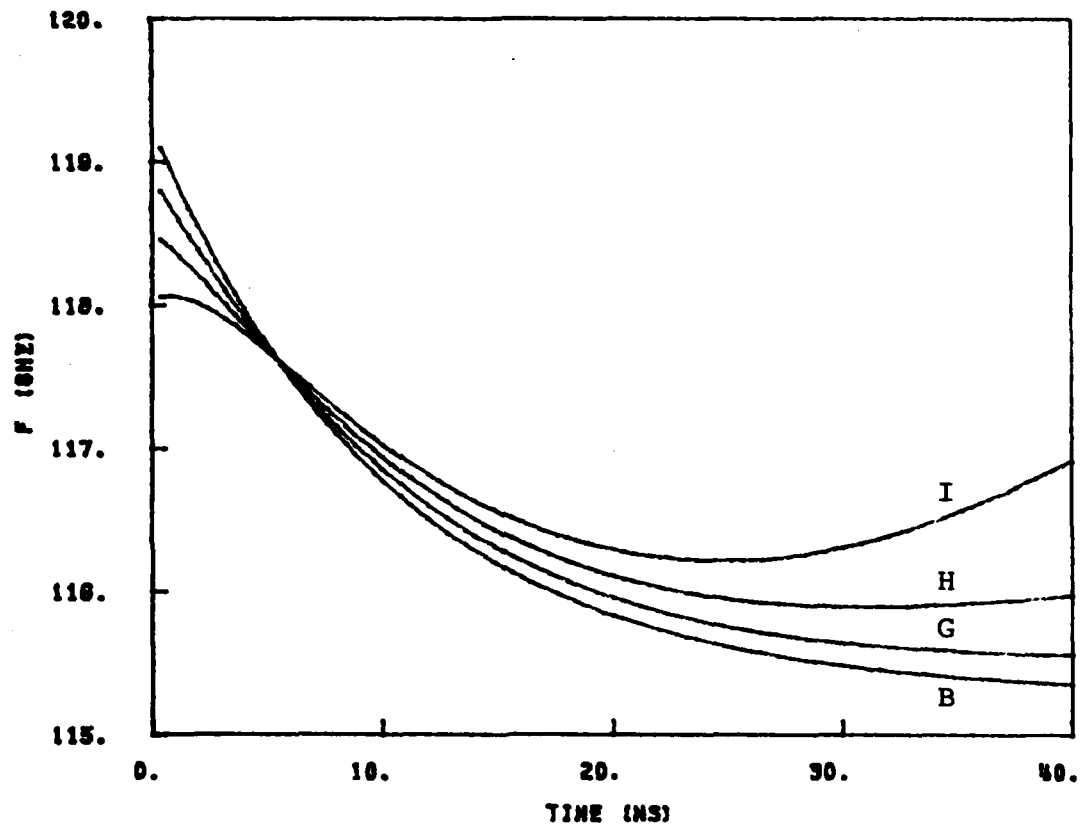
FIG. 4.5 FREQUENCY RESPONSES OF THE PULSED OSCILLATOR WITH EXPONEN-
TIALLY INCREASING CURRENT WAVEFORMS.

frequency responses of the pulsed oscillator with exponentially increasing current waveforms. For curve I, the temperature rise of the diode is $202°C$, and f_d is 1.9 GHz (f_{max} = 118.1 GHz, f_{min} = 116.2 GHz). The temperature coefficient of 9.4 MHz/°C is better than that of curve E (11.2 MHz/°C, J_{dc} increases from 45 to 75 kA/cm^2 linearly).

4.3 Current Waveform $I_{dc}(t)$ to Achieve Minimal Post Turn-On Frequency Drift

Although the post turn-on frequency drift can be reduced with linearly or exponentially increasing current waveform, it is still desirable to have a current waveform $I_{dc}(t)$ such that the minimal frequency drift during the pulse is obtained. This optimum current waveform can be derived from Eq. 2.23:

$$I_{dc}(t_1 + \Delta t) = I_{dc}(t_1) + \Delta I_{dc} \quad ,$$

where Δt is the time step, and ΔI_{dc} is the difference of dc current at $t_1 + \Delta t$ and t_1.

Then, if $\Delta f = 0$ (no frequency drift during Δt) is assumed, Eq. 2.23 becomes

$$\begin{aligned}
\Delta I_{dc} &= -(A_1/A_2)\Delta T \\
&= -(A_1/A_2)R_{th}P_d \\
&= -(A_1/A_2)R_{th}(V_{dc}I_{dc} - P_{RF}) \\
&= -(A_1/A_2)R_{th}\{[V_B(T) + R_{sc}I_{dc} + V_R(V_{RF},T)]I_{dc} - P_{RF}\} \quad ,
\end{aligned}$$

$$(4.3)$$

where

$$A_1 = \frac{\partial B_d}{\partial V_{RF}} \; \frac{1}{\partial G_d/\partial V_{RF}} \; \frac{\partial G_d}{\partial T} - \frac{\partial B_d}{\partial T} \quad ,$$

$$A_2 = \frac{\partial B_d}{\partial V_{RF}} \; \frac{1}{\partial G_d/\partial V_{RF}} \; \frac{\partial G_d}{\partial I_{dc}} - \frac{\partial B_d}{\partial I_{dc}} \quad ,$$

and ΔT is the difference of junction temperature at $t_1 + \Delta t$ and t_1.

When the temperature dependence of circuit admittance is negligible ($\partial B_c/\partial T = 0$), A_1, A_2, R_{th}, V_B, R_{sc} and V_R depend on the device dc and large-signal properties only. These parameters (dc and large-signal device admittance as functions of RF voltage, temperature, and dc current) are known at the frequency range of interest, and the optimum current waveform $I_{dc}(t)$ to achieve minimal frequency drift can be determined.

Figure 4.6 shows the optimum current waveform $J_{dc}(t)$ obtained from Eq. 4.3. The current density J_{dc} increases from 31.5 to 71.2 kA/cm^2. This waveform is chosen such that the temperature rise during the pulse is the same as that from a constant current pulse. Figure 4.7 shows the frequency responses caused by the optimum current waveform and constant current bias. It can be seen that constant frequency is achieved during the pulse with optimum current waveform. This waveform can be obtained through a pulse modulator.[16] The pulse modulator must provide fast rise-time current pulses and proper adjustment for current shaping. The magnitude of frequency drift can then be adjusted for a specific application.
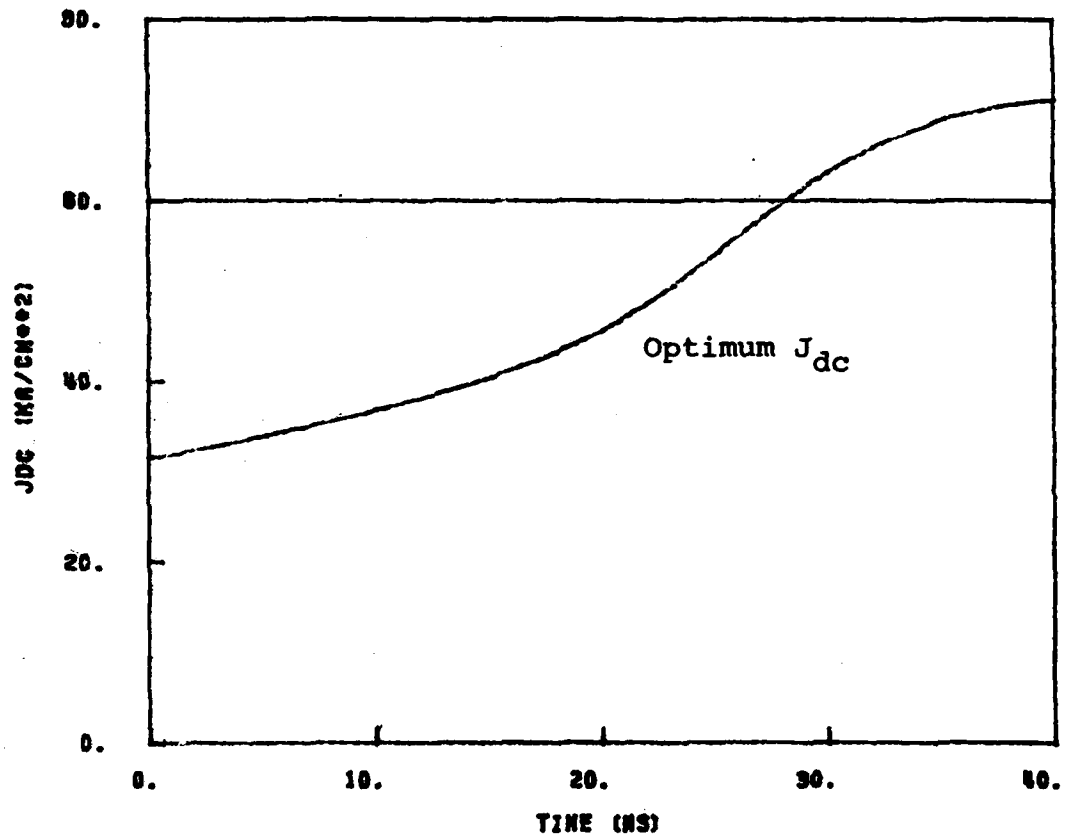
FIG. 4.6   OPTIMUM CURRENT WAVEFORM TO ACHIEVE MINIMAL POST TURN-ON

FREQUENCY DRIFT.
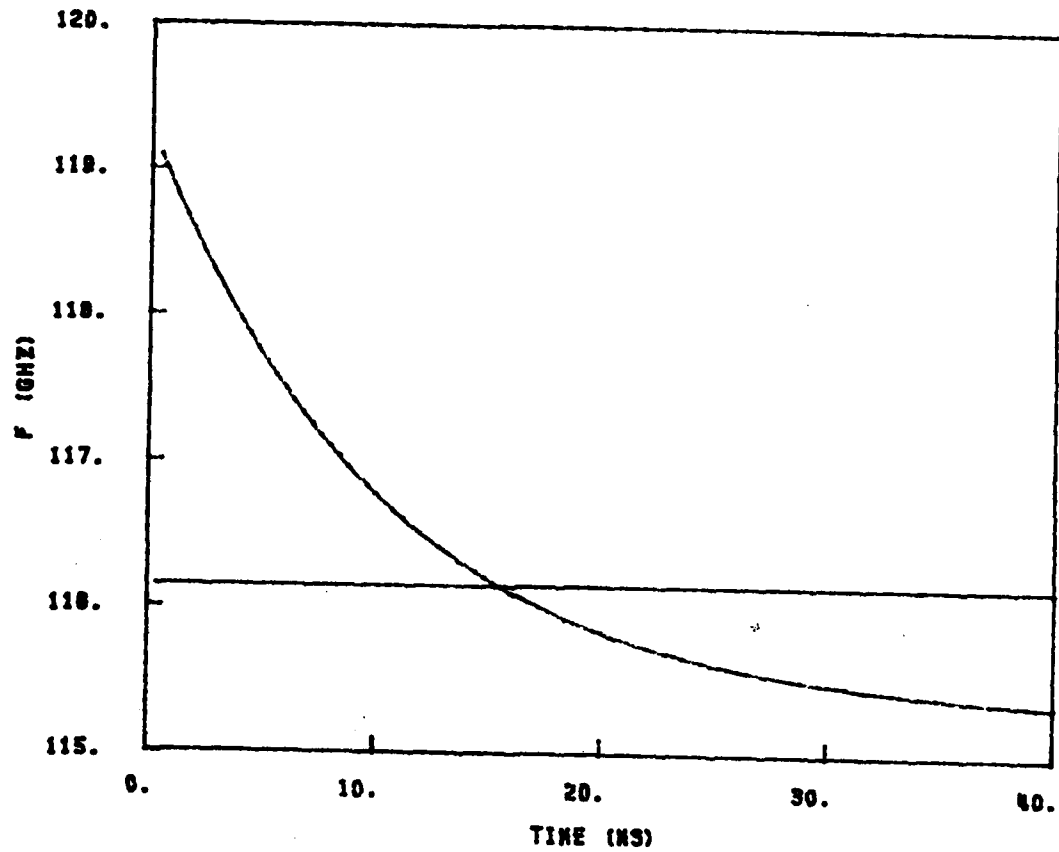
FIG. 4.7 FREQUENCY RESPONSES CAUSED BY THE OPTIMUM CURRENT WAVEFORM
AND CONSTANT CURRENT BIAS.

4.3.1 <u>Dependence of Optimum Current Waveform on the Operating Point</u>. Three operating points (A, B and C) as shown in Fig. 4.8 are used to illustrate the dependence of optimum current waveform on the operating condition. The operating points A, B and C are chosen to have maximum power at f = 115, 124 and 130 GHz, respectively, with bias current density J_{dc} = 30 kA/cm^2. The device diameter is 50 μm and the microwave circuit parameters used for different operating points are shown below.

Operating Point	G (mmho)	L (h)	C (pF)
A	19.3	1.34×10^{-12}	1.25
B	23.9	1.01×10^{-12}	1.44
C	25.9	8.89×10^{-13}	1.37

These circuit parameters are chosen to have $Q_{L,C}$ = 50. Figure 4.9 shows the optimum current waveforms for these operating points. It can be seen that the bias current may increase or decrease with time depending strongly on the operating point. J_{dc} increases with time for operating point A and decreases with time for operating point C. For the operating point b, bias current remains relatively constant during the pulse. Frequency drift during the pulse is eliminated for each operating point. Figure 4.10 shows the output power responses for these optimum current waveforms. The power variation during the pulse is very small for the operating point B. Figs. 4.9 and 4.10 indicate the possibility that constant frequency can be obtained with a constant bias current (case B) by proper selection of the operating point.

FIG. 4.8   THREE OPERATING POINTS USED TO STUDY THE DEPENDENCE OF
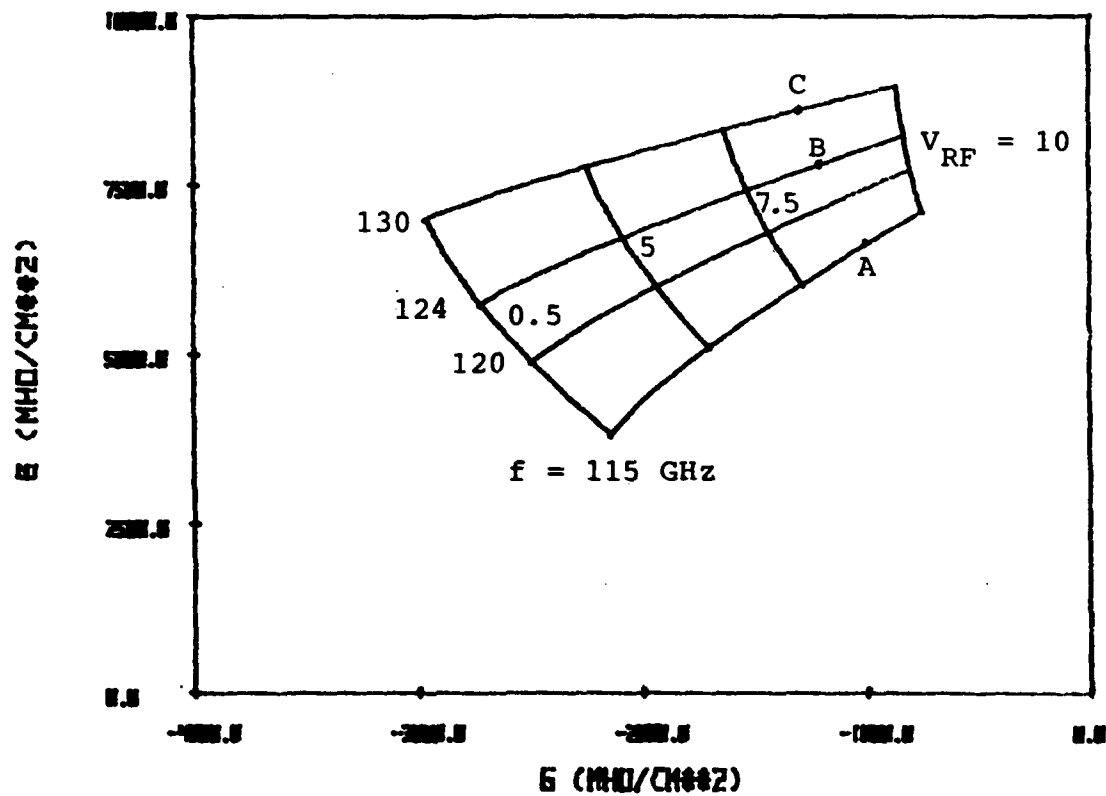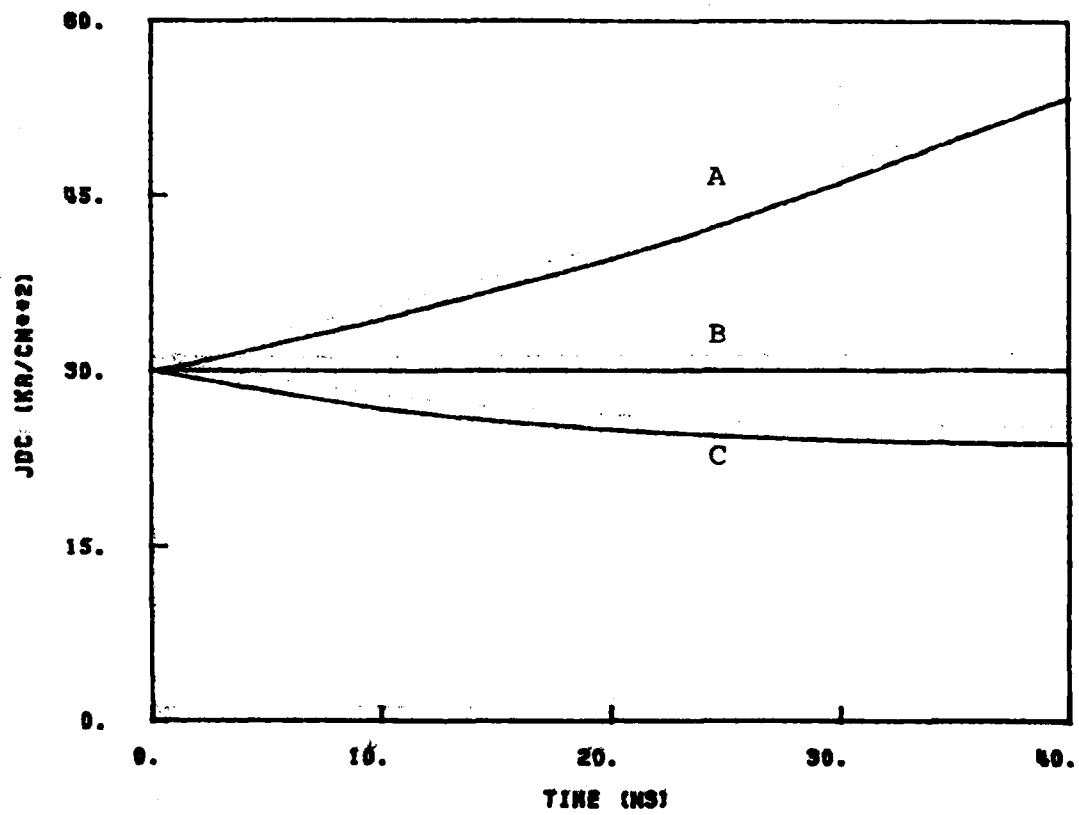OPTIMUM CURRENT WAVEFORM ON THE OPERATING POINT.

FIG. 4.9 OPTIMUM CURRENT WAVEFORMS FOR VARIOUS OPERATING POINTS.
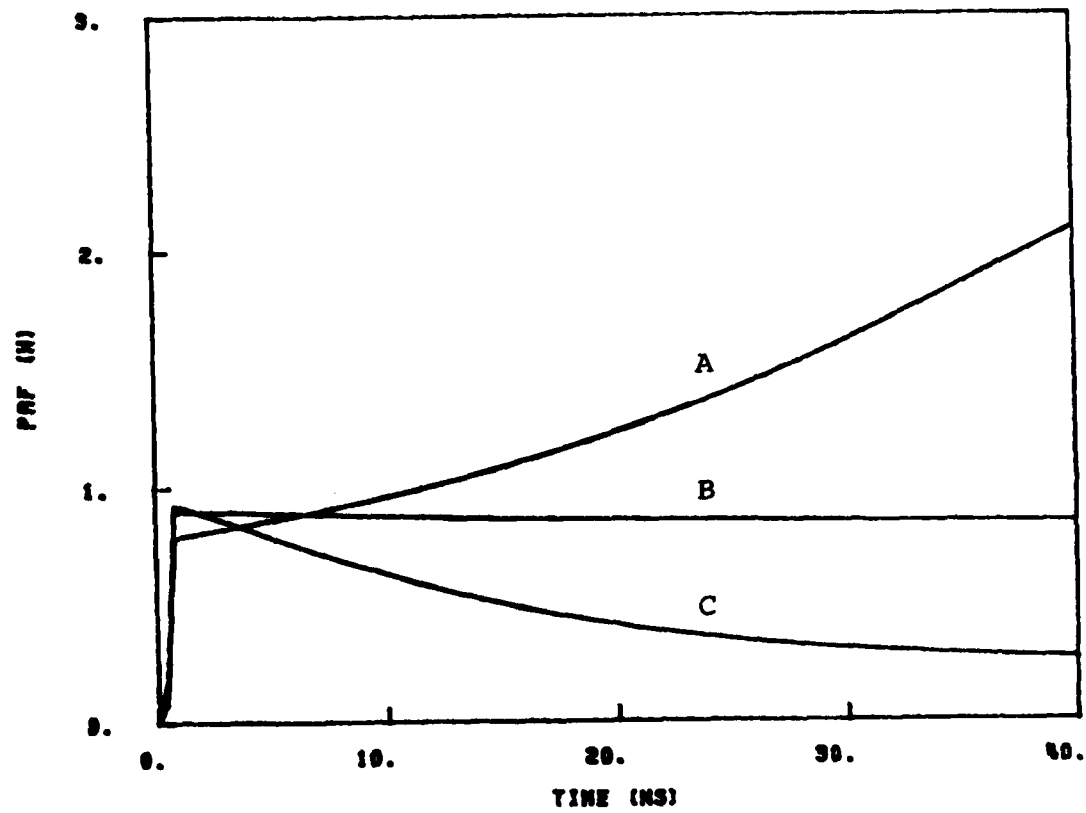
FIG. 4.10 OUTPUT POWER RESPONSES FOR VARIOUS OPERATING POINTS.

4.3.2 Device Preheating. Frequency drift can be reduced by heating the device to the steady-state temperature in a short time and keeping the temperature constant for the rest of the pulsewidth. Since the frequency drift is caused by the temperature rise, the frequency will remain constant after the steady-state temperature is reached. This preheating technique is demonstrated through an example in this section. Figure 4.11 shows a preheating bias current waveform. The bias current density J_{dc} increases from 0 to 90 kA/cm^2 with finite rise time of 1 ns, remains at 90 kA/cm^2 until t = 7.5 ns, decreases from 90 to 30 kA/cm^2 in 1 ns and remains at 30 kA/cm^2 for the rest of the pulsewidth. It can be seen from Fig. 4.12 that the junction temperature increases from 300 to 385°K in 8.5 ns and remains at that temperature. The junction temperature can be increased to this steady-state value in a shorter time by applying a higher bias current. The maximum current density used in the simulation program is 60 kA/cm^2. Although a higher bias current can be used in a practical oscillator circuit, J_{dc} of 90 kA/cm^2 is the highest possible current density used in the simulation program to generate meaningful results. The temperature response of a flat current pulse (J_{dc} = 30 kA/cm^2) is also shown for comparison. Figure 4.13 shows that the frequency is constant (f = 115 GHz) after t = 8.5 ns. The frequency transient before t = 8.5 ns is undesirable and can be reduced by faster preheating.

One disadvantage of this technique is that the power used to heat the device does not generate the RF power at the desired frequency. In the example, the operating efficiency is only 55 percent. The operating efficiency η is defined by

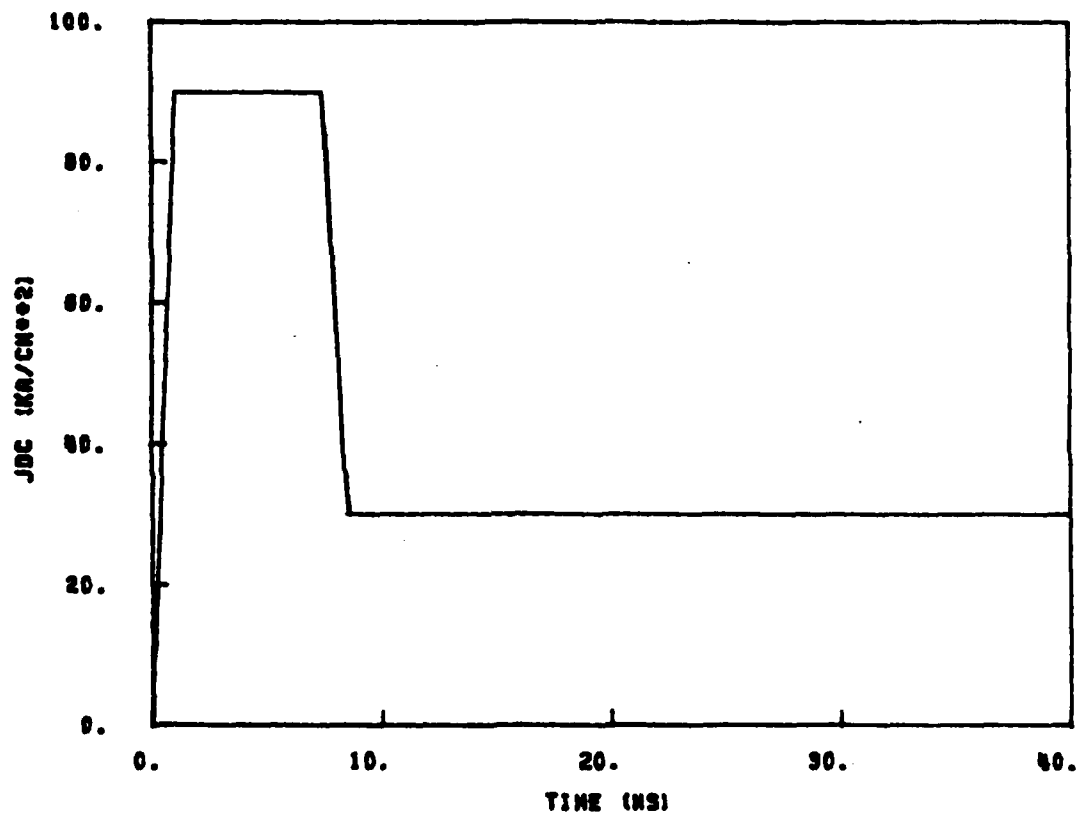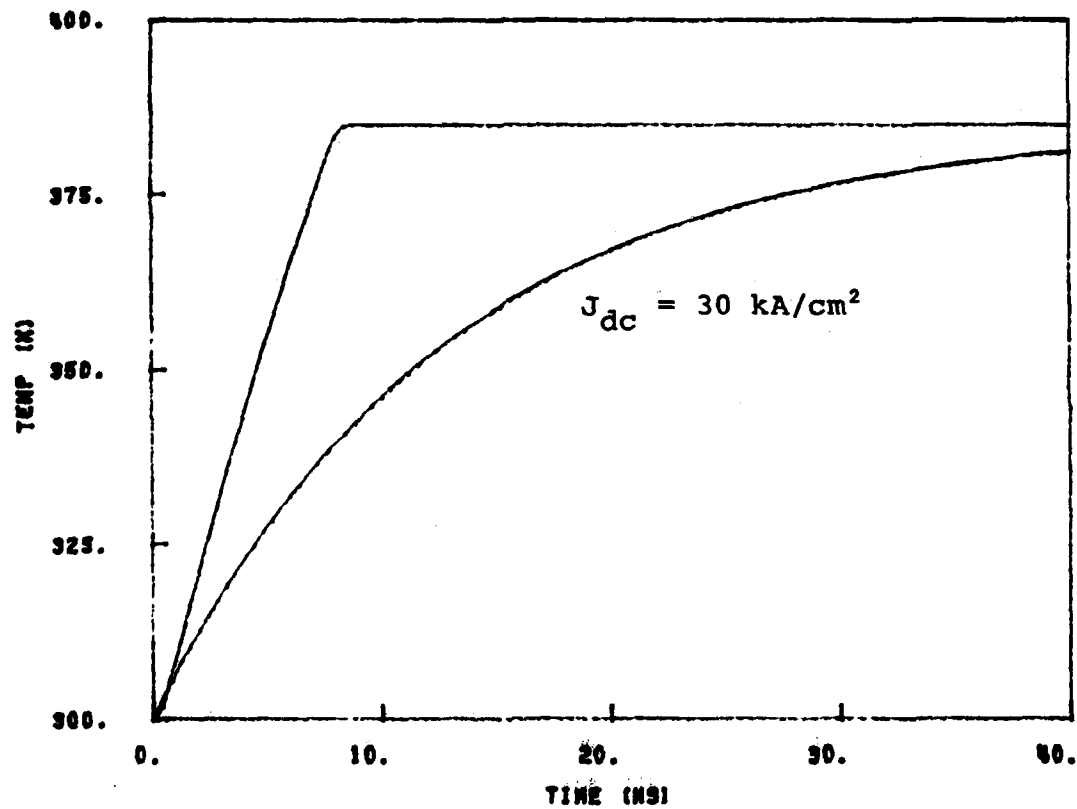FIG. 4.11 BIAS CURRENT WAVEFORM TO PREHEAT THE DEVICE.

FIG. 4.12 TEMPERATURE RESPONSES OF THE PREHEATING CURRENT WAVEFORM
AND FLAT CURRENT PULSE.
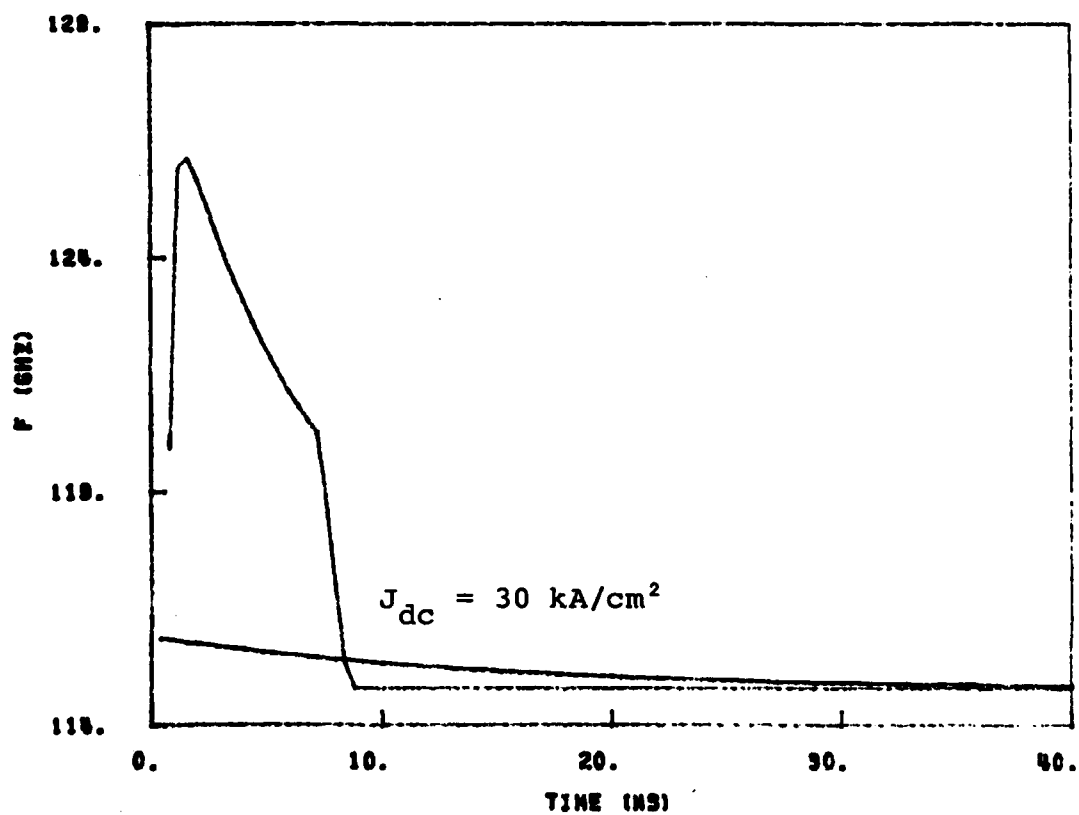
FIG. 4.13 FREQUENCY RESPONSES OF THE PREHEATING CURRENT WAVEFORM

AND FLAT CURRENT PULSE.

$$\eta = \frac{(\text{RF energy at desired frequency/total input energy})_{\text{preheating}}}{(\text{RF energy at desired frequency/total input energy})_{\text{flat current}}}$$

$$\cong \frac{31.5}{40} \times \frac{40 \times 30}{90 \times 8.5 + 30 \times 31.5} = 55 \text{ percent} \quad .$$

In the estimate, constant dc voltage is used for different current levels.

4.4 Optical Injection Compensation

The current produced by photon injection is subject to multiplication in the same way as the reverse saturation current. A small-signal analysis which describes the primary effects of photon injection on the IMPATT diodes has been derived.[25] Photon injection produces an increase in device conductance G_d and a decrease in device susceptance[26-29] B_d. Variation of device admittance with photon injection is strongly frequency dependent, and much greater variation occurs at the lower range of operating frequencies of a given IMPATT diode.[14] Therefore, the output power and oscillation frequency of the IMPATT oscillator can be controlled by photon injection. Injection at high intensity can be used to quench oscillation. Photon injection at low intensity can be used to modulate the amplitude and frequency of an IMPATT oscillator. The amount of modulation also depends on the microwave circuit and the operating condition.

It has been demonstrated that photon injection can be used to control the behavior of TRAPATT oscillators.[30] Frequency drift during the pulse may be eliminated by illuminating the device with an adequately shaped optical pulse. Under constant current bias, the effect of photon injection is to shift the oscillation higher in frequency.

The reduction in frequency drift is larger for a time-varying optical pulse that increases more rapidly in intensity.

The influence of optical current shaping on the frequency drift can be described by Eq. 4.4, which is derived in the same way as the derivation of Eq. 2.23, i.e.,

$$\frac{\partial(B_d + B_c)}{\partial f} \Delta f = A_1 \Delta T + A_3 \Delta I_{op} , \qquad (4.4)$$

where

$$A_3 = \frac{\partial B_d}{\partial V_{RF}} \frac{1}{\partial G_d / \partial V_{RF}} \frac{\partial G_d}{\partial I_{op}} - \frac{\partial B_d}{\partial I_{op}} .$$

To evaluate A_3 the device properties are summarized as follows:

1. The device susceptance B_d increases with RF voltage $(\partial B_d / \partial V_{RF} > 0)$.

2. The device conductance G_d increases with RF voltage $(\partial G_d / \partial V_{RF} > 0)$.

3. The device conductance G_d increases with optical current $(\partial G_d / \partial I_{op} > 0)$.

4. The device susceptance B_d decreases with optical current $(\partial B_d / \partial I_{op} < 0)$.

The calculated result $(A_3 > 0)$ suggests that the frequency drift during the pulse can be reduced with a time-varying optical current waveform.

Under constant current bias $(J_{dc} = 60 \text{ kA/cm}^2)$, the behavior of the IMPATT oscillator with photon injection has been studied. Figure 4.14 shows the various optical current waveforms used to study the effects of optical current shaping on the frequency drift and power variation of the pulsed IMPATT oscillator. For curve E, optical current density J_{op} increases from 0 to 1750 A/cm^2 linearly during the 40-ns pulsewidth.
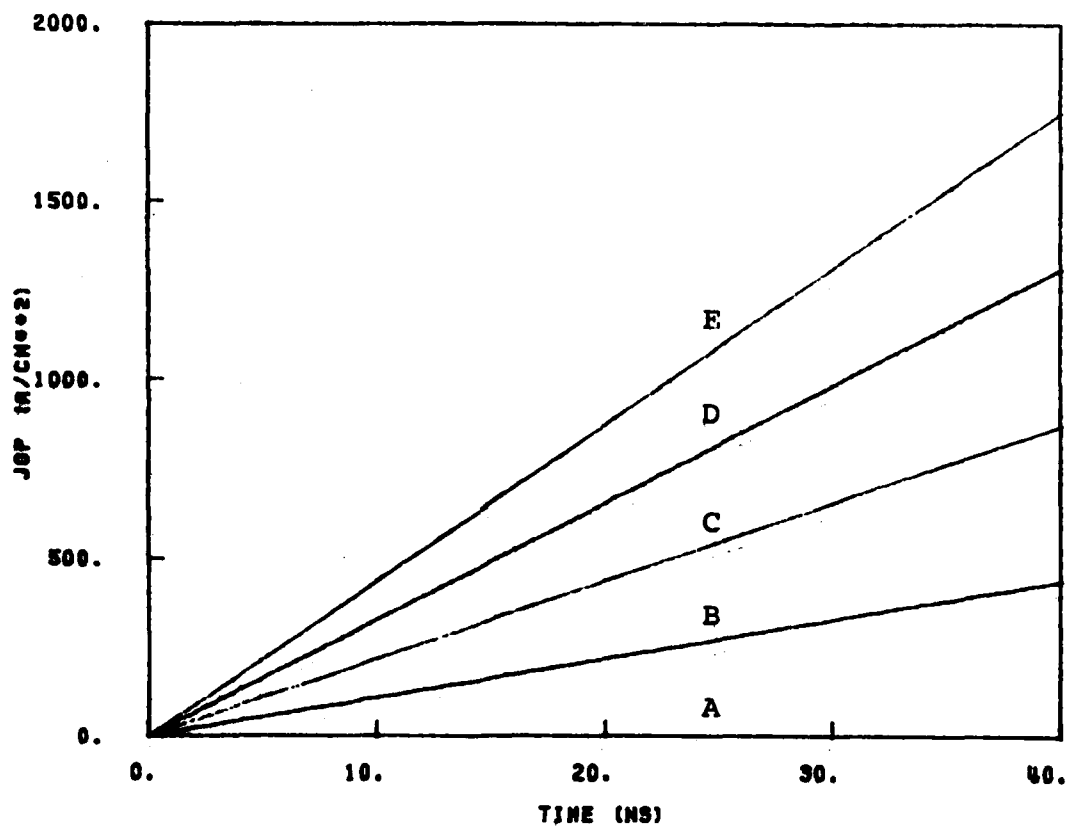
FIG. 4.14 VARIOUS OPTICAL CURRENT WAVEFORMS USED TO STUDY THE EFFECTS

OF OPTICAL CURRENT SHAPING ON THE FREQUENCY DRIFT AND POWER

VARIATION OF PULSED OSCILLATORS.

Figure 4.15 shows the frequency responses of the pulsed oscillator under various optical current waveforms. The temperature rise of the diode with optical compensation (curve E) is 169.1°C, and f_d is 2.5 GHz (f_{max} = 119.2 GHz, f_{min} = 116.7 GHz). The temperature coefficient of 14.8 MHz/°C is smaller than that without compensation (22.1 MHz/°C, curve A). It can be seen that the frequency drift decreases with upward optical compensation. For curve E, frequency decreases from 119.2 to 116.7 GHz and then increases to 117.0 GHz. The reason for this increase is that the frequency decrease caused by temperature rise is over-compensated by optical current.

Figure 4.16 shows the power variation of the pulsed oscillator under various optical current waveforms. When there is no photon injection (curve A), the output power increases from 1.3 to 3.27 W. With upward optical compensation (curve E), output power increases from 1.3 to 2.1 W and then decreases to 1.9 W. It can be seen that power variation and the frequency drift are improved with upward optical compensation.

To study the effects of exponentially and linearly increasing optical current waveforms on the frequency drift, the exponentially increasing optical current waveforms as shown in Fig. 4.17 are used in the simulation. The calculated results indicate that the temperature rise of the diode remains the same. Figure 4.18 shows the frequency responses of the pulsed oscillator with exponentially increasing optical current waveforms. For curve I, the optical current density J_{op} = 1750 $(1 - e^{-t/\tau_{th}})$ A/cm^2 and frequency decreases from 129.3 to 116.9 GHz during the pulse. This frequency drift is the same as that of the linearly increasing optical current waveform (curve E, Fig. 4.15).
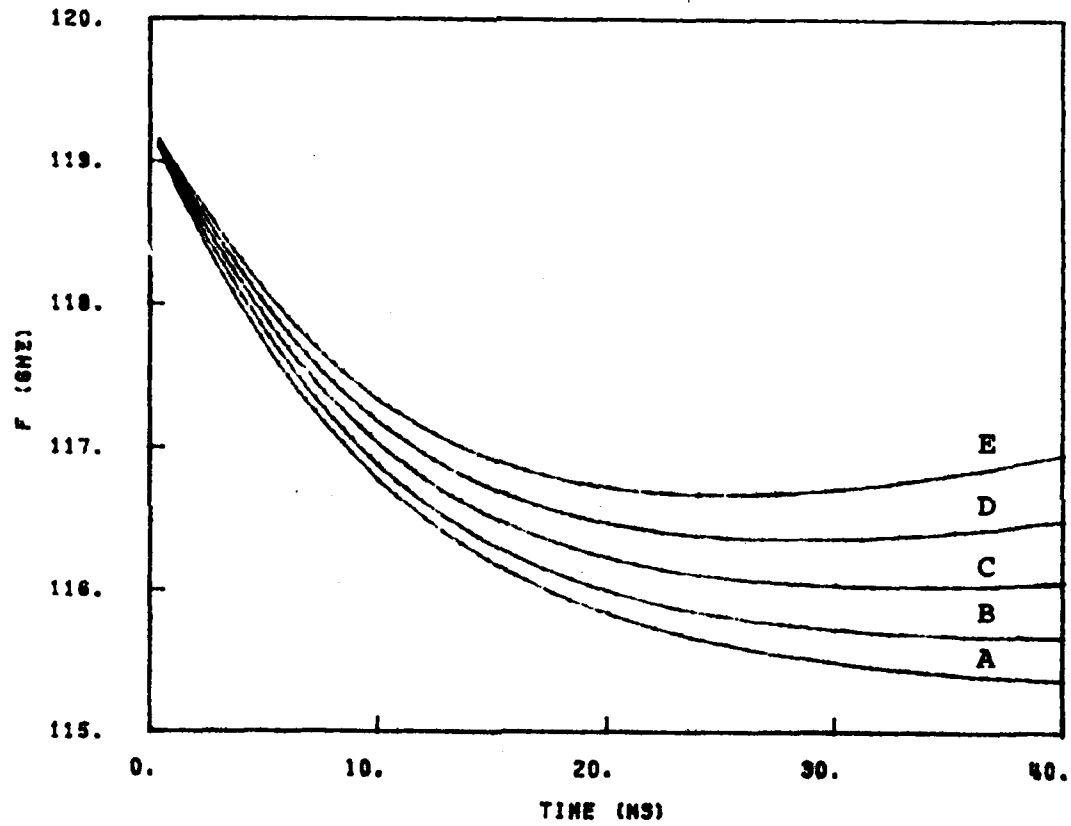
FIG. 4.15 FREQUENCY RESPONSES OF THE PULSED OSCILLATOR UNDER VARIOUS OPTICAL CURRENT WAVEFORMS.
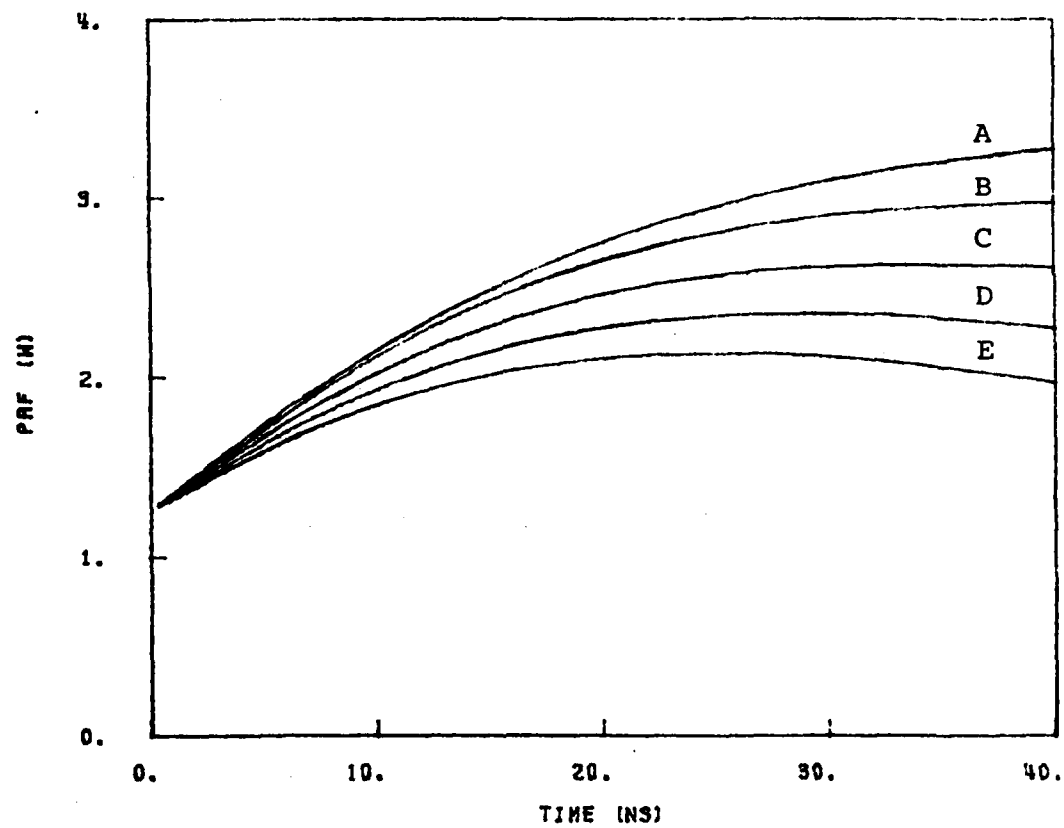
FIG. 4.16 POWER VARIATIONS OF THE PULSED OSCILLATOR UNDER VARIOUS

OPTICAL CURRENT WAVEFORMS.
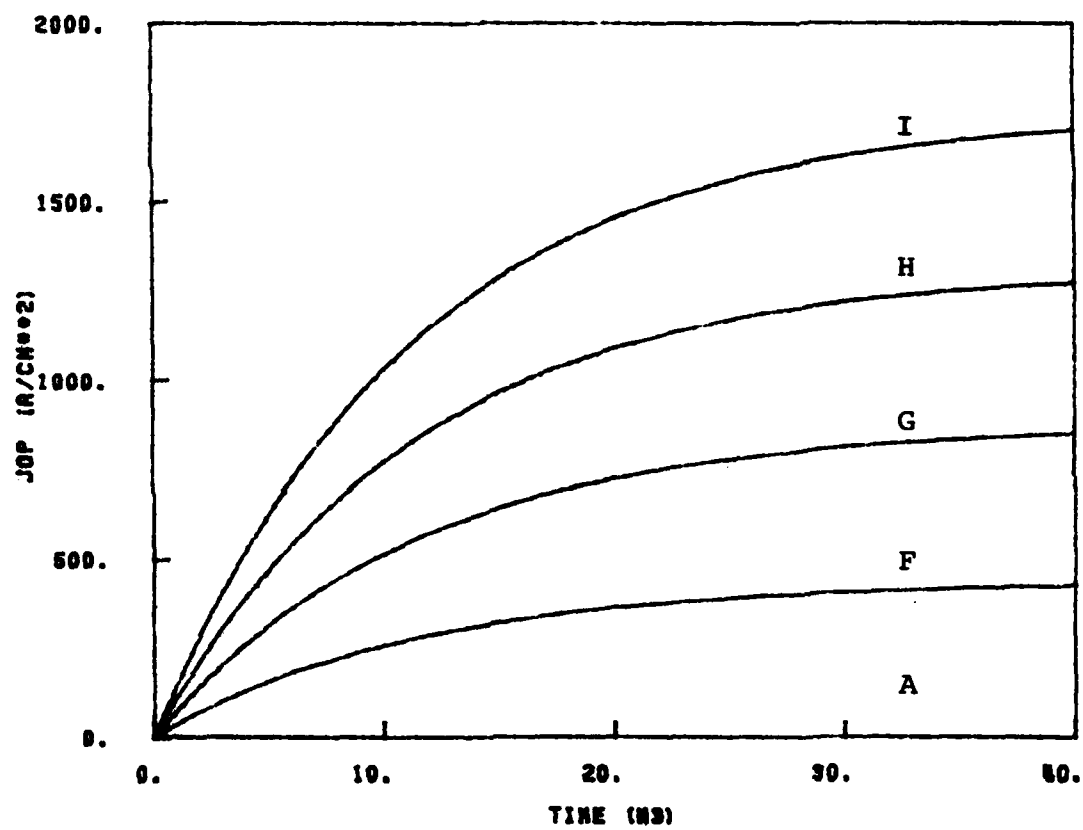
FIG. 4.17 EXPONENTIALLY INCREASING OPTICAL CURRENT WAVEFORMS.
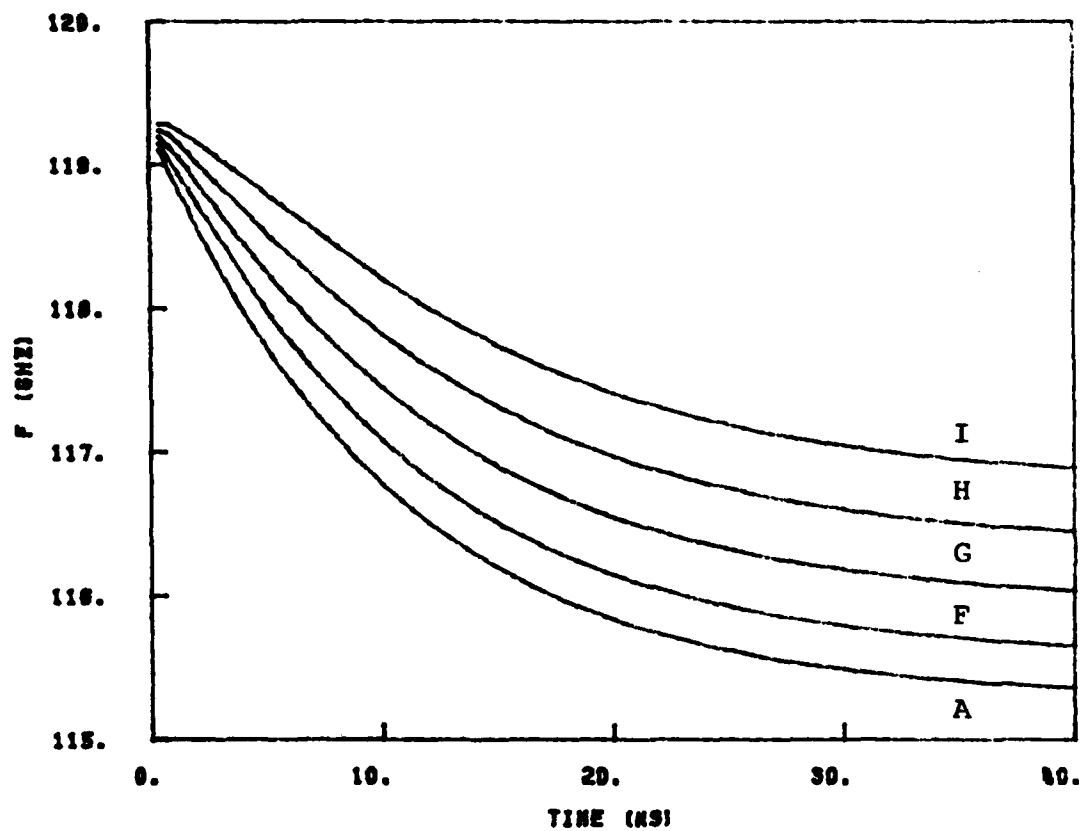
FIG. 4.18   FREQUENCY RESPONSES OF THE PULSED OSCILLATOR WITH EXPONEN-

TIALLY INCREASING OPTICAL CURRENT WAVEFORMS.

4.5 Optical Current Waveform $I_{op}(t)$ to Achieve Minimal Post Turn-On Frequency Drift

An expression of the optical current waveform $I_{op}(t)$ to achieve the minimal post turn-on frequency drift is desirable. This waveform can be obtained from Eq. 4.4:

$$I_{op}(t_1 + \Delta t) = I_{op}(t_1) + \Delta I_{op} ,$$

where Δt is the time step, and ΔI_{op} is the difference of optical current at $t_1 + \Delta t$ and t_1.

Then, if $\Delta f = 0$ (no frequency drift during Δt) and a constant dc current during the pulse is assumed, Eq. 4.4 becomes

$$\Delta I_{op} = - (A_1/A_3)\Delta T , \qquad (4.5)$$

where ΔI_{op}, A_1, A_3 and ΔT are functions of time, and ΔT is the temperature rise between $t_1 + \Delta t$ and t_1.

When the temperature dependence of circuit admittance is negligible, A_1, A_3, R_{th}, V_B, R_{sc} and V_R depend on the device dc and large-signal properties only. These parameters are known at the frequency range of interest, and the expression $I_{op}(t)$ to achieve minimal frequency drift can be determined.

The optimum optical current waveform obtained from Eq. 4.5 is shown in Fig. 4.19. The optical current density J_{op} increases from 0 to 3.7 kA/cm^2 during the 40 ns pulsewidth. In the calculation the diode is biased with constant current pulse (J_{dc} = 60 kA/cm^2). Figure 4.20 shows the frequency response caused by the optimum optical current waveform. The post turn-on frequency drift without
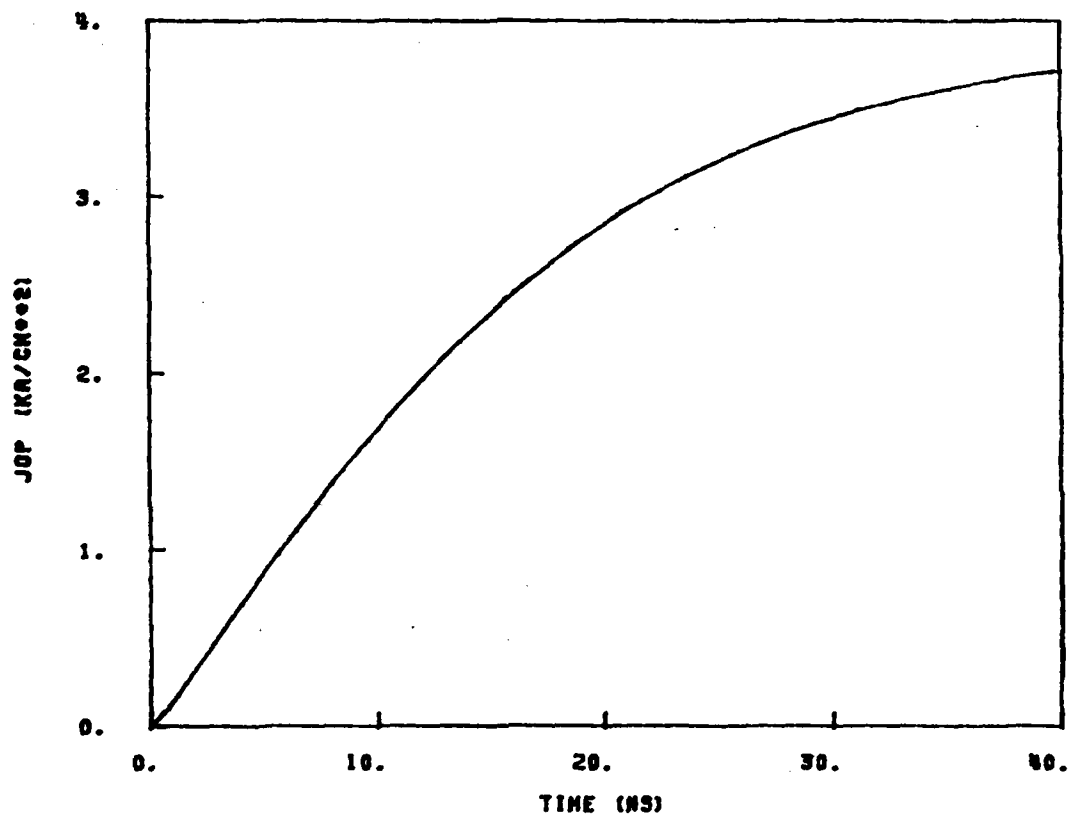
FIG. 4.19 OPTIMUM OPTICAL CURRENT WAVEFORM TO ACHIEVE MINIMAL

POST TURN-ON FREQUENCY DRIFT.
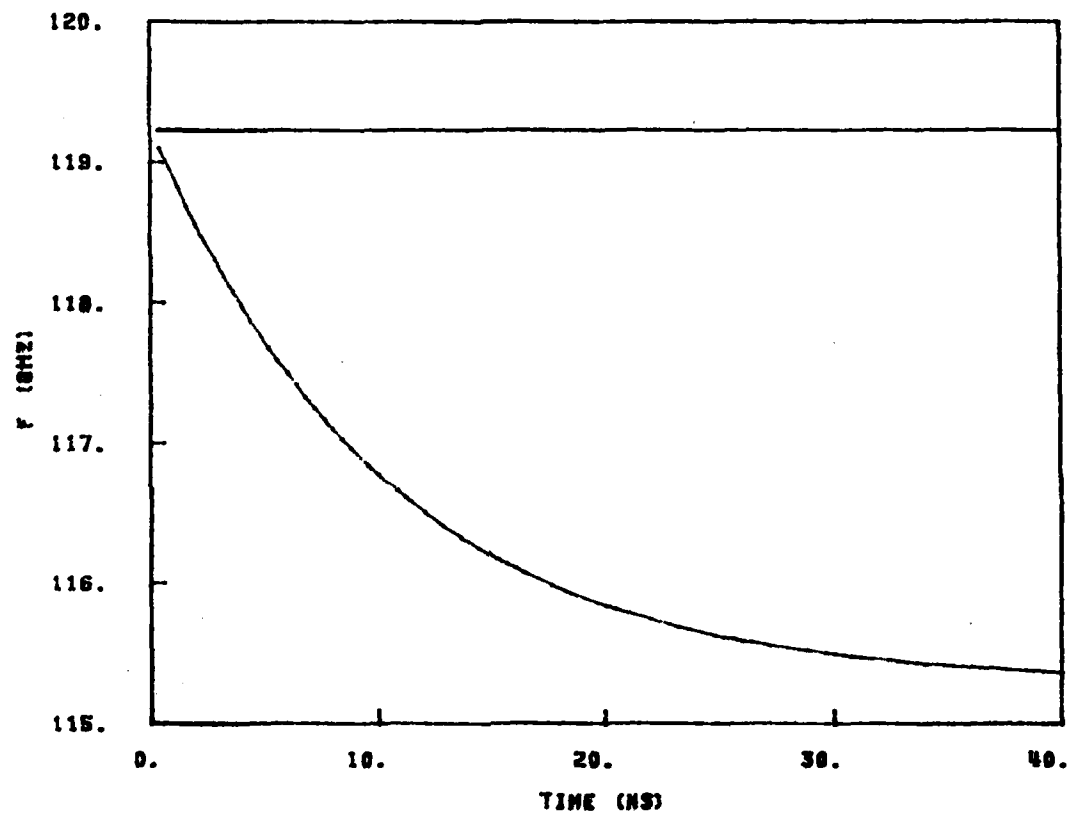
FIG. 4.20   FREQUENCY RESPONSE CAUSED BY THE OPTIMUM OPTICAL CURRENT
WAVEFORM.

optical compensation is also shown for comparison. It can be seen
that frequency drift during the pulse is eliminated.

4.6 Injection Locking

Injection locking is a conventional technique to stabilize the
frequency and tune solid-state oscillators. There are several types
of injection locking:[31]

1. Fundamental frequency injection locking: The injection
frequency f_i is nearly equal to the free-running frequency to be
locked f_o.

2. Subharmonic injection locking: f_i is nearly equal to $(1/n)f_o$,
where n is an integer larger than one. A low-frequency signal can
be used for injection but the locking bandwidth becomes narrower when
n is increased.

3. Sideband-wave injection locking: Two injection frequencies
are used; one is a low frequency signal $f_{inj,1}$ and the other with
frequency $f_{inj,2} = f_o \pm f_{inj,1}$.

CW and pulsed oscillators can be stabilized in frequency by
injection of a low-level signal into the oscillator through a circula-
tor. In the simplest case, the injection frequency is nearly equal to
that of a free-running oscillator. When the difference between two
frequencies is sufficiently small, the oscillator will be locked and
the frequency difference becomes negligible. This section describes
the performance of a short pulse (40 ns), low duty cycle, and pulsed
injection locked oscillator. The RF voltage and phase transients in
the time domain and the effects of the injection power and frequency
on the transient behavior can be studied.[32] In the calculation the
following parameters are used: injection frequency f_i = 117 GHz;

injection power P_{in} = 0.2 W (10 dB below the output power of the free-running oscillator); circuit conductance G = 20 mmho; circuit susceptance B_c = - 117 mmho; initial phase angle θ(0) = - 1.06 rad; device capacitance C_d = 0.208 pF; and injection current $I_i = \sqrt{8\ GP_{in}}$ = 0.18 A.

For a given injection current and frequency, the initial RF voltage $V_{RF}(0)$ is given by

$$V_{RF}(0) = \frac{I_i}{\sqrt{(\omega_i C_d)^2 + (G^2 + B_c^2)}} = 0.93\ V\ .$$

Without injection locking, the temperature increase causes the frequency to drift under a flat bias current pulse (J_{dc} = 60 kA/cm^2). In the case of an injection locked oscillator, the leading edge portions of the RF oscillation are not locked because of the large frequency transients during turn-on, and the oscillator is locked after the oscillation buildup is accomplished. With injection locking, frequency drift during the pulse is eliminated, and the oscillator is not locked during turn-on. When injection power is decreased, the locked portion of the pulse width decreases as shown:

I_i (A)	Locked Portion (ns)
0.18	2 to 40
0.12	3 to 21
0.06	6 to 15

Response of the PILO on the GB plane is shown in Fig. 4.21 when the injection current I_i = 0.12 and injection frequency f_i = 117 GHz. The circuit line as a function of frequency - $Y_c(f)$,
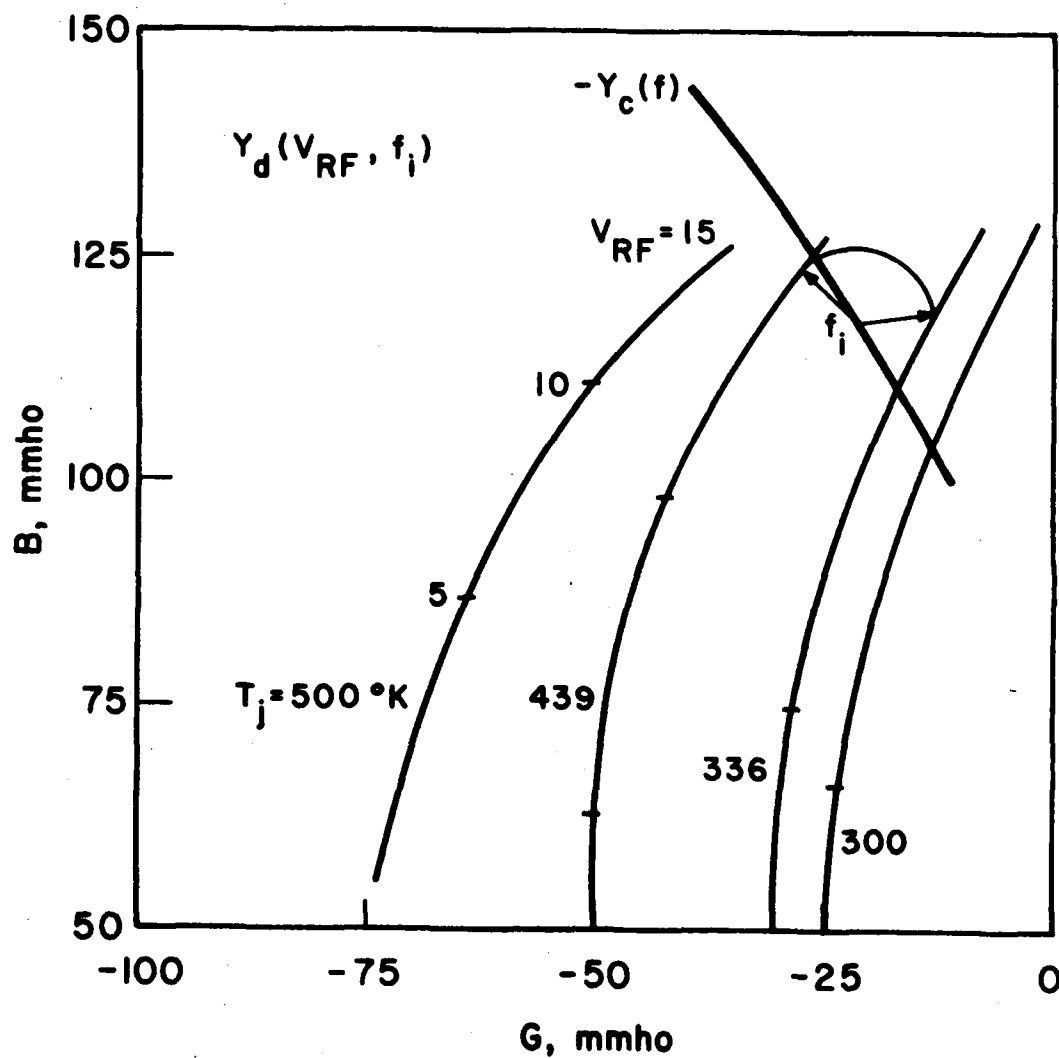
FIG. 4.21 RESPONSE OF THE PILO ON GB PLANE WHEN THE INJECTION CURRENT $I_i = 0.12$ AND INJECTION FREQUENCY $f_i = 117$ GHz.

the device line Y_d as a function of RF voltage and junction temperature with $f = f_i$, and the injection vector when the oscillator is locked are also shown. It can be seen that the oscillator is locked only when the junction temperature is between $336°K$ ($t = 3$ ns) and $439°K$ ($t = 21$ ns).

4.7 Conclusions

A number of techniques to reduce the post turn-on frequency drift were described in this chapter. Advantages and disadvantages of varactor compensation, high Q circuit, microwave switch and capacitor with negative temperature coefficient were discussed. With upward current compensation, power variation increased, although the frequency drift improved. The analytical expression of a current waveform to achieve the minimal frequency drift was derived. Elimination of the post turn-on frequency drift was demonstrated with this optimum current waveform. Frequency drift and power variation were improved with upward optical compensation. The expression of optimum optical current waveform was obtained, and the elimination of post turn-on frequency drift was illustrated. Use of injection locking to reduce the frequency drift was also studied. It was shown that the locked portion decreased with decreasing injection power as expected.

CHAPTER V. SUMMARY, CONCLUSIONS AND SUGGESTIONS
FOR FURTHER STUDY

5.1 Summary and Conclusions

The primary goal of this study was to obtain an improved understanding of pulsed oscillator properties primarily in the millimeter-wave frequency range. To reach this objective the first part of this work included an oscillator model which can be used to investigate the dynamic behaviors of pulsed and CW oscillators. The second part described the effect of external influences on device behavior and performance as oscillators, techniques to control the post turn-on frequency drift, and device and circuit design to optimize the oscillator performance.

In Chapter II the oscillator model to investigate the static and dynamic behavior of a free-running or injection locked pulsed oscillator was described. Turn-on, post turn-on and turn-off transients of the pulsed oscillator were obtained by solving the oscillator, thermal, and bias circuit equations simultaneously. Device admittance, circuit admittance, thermal resistance and thermal-time constant required for the oscillator analysis were obtained by theoretical calculation. Usefulness and limitation of this oscillator model were described. Buildup of RF oscillation, temperature increase, frequency drift, and power variation during the pulse and decay of the RF oscillation were illustrated through an example.

Oscillator turn-on transients and their dependence on device and circuit parameters were described in Chapter III.

The effects of bias current on the oscillator frequency and output power, of RF circuit on turn-on time and frequency response, of low-frequency bias circuit on the oscillator performance, and of injection signal on the turn-on transient were described. Also, influences of photon injection on output power under various bias conditions, simulated turn-on jitter and the effect of ambient temperature on turn-on transient were illustrated.

The techniques to control the post turn-on frequency drift were described in Chapter IV. Advantages and disadvantages of various techniques were discussed. Influences of bias current compensation on the frequency drift and power variation were described qualitatively. Influence of optical injection compensation on the frequency drift and use of injection locking to control the frequency drift were illustrated. The effects of the injection power and injection frequency on the locking result were discussed.

5.2 Suggestions for Further Study

Although the oscillator model developed in this investigation provides good simulation results and insight into the device-circuit interaction of oscillators, there are several additional topics which need further study. They are:

1. Experimental studies of pulsed and CW oscillators.

2. Comparison of the developed oscillator model and experimental results.

3. Full simulation (small-signal and large-signal simulation) of the optimum device design to minimize the post turn-on frequency drift.

4. Device fabrication and circuit design to minimize the post turn-on frequency drift.

APPENDIX

CIRCUIT MODEL USED IN CHAPTER IV

The circuit model used in Chapter IV is a post-in-waveguide circuit[16] which has the following circuit and package parameters:

waveguide width = 65 mil,

waveguide height = 15 mil,

radius of the bias post = 11 mil,

bias post position = 32.5 mil,

waveguide short position = 19 mil,

length of the bias coaxial line = 45 mil,

load of the bias coaxial line = 0,

characteristic impedance of the bias coaxial line = 50 Ω,

package parasitic inductor L_p = 0.03 nH, and

package parasitic capacitor C_p = 0.1 pF.

Figure A.1 shows the calculated circuit admittance as a function of frequency seen from the diode chip. In the calculation, the package inductance and capacitance are taken into consideration.
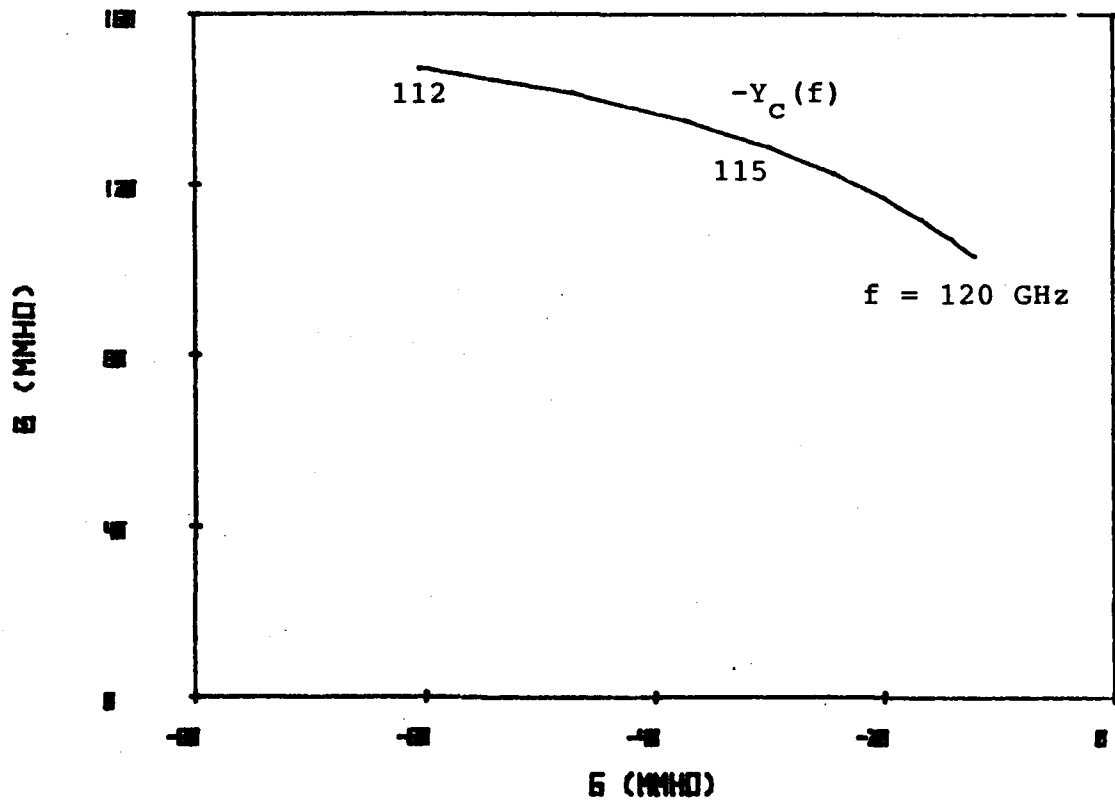
FIG. A.1   NEGATIVE OF CIRCUIT ADMITTANCE AS A FUNCTION OF FREQUENCY
SEEN FROM THE DIODE CHIP.

LIST OF REFERENCES

1. *Proceedings of the Symposium on Submillimeter Waves*, Poly-technic Press of the Polytechnic Institute of Brooklyn, New York, 1970.

2. Kihm, T.,Beebe, M., Brenneise, C. and Weglein, R. D., "A W-Band, Coherent, Pulsed-Compression Radar Transceiver Using Linear Frequency Modulation," *1981 IEEE Internal Microwave Symposium Digest*, pp. 414-416.

3. Sze, S. M., *Physics of Semiconductor Devices*, John Wiley and Sons, Inc., New York, 1969.

4. Gustafsson, L., Hasson, G. H. B. and Lundstrom, I. I., "On the Use of Describing Functions in the Study of Nonlinear Active Microwave Circuits," *IEEE Trans. on Microwave Theory and Techniques*, vol. MTT-20, No. 6, pp. 402-409, June 1972.

5. K.   awa, K., "Injection Locking of Microwave Solid-State Oscillators," *Proc. of IEEE*, vol. 61, No. 10, pp. 1386-1410, October 1973.

6. Culshaw, B., Giblin, R. A., and Blakey, P. A., *Avalanche Diode Oscillator*, Taylor & Francis Ltd., London, 1978.

7. Collin, R. E., *Foundations for Microwave Engineering*, McGraw-Hill, New York, pp. 155-156, 1966.

8. Burmawi, M. Y., "Optical Effects in Millimeter-Wave IMPATT Diodes and Oscillators," Ph.D. Dissertation, The University of Michigan, Ann Arbor, 1981.

9. Lewin, L., "A Contribution to the Theory of Probes in Wave-guides," *Inst. of Electrical Engineers Proceedings*, vol. 105, pt. C, pp. 109-116, 1958.

10. Chang, K. and Ebert, R. L., "W-Band Power Combiner Design," *IEEE Trans. on Microwave Theory and Techniques*, vol. MTT-28, No. 4, pp. 295-304, April 1980.

11. Gibbons, G., "Transient Temperature Response of an Avalanche Diode," *Solid-State Electronics*, vol. 133, No. 8, pp. 799-806, August 1969.

12. DiLorenzo, J. V., Niehaus, W. C., Velerbir, J. R., Jr. and Iglesias, D. E., "Beam-Lead Plated Heat Sink GaAs IMPATT: Part I. Performance," *IEEE Trans. on Electron Devices*, vol. ED-22, No. 8, pp. 509-514, August 1975.

13. Haitz, R. H., Stover, H. L. and Tolar, N. J., "A Method for Heat Flow Resistance Measurements in Avalanche Diodes," *IEEE Trans. on Electron Devices*, vol. ED-16, No. 5, pp. 438-444, May 1969.

14. Schroeder, W. E. and Haddad, G. I., "The Effect of Temperature on the Operation of an IMPATT Diode," *Proc. of IEEE* (Lett.), vol. 59, No. 8, pp. 1242-1244, August 1971.

15. Makino, T., "Effect of the Operational Modes on the Temperature Dependence of the Gunn Diode Admittance," *Solid-State Electronics*, vol. 22, pp. 761-769, 1979.

16. Fong, T. T. and Kuno, H. J., "Millimeter-Wave Pulsed IMPATT Sources," *IEEE Trans. on Microwave Theory and Techniques*, vol. MTT-27, No. 5, pp. 492-499, May 1979.

17. Chudobiak, W. J., "The Effect of Junction Temperature on the Output Power of a Silicon IMPATT Diode," *Proc. of IEEE*, vol. 60, pp. 340-341, March 1972.

18. Misawa, T., "Negative Resistance in p-n Junctions Under Avalanche Breakdown Condition, Part I & II," *IEEE Trans. on Electron Devices*, vol. ED-13, No. 1, pp. 137-151, January 1966.

19. Hirachi, Y., Nakagami, T., Toyama, Y., and Fukukawa, Y., "High-Power 50-GHz Double-Drift Region IMPATT Oscillators with Improved Bias Circuits for Eliminating Low-Frequency Instabilities," *IEEE Trans. on Microwave Theory and Techniques*, vol. MTT-24, No. 11, pp. 731-737, November 1976.

20. Bracket, C. A., "The Elimination of Tuning-Induced Burnout and Bias-Circuit Oscillations in IMPATT Oscillators," *Bell System Tech. J.*, vol. 52, No. 3, pp. 271-307, March 1973.

21. Vyse, B. and Levinson, H., "The Stability of Magnetrons Under Short Pulse Conditions," *IEEE Trans. on Microwave Theory and Techniques*, vol. 29, No. 7, pp. 739-745, July 1981.

22. Howes, M. J. and Morgan, D. V., *Microwave Devices, Device Circuit Interactions*, Wiley-Interscience, New York, 1976.

23. Morgan, D. V. and Howes, M. J., *Microwave Solid State Devices and Applications*, Peter Peregrinus Ltd., London, 1980.

24. Kondo, A., Ishii, T. and Shirahata, K., "Simple Stabilizing Method for Solid-State Microwave Oscillators," *IEEE Trans. on Microwave Theory and Techniques*, vol. MTT-22, No. 11, pp. 970-972, November 1974.

25. Sanderson, A. C. and Jordan, A. G., "Electron Beam Control of IMPATT Diodes," *Solid State Electronics*, vol. 15, No. 1, pp. 142-144, January 1972.

26. Gerlach, W. A. and Wellman, R., "The Behavior of a Pulsed Millimeter Wave (70 GHz) IMPATT Diode Oscillator During Laser Illumination," IEEE 1980 Int. Microwave Symposium Digest, pp. 70-72.

27. Kiehl, R. A., "Optical Control of IMPATT Oscillator Dynamics," 1978 IEDM Tech. Digest, pp. 286-289.

28. Forrest, J. R. and Seeds, A. J., "Analysis of the Optically Controlled IMPATT Oscillator," Solid-State and Electron Devices, vol. 3, No. 5, pp. 161-169, September 1979.

29. Sun, H. J., Gutmann, R. J. and Borrego, J. M., "Optical Tuning in GaAs MESFET Oscillators," IEEE 1981 Int. Microwave Symposium Digest, pp. 40-42.

30. Kiehl, R. A. and Eernisse, E. P., "Control of TRAPATT Oscillations by Optically Generated Carriers," IEEE Trans. on Electron Devices, vol. ED-24, No. 3, pp. 275-277, March 1977.

31. Okamoto, H. and Ikeda, M., "Cavity Stabilization and Electronic Tuning of a Millimeter-Wave IMPATT Diode Oscillator by Parametric Interaction," IEEE Trans. on Microwave Theory and Techniques, vol. MTT-26, No. 6, pp. 420-424, June 1978.

32. Parlidis, D., Hartnagel, H. L. and Tomizawa, K., "Dynamic Considerations of Injection Locked Pulsed Oscillators with Very Fast Switching Characteristics," IEEE Trans. on Microwave Theory and Techniques, vol. MTT-26, No. 3, pp. 162-169, March 1978.

REPORT DOCUMENTATION PAGE		READ INSTRUCTIONS BEFORE COMPLETING FORM
1. REPORT NUMBER 019795 1-T	2. GOVT ACCESSION NO. AD-A135 335	3. RECIPIENT'S CATALOG NUMBER
4. TITLE (and Subtitle) OPTIMUM DESIGN OF MILLIMETER-WAVE IMPATT DIODE OSCILLATORS		5. TYPE OF REPORT & PERIOD COVERED Interim Tech
		6. PERFORMING ORG. REPORT NUMBER Technical Report No. 165
7. AUTHOR(s) Y. S. Hwang		8. CONTRACT OR GRANT NUMBER(s) DAAG29-82-K-0083
9. PERFORMING ORGANIZATION NAME AND ADDRESS Electron Physics Laboratory The University of Michigan Ann Arbor, MI 48109-1109		10. PROGRAM ELEMENT, PROJECT, TASK AREA & WORK UNIT NUMBERS 18619-EL
11. CONTROLLING OFFICE NAME AND ADDRESS U. S. Army Research Office PO Box 12211 Research Triangle Park, NC 27709		12. REPORT DATE October 1983
		13. NUMBER OF PAGES 164
14. MONITORING AGENCY NAME & ADDRESS(if different from Controlling Office)		15. SECURITY CLASS. (of this report) Unclassified
		15a. DECLASSIFICATION DOWNGRADING SCHEDULE

16. DISTRIBUTION STATEMENT (of this Report)

Approved for public release; distribution unlimited.

17. DISTRIBUTION STATEMENT (of the abstract entered in Block 20, if different from Report)

18. SUPPLEMENTARY NOTES

The findings in this report are not to be construed as an official Department of the Army position, unless so designated by other authorized documents.

19. KEY WORDS (Continue on reverse side if necessary and identify by block number)

Pulsed IMPATT diode millimeter-wavelength oscillators
Quasi-static oscillator model
Si double-drift diode
Pulsed behavior
Optimum bias current

20. ABSTRACT (Continue on reverse side if necessary and identify by block number)

The limitations and control of pulsed IMPATT diode millimeter-wavelength oscillators are described. A quasi-static oscillator model is established for characterizing amplitude and frequency behavior during pulsed operation in response to external influences such as bias current, temperature, optical injection, locking signal injection and RF circuit. The effect of these external parameters in oscillator turn-on, turn-off, frequency chirp during the pulse, and start-up jitter are given for a millimeter-wavelength oscillator using a Si double-drift diode. Methods of controlling the pulsed behavior including bias current

DD FORM 1473
1 JAN 73

UNCLASSIFIED

20. Abstract (cont.)

compensation, optical compensation and injection locking are analyzed and applied to a pulsed millimeter-wave oscillator example. The optimum bias current and optical current waveforms which eliminate post turn-on frequency drift are presented.

END

FILMED

1-84

DTIC